Identifying and Characterizing Novel Targets against Rhabdomyosarcoma Disease Relapse

Thao Quang Pham

A dissertation
submitted in partial fulfillment of the
requirements for the degree of:

Doctor of Philosophy

University of Washington
2020

Reading Committee:
Eleanor Y Chen, Chair
Douglas S Hawkins
Lisa A Maves

Program Authorized to Offer Degree
Pathology

University of Washington

Abstract

Identifying and Characterizing Novel Targets against Rhabdomyosarcoma Disease Relapse

Thao Quang Pham

Chair of Supervisory Committee:
Associate Professor Eleanor Y Chen
Department of Pathology

Rhabdomyosarcoma (RMS) is the most common soft tissue pediatric sarcoma. Patients with relapsed or metastatic disease are faced with a poor survival outlook. Self-renewal of tumor propagating cells (TPCs) is believed to be responsible for driving RMS disease relapse through resistance to conventional therapies and recapitulation of RMS tumor heterogeneity. Identifying novel regulators of TPC activity may provide insight into potential therapeutic targets. In this dissertation, I identify and characterize GRK5 and HDAC6 as novel regulators of RMS cell growth and self-renewal. GRK5, a G-protein receptor kinase, regulates cell cycle in a kinase-independent manner to promote RMS tumor cell growth. Loss of GRK5 results in significant reduction of RMS self-renewal capacity due to increased cell death. HDAC6, a histone deacetylase, promotes RMS tumor growth by modulating cell cycle progression and tumor cell differentiation. Depletion of HDAC6 reduces RMS self-renewal capacity by limiting dilution assays and expression of stem-cell markers *SOX2, NANOG* and *OCT4. In vivo* inhibition of GRK5 and HDAC6 with small molecule inhibitors results in reduced RMS tumor cell growth, demonstrating their potential as therapeutic targets. Current *in vitro* approaches for studying RMS TPCs are unspecific, with *in vivo* methods being time intensive and costly. I will present preliminary data identifying CD133 as a potential marker for embryonal rhabdomyosarcoma (ERMS) TPCs for rapid *in vitro* characterization of TPC behavior. Collectively, my findings demonstrate the potential of RMS TPCs as therapeutic targets against RMS disease relapse and metastasis.

Acknowledgements

Special thanks to Eleanor Chen, Michael Phelps, Terra Vleeshouwer-Neumann and all undergraduates from the Chen lab for providing valuable feedback and insight in guiding me to where I am today. I would also like to thank William Mahoney, Megan Barker and all members of the Molecular Medicine and Mechanism of Disease PhD program for their contributions to my training. Finally, I would like to thank my Mom, Dad, sisters, and brothers as well as my friends for always providing me with support during difficult times.

Table of Contents

Chapter 1: Introduction

AUTHORS: Thao Pham[1], Eleanor Y. Chen[1]

1. Department of Pathology, University of Washington, Seattle, WA

Overview

Just as each individual patient is unique, each cancer possesses unique characteristics that make treatment difficult. Surgery, radiation and chemotherapy kill both healthy and cancerous cells, resulting in harmful side effects to the patient. Recent advancements in immunotherapy and small molecule inhibitors have shown personalized, more targeted therapies provide a better standard of care. However, concern over disease relapse remains. Relapsed disease often is more aggressive and resistant against previously administered treatment. Thus, there remains the need of understanding the mechanism behind cancer disease relapse and the possible ways of treating it.

Chapter 1 will highlight our current understanding behind rhabdomyosarcoma (RMS), a common pediatric sarcoma, and introduce key concepts that are explored in further chapters. Chapter 2 presents results of a study into G-protein coupled receptor 5's (*GRK5)* role in RMS disease and its potential as a therapeutic target. Chapter 3 will focus on histone deacetylase 6 (*HDAC6)* and its role in RMS disease. Chapter 4 explores the potential role of tumor propagating cells (TPC) driving RMS disease relapse and how we may better study them. Chapter 5 will have concluding remarks and discuss how the research in this thesis contributes to our understanding of RMS disease and how to potentially treat it.

Rhabdomyosarcoma (RMS)

Sarcomas are a heterogeneous group of cancers derived from the mesenchymal cell lineage[1]. Mesenchymal cells give rise to both skeletal and smooth muscle, as well as fat, bone and cartiledge[2]. Sarcomas that present in areas other than bone are categorized as soft tissue sarcomas[1,2]. Identification and categorization of soft-tissue sarcomas require biopsy of a tumor for histological and genetic testing[1]. Soft tissue sarcomas are considered quite rare, with an incidence rate of less than 1%[1–3]. 7.4% of cancer cases in children and young adults under the age 20 are categorized as being soft tissue sarcomas. Of these cases, 40% are identified as rhabdomyosarcoma (RMS)[2]. RMS is the most common soft tissue pediatric sarcoma. Histological and genetic characterization of RMS tumors show classic hallmarks of myogenesis, resulting in the use of the term "muscle" cancer[4]. This includes RMS tumors expressing myogenic markers such as *MYF5* and *MYOD*[5,6]. However, this term may be misleading as RMS tumors can present in connective or bone tissue. RMS tumors can be further categorized into subtypes, such as embryonal, alveolar, pleomorphic, spindle cell/sclerosing or anaplastic[1,7]. Embryonal (ERMS) and alveolar (ARMS) will be the focus of further discussion.

Embryonal Rhabdomyosarcoma (ERMS)

ERMS is the most common RMS subtype, accounting for about 75% of confirmed cases in patients younger than 20 years of age[2]. ERMS tends to present in children younger than 5 years old[2]. RMS tumors are categorized as ERMS subtype based upon distinct histological and genetic signatures. ERMS tumors histologically resemble an unorganized, heterogeneous population of cells that have arrested during various stages of myogenesis[1] (Figure 1). Compared to ARMS, ERMS typically do not contain a fusion protein resulting from a translocation event, leading to the term “Fusion Negative RMS” (FNRMS). ERMS tumors tend to present in the head and neck region (29%), with other common locations being the genital and urinary organs (18% and 10%)[2]. The average 5-year survival rate for patients diagnosed with ERMS varies based upon initial staging criteria set by the Intergroup Rhabdomyosarcoma Study (IRS). Stage I patients who present with localized disease that can be completely resected have the highest 5-year survival rate, at around greater than 90%[1]. Stage II, III and IV patients present with more metastatic disease progression at diagnosis and have worse 5-year survival projections at 80%, 70% and 30% respecitively[1]. Overall, the 5-year survival rate for RMS is 64%, with ERMS patients seeing a slightly higher rate of 68%[2]. This is partially explained due to ERMS cases having superior outcomes compared to other subtypes, such as ARMS[2]. However, patients that present with relapsed ERMS disease, on average, will see their 5-year survival rate fall to 26% resulting in a need for additional treatment options[8].

ERMS are also unique in their relatively low mutation burden when compared to other more commonly known cancers[9]. This is due to the relatively early onset of RMS in patients compared to other cancer types. Loss of heterozygosity (LOH) of 11p15.5 is believed to be a landmark event in the development of ERMS[1,10,11]. LOH at 11p15.5 leads to loss of imprinting control over the *IGF2* locus, resulting in overexpression of this potent growth factor[1,11,12]. The second most frequent genetic lesion found in ERMS tumors are mutations in genes in the RAS signaling pathway. Independent studies have shown that activating mutations in the RAS pathway are found in at least 45% of ERMS cases, with alterations of *NRAS* being the most common[12–16]. Other common mutations found in ERMS include those to several tyrosine kinases (*FGFR, PDGFRA, ERBB2)* and PI3K signaling family (*PIK3CA, PIK3CD, PTEN)*[11,14]. Thus, genetic diseases such as Costello Syndrome (germline *HRAS* mutation), Noonan Syndrome (*NRAS, KRAS, PTPN11* mutations) and Neurofibromatosis (*NF1* mutation) increases the chances a patient will develop ERMS[12]. In total, ERMS tumors carry far more clonal mutations compared to subclonal mutations, indicating a low level of mutation accumulation throughout the history of the tumor[12]. Molecular alterations commonly found in other cancer types appear to not apply in

ERMS. *TP53*, a potent tumor suppressor commonly found mutated in other cancer types (38%-50%), is less affected in ERMS (5.3%-12%)[11,14,17]. Activation of the *WNT* signaling pathway has been found in various cancers such as leukemia and breast cancer[18]. Silencing of canonical *WNT* signaling in chronic lymphocytic leukemia (CLL) was found to increase apoptosis *in vitro*[18]. However, in ERMS activation of WNT/B-catenin signaling results in tumor-suppressive effects, such as ERMS tumor cell differentiation, growth and reduced self-renewal[19]. During adult muscle regeneration, activation of canonical WNT signaling in muscle satellite cells is necessary for differentiation, indicating a defective myogenic process in ERMS is driving tumor cell growth[20,21]. Due to ERMS sharing common characteristics to cells undergoing myogenesis, various studies have investigated the role of myogenic markers in ERMS pathogenesis. MYOD, a myogenic marker, that typically functions to drive muscle cell differentiation, has been found to act in aberrant roles in ERMS[22–26]. Mutations to *MYOD* in combination with those in the PI3K-AKT pathway confer an aggressive form of ERMS[27]. A specific mutation to the DNA-binding site of MYOD, L122R, was shown to confer recognition of MYOD to MYC, a proto-oncogene, gene target sites[28]. The epigenetic landscape of MYOD gene targets in ERMS has also been found to be altered compared to primary muscle cells[25]. Taken together, while ERMS may possess myogenic markers, their ability to fully commit to muscle differentiation is defective.

Alveolar Rhabdomyosarcoma (ARMS)

ARMS is the second most common RMS subtype, making up 20%-31% of RMS cases[1,29]. ARMS presents in patients over a wider range of ages compared to ERMS[2]. ARMS is characterized by the histological presentation of an alveolar pattern of small, undifferentiated cells along with a fusion protein between *PAX3/PAX7* and *FOXO1A* (Figure 1B)[1]. Tumors typically present in the extremities of patients (39%) and in the head and neck area (22%)[2]. 5-year survival rates of ARMS patients are lower than ERMS, at around 59%[2]. Patients who experienced relapsed ARMS disease are faced with a 5% 5-year survival rate, making ARMS the most aggressive RMS subtype[8].

80% of ARMS cases have a detectable fusion protein of either *PAX3/FOXO1* (60%) or *PAX7/FOXO1* (20%)[30]. Rarer fusion proteins have also been identified, such as *PAX3/NCOA1*[31]. The remaining 20% of histologically characterized ARMS tumors have no detectable fusion protein and are clinically and molecularly indistinguishable from FNRMS[30,32]. ARMS presenting without the presence of a fusion protein have a better outlook when compared to fusion protein positive ARMS[32]. The most common fusion protein variants found in ARMS result from a chromosomal translocation event between chromosome 2 (*PAX3)* or

chromosome 1 *(PAX7)* with *FOXO1* on chromosome 13[33,34]. This fuses together the amino-terminal domain of the PAX3/PAX7 with the DNA-binding of FOXO1[33,34]. While the presence of PAX3/PAX7-FOXO1 is necessary for ARMS pathogenesis and confers a more aggressive nature, *in vivo* studies have shown it is not sufficient for ARMS tumorigenesis[35,36]. Additional mutations to tumor suppressor genes *Tp53* and *Cdkn2a* were required in a mouse model of ARMS for tumors to arise[37]. Similar to ERMS, ARMS tumors carry a relatively low mutation burden compared to other cancer types[12]. Sequencing analysis of primary ARMS tumors showed a high percentage of chromosomal amplification in fusion positive ARMS[12]. PAX3-FOXO1 tumors saw whole chromosomal duplication of the oncogene whereas PAX7-FOXO1 samples saw frequent focal amplication[12]. This chromosomal duplication event in combination with focal amplification of *CDK4, MYCN* or LOH at 11p is believed to be the penultimate step before ARMS tumorigenesis in patients[12]. Investigation into the role of PAX3/PAX7-FOXO1 in ARMS revealed multiple functions. PAX3-FOXO1 expression is able to rescue a *Pax3* deficient mouse model by activating *Pax3* target genes, including *Myod,* indicating its ability to activate genes responsible for driving myogenic differentiation[38,39]*.* However, at the same time, PAX3-FOXO1 works to both inhibit MYOD activation of differentiation genes and turn on proliferation genes in ARMS. PAX3-FOXO1 directly upregulates *JARID2* expression resulting in JARID2-EZH2 mediated recruitment of the PRC2 complex histone repressor complex to *MYOG* and *MYLH*[40,41]*.* At the same time, PAX3-FOXO1 works to turn on various proliferation and pro-survival genes including *IGFR4, MYCN, MET, IGF1R* and *BCL2L1*[11,42–45]*.* This combination of activity by PAX3-FOXO1 helps to create ARMS's characteristic presentation of tumor cells defective in terminal muscle differentiation. While ARMS and ERMS tumor cells may have hijacked different pathways to drive tumor cell proliferation, they both converge downstream in blocking activation of genes required for terminal differentiation (Figure 1C).

Current standard treatment of care for RMS patients

Surgical resection of the primary tumor is commonly the first method of attack in treating patients with RMS[11,46]. A grouping system devised by the IRS to classify patients following surgery is a useful predicator for patient outcome and a guide for further treatment[46]. This grouping system combines together tumor staging (I-IV) with pathological features and the effectiveness of initial tumor resection[11]. Patients with localized disease that is completely resected (Group I) see a 83% 3-year failure-free survival (FFS) rate[46]. Those with evidence of regional spread (Group II) or with advance presentation with incomplete resection (Group III) see a drop in their FFS rate to 86% and 73% respectively. Those in Group IV have distant

metastatic disease and have a >30% FFS rate[46]. To better treat RMS patients, the Children's Oncology Group (COG) used the IRS grouping system to place patients into 3 risk stratification levels (low, intermediate and high risk)[11,46]. Low-risk RMS patients, which included only ERMS cases in Group I/II, are given 45 weeks of a combination of either vincristine and, actinomycin-D (VA) or vincristine, actinomycin-D and cyclophosphamide (VAC)[46]. These patients saw a 5-year FFS of 85% and 93% respectively[46]. Intermediate-risk patients (ERMS Group III and ARMS Group I-III) typically receive VAC with or without alternating cycles of vincristine/topotecan/cyclophosphamide (VTV)[46]. This results in a 4-year FFS of 73% for VAC treatment and 68% VAC/VTC treatment[46]. High-risk RMS patients (Group IV ERMS and ARMS of any age) see an increase in the types of chemotherapeutic agents they may receive. Vincristine alongside irinotecan (VI) has been used in combination with interval-compressed additions of vincristine/doxorubicin/cyclophosphamide and alternating ifosfamide/etoposide[46]. A study of high-risk RMS patients who received this treatment combination saw a preliminary result of 18-month FFS of 66% and overall survival of 80%[46]. Concern remain about the duration over which RMS patients may receive chemotherapy. Chemotherapeutic agents present concerns over toxicity overexposure, and thus, determining the optimal period of treatment is critical[47].

However, the major concern RMS patients face today is disease relapse. Following disease relapse, the median survival of RMS patients is 0.8 years with the estimated 5-year survival rate being 17%[8]. Individuals who received a more intensive treatment combination were shown to respond worse following disease relapse, compared to those who were in a lower risk group[8,11]. Thus, there remains a need for alternative therapeutic options for relapsed or metastatic RMS disease. Novel therapeutic targets against RMS would also allow for the potential of reduced use of chemotherapeutics to improve patient quality of life.

Identification of molecular therapeutic targets

While a molecular target against RMS may show promise in the lab, their success in the clinic remains limited. *IGF1R* is a receptor tyrosine kinase that is found to be highly upregulated in ARMS[48]. A phase II clinical trial tested an IGF1R monoclonal antibody, R1507, in a cohort of RMS patients[48]. They found that only 1 RMS patient saw partial response to the treatment[48]. A subsequent phase II trial of another IGF1R inhibitor, in combination with an mTOR inhibitor, also showed no significant response in RMS patients[49]. There currently exists the need for further studies in identifying novel therapeutic targets that show promise in both the lab and clinic.

Therapeutic targeting of protein kinases has been demonstrated to be an effective treatment option for a variety of cancers[50]. There exists at least 500 kinases in the human genome, many of which have been linked to the promotion of cancer progression and relapse[50,51]. The roles of kinases in the pathogenesis of cancer and other human diseases have been studied extensively over the past 20 years[52]. However, there currently exist only 48 FDA-approved kinase inhibitors, many of which share the same targets[52]. Of the 48 FDA-approved kinase inhibitors, none have been tested for their therapeutic effects against advanced RMS disease[52]. While previous studies have shown MEK, CDK4/6 and WEE1 as promising kinase targets for inhibiting tumor growth, druggable kinases against RMS self-renewal have been poorly characterized[53,54]. The study by Chen et al (2014) shows that chemical inhibition of glycogen synthase kinase 3 (GSK3) reduces ERMS tumor growth and self-renewal, demonstrating the therapeutic potential for targeting protein kinases that play a role in the regulation of RMS tumor growth and self-renewal[19]. Therefore, our lab performed a siRNA library screen against the entire human kinome (714 kinases) to identify novel molecular targets that regulate RMS cell growth. I shall go into detail regarding one promising candidate, *GRK5,* in a later chapter.

Histone deacetylases (HDACs) are a class of epigenetic modifiers implicated in various cancers including osteosarcoma, lung cancer and RMS[55,56]. Previous work done by the Chen lab has identified the role of HDACs in regulating ERMS cell growth, motility and differentiation[57,58]. Treatment of ERMS cancer cell lines with two pan HDAC inhibitors, TSA and SAHA, resulted in reduced tumor growth through induction of myogenic differentiation[57]. This was found to be through HDAC modulation of Notch1 and EphrinB1 signaling pathways[58]. Our subsequent study utilizing a high throughput CRISPR/Cas9 screen, identified HDAC3 as a major repressor of ERMS differentiation[58]. HDAC3, in tandem with NCOR, forms a complex that repress MYOD/E2A-mediated transcription of myogenic differentiation genes[58]. Disruption of either HDAC3 or NCOR1/2 results in significant ERMS cancer cell differentiation[58]. HDAC3 was also implicated in suppressing the expression of *PAX3-FOXO1* in ARMS through a HDAC3-SMARCA4-miR-27a signaling axis, expanding its role across both ERMS and ARMS[59]. From our high throughput CRISPR/Cas9 screen of class I/II HDACs, we identified additional HDACs that potentially play a role in regulating RMS tumor cell growth[58]. I will discuss our findings on one of these candidate HDACs, HDAC6, in a later chapter.

Tumor propagating cells (TPCs) as potential drivers of RMS relapse

Liquid and solid tumors are comprised of a hierarchical system of cells, each possessing different characteristics. Early studies of acute myeloid leukemia (AML) suggested the existence of a small, subpopulation of cells that behaved similar to hematopoietic stem cells[60]. Stem cells possess the ability of self-renewal, which allows for continued propagation of itself and progenitor daughter cells[61]. While the majority of AML cells were post mitotic, researchers believed leukemic stem cells functioned as a driving source of new cancer cells[60]. This concept gave rise to what is known as the cancer stem cell theory[60,61]. Tumor propagating cells (TPCs), also commonly known as cancer stem cells, are thought to be responsible for metastasis and relapse of some cancer types, such as leukemia, breast and lung cancer[61–64]. TPCs possess stem cell-like characteristics that allow for the recapitulation of tumor heterogeneity in its entirety[61]. Tumor heterogeneity, and the role of TPCs, have been implicated as a mechanism behind cancer acquired resistance to therapeutic agents[61,65]. Chronic myeloid leukemia (CML) TPCs are characterized by the oncogene BCR-ABL and high levels of CD34 expression[66]. While CML patients treated with Gleevec, a BCR-ABL inhibitor, see significant reduction in disease burden, CML TPCs were found to still persist[66,67]. Quiescent CML TPCs isolated from patients in chronic phase at diagnosis showed resistant to Gleevec treatment *in vitro*[67]*.* There is also evidence indicating the role of chemotherapeutic resistant TPCs driving disease relapse in solid tumors, such as pancreatic and breast cancer[68,69]. Prolonged treatment of pancreatic adenocarcinoma cancer cell lines with Gemcitabine results in favored survival of CD133 positive TPCs *in vitro* and *in vivo*[68]. Pancreatic adenocarcinoma TPCs were also seen to be more resistant to chemotherapeutic induced cell death[68]. In breast cancer, prolonged exposure of HER2 overexpressing breast cancer cells with tastuzumab, a HER2 receptor antibody, results in TPC mediated resistance through PTEN inactivation and an IL6 inflammatory loop[69]. However, studies have shown that targeting TPCs and bulk cancer cells together may provide a more effective form of treatment. Inhibition of β-catenin or HDACs in combination with Imatinib, a BCR-ABL antibody, effectively induces CML TPC apoptosis and delays disease recurrence *in vivo*[70,71]*.* Treatment of pancreatic cancer cell lines with a STAT3 small molecule inhibitor reduces TPC self-renewal capacity *in vitro* as well as tumor growth and relapse *in vivo*[72]. Metformin, an anti-diabetic, in combination with doxorubicin, a chemotherapeutic agent, reduced tumor growth and disease relapse in a breast cancer xenograft mouse model[73]. Taken together, these findings highlight the role of cancer TPCs in driving disease relapse and metastasis.

As RMS shares many similarities to normal muscle development, it has been theorized that there exists a TPC population that function similarly to muscle satellite cells. Muscle

satellite cells serve as a stem cell progenitor population, responsible for maintaining muscle cell homeostasis[74]. Following injury to muscle fibers, muscle satellite cells undergo clonal expansion via asymmetric division to drive regeneration[75]. These muscle satellite cells express certain myogenic factors, such as *MYF5*¸that indicate their stage during myogenesis[75]. A potential TPC population with self-renewal capacity has been identified in a transgenic zebrafish model of ERMS[76]. *myf5* positive ERMS tumor cells were shown to possess the ability to generate new, heterogeneous tumors following transplantation into new zebrafish hosts[76]. Disruption of certain molecular targets, such as GSK3, has been shown to deplete TPC populations and reduce the ability of ERMS self-renewal[19]. However, in some RMS cancer cell lines, *MYF5* was not found to be differentially expressed between potential TPCs and total cell population, making it a less ideal TPC marker (Figure 2).

The spheroid assay is a surrogate *in vitro* assay that is commonly used to assess self-renewal capacity in cancer cells[77]. Cells are grown in suspension in medium containing a collection of various growth factors such as EGF, FGF and bFGF[77]. However, the medium in which spheroids are grown may propagate potential TPCs as well as cells that possess only stem-cell like characteristics[77]. Therefore, the gold standard to test self-renewal of potential TPCs remains clonal serial repopulation assays[61].

CD133 is a transmembrane glycoprotein that is used to label both cancer TPCs and normal stem cells[78–81]. Transplanted CD133 positive human derived cells showed greater regenerative capacity than human myoblasts in a muscle injury mouse model[80]. A subset of CD133 positive donor cells expressed both *PAX7* and *MYOD,* markers of quiescent and activated muscle satellite cells[79]. CD133 expressing glioblastoma cells contained elevated levels of neural precursor genes compared to CD133 negative cells[82]. Samples of recurrent glioblastoma tumors also showed significantly higher expression of CD133 compared to newly diagnosed tumors[82]. In human ERMS, CD133-positive cells have also been found to possess stem-like characteristics and are resistant to standard-of-care chemotherapy[83]. CD133 positive ERMS and ARMS cells were shown to have higher expression of skeletal muscle progenitor genes, such as PAX7 and cMET[84]. However, the antibodies used in these studies identified dramatically different percentages of CD133 positive RMS cells. A potential explanation for the discrepancy may be due to differences in antibody specificity, as one was monoclonal and the other polyclonal[83,84]. In addition, commonly recognized CD133 epitopes have the potential to be hidden or inaccessible due to changes in glycosylation patterns, which may also impact accurate CD133 representation[85,86]. Therefore, in a later chapter I will introduce our preliminary

findings in endogenously labeling CD133 expressing RMS cells for further cellular characterization.

Figures

Figure 1

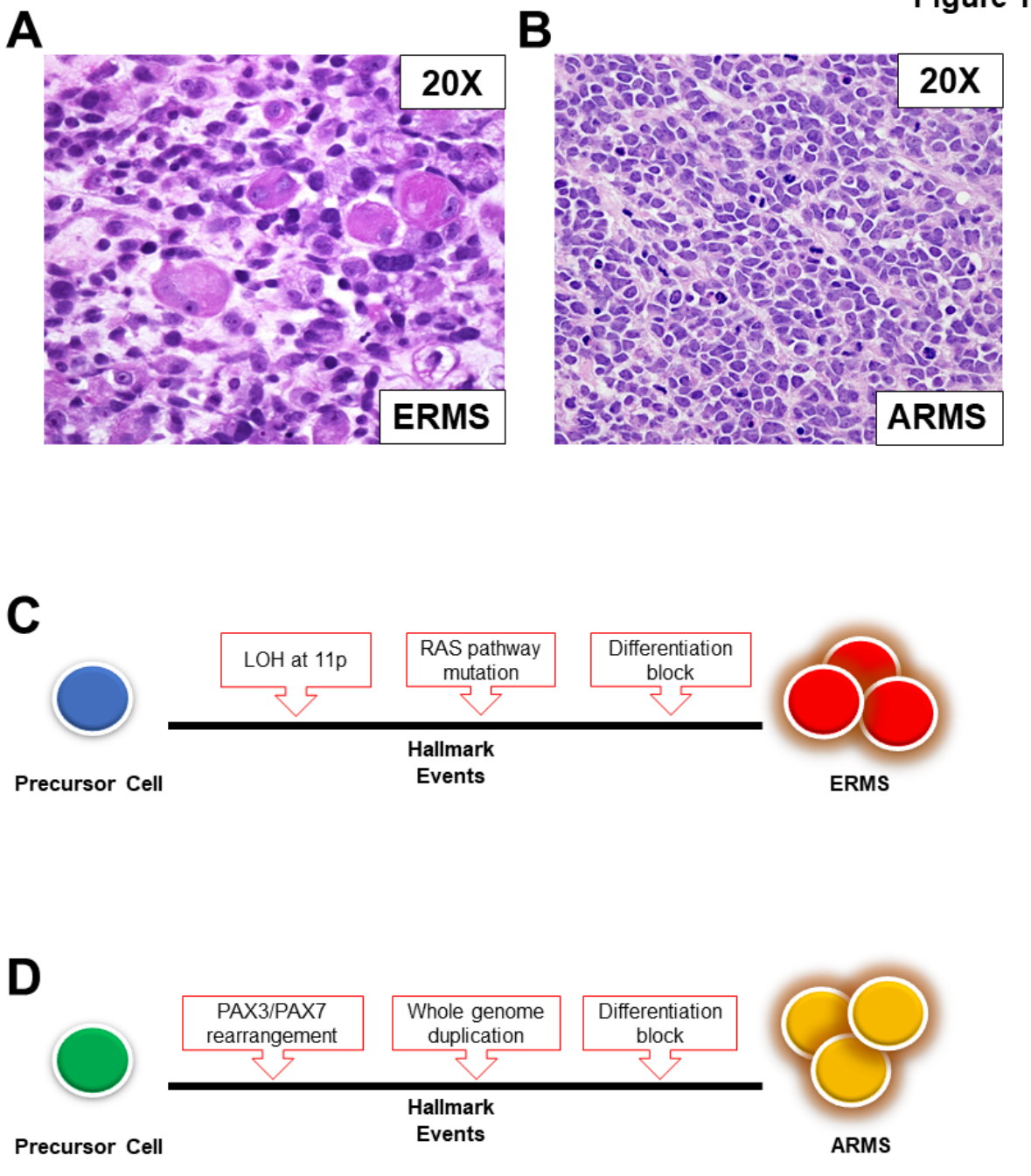

Figure 2

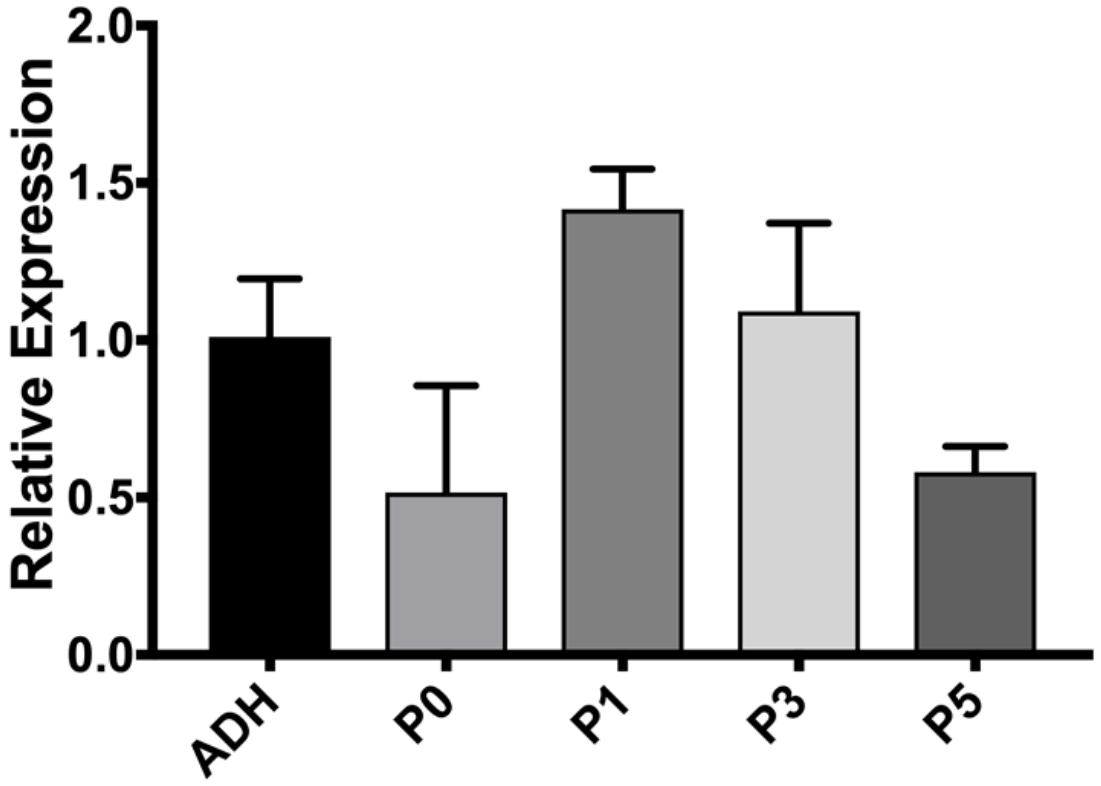

Figure Legends

Figure 1. Embryonal (ERMS) and alveolar (ARMS) rhabdomyosarcoma are histologically and molecular distinct. (A-B) Hematoxylin and eosin (H&E)-stained histology images showing distinguishing characteristics of ERMS and ARMS tumors. **(C-D)** Summarization of major hallmark events that result in the development of ERMS and ARMS.

Figure 2. *MYF5* expression levels are similar between adherent and potential TPCs. Quantitative PCR (qPCR) analysis to assess *MYF5* expression between total adherent cells (ADH) and serially passaged potential TPCs (P0 = passage 0, P1 = passage 1, P3 = passage 3, P5 = passage 5). Error bars represent 3 technical replicates from an independent biological experiment.

References

1. Skubitz, K. M. & D'Adamo, D. R. Sarcoma. *Mayo Clinic Proceedings* **82**, 1409–1432 (2007).

2. Ries, L. *et al. Cancer Incidence and Survival among Children and Adolescents: United States SEER Program 1975-1995*. (National Cancer Institute, SEER Program., 1999).

3. Clark, M. A., Fisher, C., Judson, I. & Thomas, J. M. Soft-Tissue Sarcomas in Adults. *New England Journal of Medicine* **353**, 701–711 (2005).

4. Keller, C. & Guttridge, D. C. Mechanisms of impaired differentiation in rhabdomyosarcoma. *FEBS J* **280**, 4323–4334 (2013).

5. Clark, J. *et al.* Expression of members of the myf gene family in human rhabdomyosarcomas. *Br J Cancer* **64**, 1039–1042 (1991).

6. Kumar, S., Perlman, E., Harris, C. A., Raffeld, M. & Tsokos, M. Myogenin is a Specific Marker for Rhabdomyosarcoma: An Immunohistochemical Study in Paraffin-Embedded Tissues. *Modern Pathology* **13**, 988–993 (2000).

7. Pappo, A. S. & Dirksen, U. Rhabdomyosarcoma, Ewing Sarcoma, and Other Round Cell Sarcomas. *JCO* **36**, 168–179 (2017).

8. Pappo, A. S. *et al.* Survival After Relapse in Children and Adolescents With Rhabdomyosarcoma: A Report From the Intergroup Rhabdomyosarcoma Study Group. *JCO* **17**, 3487–3493 (1999).

9. Armitage, P. & Doll, R. The Age Distribution of Cancer and a Multi-stage Theory of Carcinogenesis. *Br J Cancer* **8**, 1–12 (1954).

10. Scrable, H. *et al.* A model for embryonal rhabdomyosarcoma tumorigenesis that involves genome imprinting. *Proc Natl Acad Sci U S A* **86**, 7480–7484 (1989).

11. Skapek, S. X. *et al.* Rhabdomyosarcoma. *Nature Reviews Disease Primers* **5**, 1–19 (2019).

12. Chen, L. *et al.* Clonality and Evolutionary History of Rhabdomyosarcoma. *PLoS Genet* **11**, (2015).

13. Stratton, M. R., Fisher, C., Gusterson, B. A. & Cooper, C. S. Detection of Point Mutations in N-ras and K-ras Genes of Human Embryonal Rhabdomyosarcomas Using Oligonucleotide Probes and the Polymerase Chain Reaction. *Cancer Res* **49**, 6324–6327 (1989).

14. Shern, J. F. *et al.* Comprehensive genomic analysis of rhabdomyosarcoma reveals a landscape of alterations affecting a common genetic axis in fusion-positive and fusion-negative tumors. *Cancer Discov* **4**, 216–231 (2014).

15. Martinelli, S. *et al.* RAS signaling dysregulation in human embryonal Rhabdomyosarcoma. *Genes, Chromosomes and Cancer* **48**, 975–982 (2009).

16. Seki, M. *et al.* Integrated genetic and epigenetic analysis defines novel molecular subgroups in rhabdomyosarcoma. *Nature Communications* **6**, 1–8 (2015).

17. Olivier, M., Hollstein, M. & Hainaut, P. TP53 Mutations in Human Cancers: Origins, Consequences, and Clinical Use. *Cold Spring Harb Perspect Biol* **2**, (2010).

18. Zhan, T., Rindtorff, N. & Boutros, M. Wnt signaling in cancer. *Oncogene* **36**, 1461–1473 (2017).

19. Chen, E. Y. *et al.* Glycogen synthase kinase 3 inhibitors induce the canonical WNT/β-catenin pathway to suppress growth and self-renewal in embryonal rhabdomyosarcoma. *Proc Natl Acad Sci U S A* **111**, 5349–5354 (2014).

20. Brack, A. S., Conboy, I. M., Conboy, M. J., Shen, J. & Rando, T. A. A Temporal Switch from Notch to Wnt Signaling in Muscle Stem Cells Is Necessary for Normal Adult Myogenesis. *Cell Stem Cell* **2**, 50–59 (2008).

21. von Maltzahn, J., Chang, N. C., Bentzinger, C. F. & Rudnicki, M. A. Wnt Signaling in Myogenesis. *Trends Cell Biol* **22**, 602–609 (2012).

22. Tenente, I. M. *et al.* Myogenic regulatory transcription factors regulate growth in rhabdomyosarcoma. *eLife* **6**,.

23. Weintraub, H. *et al.* Activation of muscle-specific genes in pigment, nerve, fat, liver, and fibroblast cell lines by forced expression of MyoD. *Proc Natl Acad Sci U S A* **86**, 5434–5438 (1989).

24. Tapscott, S. J., Thayer, M. J. & Weintraub, H. Deficiency in rhabdomyosarcomas of a factor required for MyoD activity and myogenesis. *Science* **259**, 1450–1453 (1993).

25. MacQuarrie, K. L. *et al.* Comparison of Genome-Wide Binding of MyoD in Normal Human Myogenic Cells and Rhabdomyosarcomas Identifies Regional and Local Suppression of Promyogenic Transcription Factors. *Mol Cell Biol* **33**, 773–784 (2013).

26. Yao, Z. *et al.* Comparison of endogenous and overexpressed MyoD shows enhanced binding of physiologically bound sites. *Skelet Muscle* **3**, 8 (2013).

27. Kohsaka, S. *et al.* A recurrent neomorphic mutation in MYOD1 defines a clinically aggressive subset of embryonal rhabdomyosarcoma associated with PI3K-AKT pathway mutations. *Nature Genetics* **46**, 595–600 (2014).

28. Antwerp, M. E. V., Chen, D. G., Chang, C. & Prochownik, E. V. A point mutation in the MyoD basic domain imparts c-Myc-like properties. *PNAS* **89**, 9010–9014 (1992).

29. Ramadan, F., Fahs, A., Ghayad, S. E. & Saab, R. Signaling pathways in Rhabdomyosarcoma invasion and metastasis. *Cancer Metastasis Rev* (2020) doi:10.1007/s10555-020-09860-3.

30. Sorensen, P. H. B. *et al.* PAX3-FKHR and PAX7-FKHR Gene Fusions Are Prognostic Indicators in Alveolar Rhabdomyosarcoma: A Report From the Children's Oncology Group. *JCO* **20**, 2672–2679 (2002).

31. Wachtel, M. *et al.* Gene Expression Signatures Identify Rhabdomyosarcoma Subtypes and Detect a Novel t(2;2)(q35;p23) Translocation Fusing PAX3 to NCOA1. *Cancer Res* **64**, 5539–5545 (2004).

32. Williamson, D. *et al.* Fusion Gene–Negative Alveolar Rhabdomyosarcoma Is Clinically and Molecularly Indistinguishable From Embryonal Rhabdomyosarcoma. *JCO* **28**, 2151–2158 (2010).

33. Barr, F. G. *et al.* Rearrangement of the PAX3 paired box gene in the paediatric solid tumour alveolar rhabdomyosarcoma. *Nat Genet* **3**, 113–117 (1993).

34. Davis, R. J., D'Cruz, C. M., Lovell, M. A., Biegel, J. A. & Barr, F. G. Fusion of PAX7 to FKHR by the Variant t(1;13)(p36;q14) Translocation in Alveolar Rhabdomyosarcoma. *Cancer Res* **54**, 2869–2872 (1994).

35. Lam, P. Y. P., Sublett, J. E., Hollenbach, A. D. & Roussel, M. F. The Oncogenic Potential of the Pax3-FKHR Fusion Protein Requires the Pax3 Homeodomain Recognition Helix but Not the Pax3 Paired-Box DNA Binding Domain. *Molecular and Cellular Biology* **19**, 594–601 (1999).

36. Scheidler, S., Fredericks, W. J., Rauscher, F. J., Barr, F. G. & Vogt, P. K. The hybrid PAX3-FKHR fusion protein of alveolar rhabdomyosarcoma transforms fibroblasts in culture. *PNAS* **93**, 9805–9809 (1996).

37. Nishijo, K. *et al.* Credentialing a Preclinical Mouse Model of Alveolar Rhabdomyosarcoma. *Cancer Res* **69**, 2902–2911 (2009).

38. Relaix, F. *et al.* The transcriptional activator PAX3-FKHR rescues the defects of Pax3 mutant mice but induces a myogenic gain-of-function phenotype with ligand-independent activation of Met signaling in vivo. *Genes Dev.* **17**, 2950–2965 (2003).

39. Calhabeu, F., Hayashi, S., Morgan, J. E., Relaix, F. & Zammit, P. S. Alveolar rhabdomyosarcoma-associated proteins PAX3/FOXO1A and PAX7/FOXO1A suppress the transcriptional activity of MyoD-target genes in muscle stem cells. *Oncogene* **32**, 651–662 (2013).

40. Walters, Z. S. *et al.* JARID2 is a direct target of the PAX3-FOXO1 fusion protein and inhibits myogenic differentiation of rhabdomyosarcoma cells. *Oncogene* **33**, 1148–1157 (2014).

41. Ciarapica, R. *et al.* The Polycomb group (PcG) protein EZH2 supports the survival of PAX3-FOXO1 alveolar rhabdomyosarcoma by repressing FBXO32 (Atrogin1/MAFbx). *Oncogene* **33**, 4173–4184 (2014).

42. Cao, L. *et al.* Genome-wide Identification of PAX3-FKHR Binding Sites in Rhabdomyosarcoma Reveals Candidate Target Genes Important for Development and Cancer. *Cancer Res* **70**, 6497–6508 (2010).

43. Gryder, B. E. *et al.* PAX3-FOXO1 Establishes Myogenic Super Enhancers and Confers BET Bromodomain Vulnerability. *Cancer Discov* CD-16-1297 (2017) doi:10.1158/2159-8290.CD-16-1297.

44. Linardic, C. M. PAX3-FOXO1 Fusion Gene in Rhabdomyosarcoma. *Cancer Lett* **270**, 10–18 (2008).

45. Margue, C. M., Bernasconi, M., Barr, F. G. & Schäfer, B. W. Transcriptional modulation of the anti-apoptotic protein BCL-XL by the paired box transcription factors PAX3 and PAX3/FKHR. *Oncogene* **19**, 2921–2929 (2000).

46. Malempati, S. & Hawkins, D. S. Rhabdomyosarcoma: Review of the Children's Oncology Group (COG) Soft-Tissue Sarcoma Committee Experience and Rationale for Current COG Studies. *Pediatr Blood Cancer* **59**, 5–10 (2012).

47. Bisogno, G. & Hawkins, D. S. An unresolved issue in rhabdomyosarcoma treatment: The duration of chemotherapy. *Pediatric Blood & Cancer* **n/a**, e28174.

48. Pappo, A. S. *et al.* A phase 2 trial of R1507, a monoclonal antibody to the insulin-like growth factor-1 receptor (IGF-1R), in patients with recurrent or refractory rhabdomyosarcoma, osteosarcoma, synovial sarcoma, and other soft tissue sarcomas: Results of a Sarcoma Alliance for Research Through Collaboration study. *Cancer* **120**, 2448–2456 (2014).

49. Wagner, L. M. *et al.* Phase II study of cixutumumab in combination with temsirolimus in pediatric patients and young adults with recurrent or refractory sarcoma: A report from the children's oncology group. *Pediatric Blood & Cancer* **62**, 440–444 (2015).

50. Gross, S., Rahal, R., Stransky, N., Lengauer, C. & Hoeflich, K. P. Targeting cancer with kinase inhibitors. *J Clin Invest* **125**, 1780–1789 (2015).

51. Hanahan, D. & Weinberg, R. A. Hallmarks of Cancer: The Next Generation. *Cell* **144**, 646–674 (2011).

52. Roskoski, R. Properties of FDA-approved small molecule protein kinase inhibitors. *Pharmacological Research* **144**, 19–50 (2019).

53. Yohe, M. E. *et al.* MEK inhibition induces MYOG and remodels super-enhancers in RAS-driven rhabdomyosarcoma. *Science Translational Medicine* **10**, eaan4470 (2018).

54. Stewart, E. *et al.* Identification of Therapeutic Targets in Rhabdomyosarcoma through Integrated Genomic, Epigenomic, and Proteomic Analyses. *Cancer Cell* **0**, (2018).

55. Deskin, B. *et al.* Inhibition of HDAC6 Attenuates Tumor Growth of Non-Small Cell Lung Cancer. *Translational Oncology* **13**, 135–145 (2020).

56. Blattmann, C. *et al.* Enhancement of Radiation Response in Osteosarcoma and Rhabomyosarcoma Cell Lines by Histone Deacetylase Inhibition. *International Journal of Radiation Oncology*Biology*Physics* **78**, 237–245 (2010).

57. Vleeshouwer-Neumann, T. *et al.* Histone Deacetylase Inhibitors Antagonize Distinct Pathways to Suppress Tumorigenesis of Embryonal Rhabdomyosarcoma. *PLoS One* **10**, (2015).

58. Phelps, M. P., Bailey, J. N., Vleeshouwer-Neumann, T. & Chen, E. Y. CRISPR screen identifies the NCOR/HDAC3 complex as a major suppressor of differentiation in rhabdomyosarcoma. *PNAS* **113**, 15090–15095 (2016).

59. Bharathy, N. *et al.* The HDAC3–SMARCA4–miR-27a axis promotes expression of the PAX3:FOXO1 fusion oncogene in rhabdomyosarcoma. *Sci. Signal.* **11**, eaau7632 (2018).

60. Dick, J. E. Stem cell concepts renew cancer research. *Blood* **112**, 4793–4807 (2008).

61. Kreso, A. & Dick, J. E. Evolution of the Cancer Stem Cell Model. *Cell Stem Cell* **14**, 275–291 (2014).

62. Kaur, G. *et al.* G-protein coupled receptor kinase (GRK)-5 regulates proliferation of glioblastoma-derived stem cells. *Journal of Clinical Neuroscience* **20**, 1014–1018 (2013).

63. Lawson, D. A. *et al.* Single-cell analysis reveals a stem-cell program in human metastatic breast cancer cells. *Nature* **526**, 131–135 (2015).

64. Jahchan, N. S. *et al.* Identification and targeting of long-term tumor-propagating cells in small cell lung cancer. *Cell Rep* **16**, 644–656 (2016).

65. Vidal, S. J., Rodriguez-Bravo, V., Galsky, M., Cordon-Cardo, C. & Domingo-Domenech, J. Targeting cancer stem cells to suppress acquired chemotherapy resistance. *Oncogene* **33**, 4451–4463 (2014).

66. Graham, S. M. *et al.* Primitive, quiescent, Philadelphia-positive stem cells from patients with chronic myeloid leukemia are insensitive to STI571 in vitro. *Blood* **99**, 319–325 (2002).

67. Bhatia, R. *et al.* Persistence of malignant hematopoietic progenitors in chronic myelogenous leukemia patients in complete cytogenetic remission following imatinib mesylate treatment. *Blood* **101**, 4701–4707 (2003).

68. Hermann, P. C. *et al.* Distinct Populations of Cancer Stem Cells Determine Tumor Growth and Metastatic Activity in Human Pancreatic Cancer. *Cell Stem Cell* **1**, 313–323 (2007).

69. Korkaya, H. *et al.* Activation of an IL6 Inflammatory Loop Mediates Trastuzumab Resistance in HER2+ Breast Cancer by Expanding the Cancer Stem Cell Population. *Molecular Cell* **47**, 570–584 (2012).

70. Heidel, F. H. *et al.* Genetic and Pharmacologic Inhibition of β-Catenin Targets Imatinib-Resistant Leukemia Stem Cells in CML. *Cell Stem Cell* **10**, 412–424 (2012).

71. Zhang, B. *et al.* Effective Targeting of Quiescent Chronic Myelogenous Leukemia Stem Cells by Histone Deacetylase Inhibitors in Combination with Imatinib Mesylate. *Cancer Cell* **17**, 427–442 (2010).

72. Li, Y. *et al.* Suppression of cancer relapse and metastasis by inhibiting cancer stemness. *PNAS* **112**, 1839–1844 (2015).

73. Hirsch, H. A., Iliopoulos, D., Tsichlis, P. N. & Struhl, K. Metformin Selectively Targets Cancer Stem Cells, and Acts Together with Chemotherapy to Block Tumor Growth and Prolong Remission. *Cancer Res* **69**, 7507–7511 (2009).

74. Bentzinger, C. F., Wang, Y. X. & Rudnicki, M. A. Building Muscle: Molecular Regulation of Myogenesis. *Cold Spring Harb Perspect Biol* **4**, a008342 (2012).

75. Gurevich, D. B. *et al.* Asymmetric division of clonal muscle stem cells coordinates muscle regeneration in vivo. *Science* **353**, aad9969 (2016).

76. Ignatius, M. S. *et al.* In Vivo Imaging of Tumor-Propagating Cells, Regional Tumor Heterogeneity, and Dynamic Cell Movements in Embryonal Rhabdomyosarcoma. *Cancer Cell* **21**, 680–693 (2012).

77. Pastrana, E., Silva-Vargas, V. & Doetsch, F. Eyes Wide Open: A Critical Review of Sphere-Formation as an Assay For Stem Cells. *Cell Stem Cell* **8**, 486–498 (2011).

78. Meng, J., Muntoni, F. & Morgan, J. CD133+ cells derived from skeletal muscles of Duchenne muscular dystrophy patients have a compromised myogenic and muscle regenerative capability. *Stem Cell Research* **30**, 43–52 (2018).

79. Meng, J. *et al.* Human Skeletal Muscle–derived CD133+ Cells Form Functional Satellite Cells After Intramuscular Transplantation in Immunodeficient Host Mice. *Molecular Therapy* **22**, 1008–1017 (2014).

80. Negroni, E. *et al.* In Vivo Myogenic Potential of Human CD133+ Muscle-derived Stem Cells: A Quantitative Study. *Molecular Therapy* **17**, 1771–1778 (2009).

81. Chen, X. *et al.* p53 positively regulates the expression of cancer stem cell marker CD133 in HCT116 colon cancer cells. *Oncol Lett* **16**, 431–438 (2018).

82. Liu, G. *et al.* Analysis of gene expression and chemoresistance of CD133+ cancer stem cells in glioblastoma. *Mol Cancer* **5**, 67 (2006).

83. Walter, D. *et al.* CD133 Positive Embryonal Rhabdomyosarcoma Stem-Like Cell Population Is Enriched in Rhabdospheres. *PLOS ONE* **6**, e19506 (2011).

84. Pressey, J. G. *et al.* CD133 marks a myogenically primitive subpopulation in rhabdomyosarcoma cell lines that are relatively chemoresistant but sensitive to mutant HSV. *Pediatric Blood & Cancer* **60**, 45–52 (2013).

85. Bidlingmaier, S., Zhu, X. & Liu, B. The utility and limitations of glycosylated human CD133 epitopes in defining cancer stem cells. *J Mol Med (Berl)* **86**, 1025–1032 (2008).

86. Glumac, P. M. & LeBeau, A. M. The role of CD133 in cancer: a concise review. *Clinical and Translational Medicine* **7**, 18 (2018).

Chapter 2: Characterization of GRK5 as a novel regulator of rhabdomyosarcoma tumor cell growth and self-renewal

AUTHORS: Thao Pham[1], Kristin Robinson[1], Terra Vleeshouwer-Neumann[1], James E. Annis[2], Eleanor Y. Chen[1*]

1. Department of Pathology, University of Washington, Seattle, WA

2. Quellos HTS Core, Institute for Stem Cell and Regenerative Medicine, University of Washington, Seattle, WA

Introduction

Rhabdomyosarcoma (RMS) is the most common pediatric soft-tissue cancer. There are two major subtypes of RMS, each with distinct histologic features and genetic alterations. Embryonal rhabdomyosarcoma (ERMS) typically harbors mutations in the *RAS* pathway[1]. Alveolar rhabdomyosarcoma (ARMS) is characterized by the presence of the PAX3- or PAX7-FOXO1 fusion[2]. Other RMS subtypes include spindle cell (SC/S), pleomorphic (PRMS) and those not otherwise specified (NOS). While the prognosis is good for patients with localized disease, the survival rate for patients with relapsed RMS is only 10-30%[3], highlighting an urgent need for more effective treatment options for disease relapse. Tumor propagating cells (TPCs) are thought to be responsible for metastasis and relapse of some cancer types, such as breast and lung cancer[4–7], and possess stem cell-like characteristics that allow for the recapitulation of tumor heterogeneity in its entirety[7]. A potential TPC population with self-renewal capacity has been identified in a conserved transgenic zebrafish model of ERMS[8]. In human ERMS, CD133-positive cells have also been found to possess stem-like characteristics and are resistant to standard-of-care chemotherapy[9]. Targeting stem-like features of RMS would therefore provide novel therapeutic avenues for treating RMS disease relapse and metastasis.

Therapeutic targeting of protein kinases has been demonstrated to be an effective treatment option for a variety of cancers[10]. There exists at least 500 kinases in the human genome, many of which have been linked to the promotion of cancer progression and relapse[10,11]. The roles of kinases in the pathogenesis of cancer and other human diseases have been studied extensively over the past 20 years[12]. However, there currently exists only 48 FDA-approved kinase inhibitors, many of which share the same targets[12]. Of the 48 FDA-approved kinase inhibitors, none have shown beneficial therapeutic effects against advanced RMS disease[12]. While previous studies have shown MEK, CDK4/6 and WEE1 as promising kinase targets for inhibiting tumor growth, druggable kinases against RMS self-renewal have been poorly characterized[13,14]. The study by Chen et al (2014) shows that chemical inhibition of glycogen synthase kinase 3 (GSK3) reduces ERMS tumor growth and self-renewal, demonstrating the therapeutic potential for targeting protein kinases that play a role in the regulation of RMS tumor growth and self-renewal[15].

G-protein coupled receptor kinase 5 (*GRK5)* belongs to a family of serine/threonine kinases[16] and plays an important role in cardiovascular disease pathogenesis and early heart development[17–19]. GRK5 targets the β-adrenergic receptors, members of the G-protein coupled receptors family (GPCRs), leading to their desensitization and down regulation in cardiomyocytes[20], and is upregulated during heart failure[21]. GRK5 can also function in a non-

GPCR-dependent manner to regulate HDAC5 activity in cardiomyocytes, promoting maladaptive hypertrophy and heart failure[22]. While GRK5 has been extensively studied for its role in heart disease, the role of GRK5 in cancer pathogenesis is poorly characterized. To date, GRK5 has been shown to play a role in the pathogenesis of lung, brain and prostate cancer[4,23,24]. In non-small cell lung cancer (NSCLC) and glioblastoma multiforme (GMB), GRK5 is highly expressed in primary patient specimens and depletion of GRK5 results in reduced cell growth[4,23]. Loss of GRK5 in NSCLC and prostate cancer cell lines also results in cell cycle arrest[23,24]. However, the role of GRK5 in RMS pathogenesis is unknown. GRK5 possesses a unique combination of kinase activity and non-enzymatic protein domains for interacting with substrates, making it an attractive target for drug design in translational applications[20,25,26].

In this study, we have identified GRK5 as a novel regulator of RMS self-renewal in a high-throughput siRNA library screen against the human kinome (714 kinases). Using the CRISPR/Cas9-based genetic editing strategy, we show that GRK5 loss-of-function reduces RMS self-renewal capacity *in vitro* and *in vivo* through increased programmed cell death. GRK5 regulates cell cycle progression to promote ERMS tumor cell growth in a kinase-independent manner. *NFAT1*, a transcription factor involved in T-cell maturation[27], is a key player in GRK5-mediated cell cycle progression. Treatment of RMS xenografts with a selective GRK5 inhibitor, CCG-215022, results in a significant reduction of tumor growth, demonstrating the potential of GRK5 as a therapeutic target in RMS.

Results

A siRNA library screen of the human kinome identifies GRK5 as a novel regulator of ERMS self-renewal.

To identify potential candidate kinases that are essential for self-renewal of ERMS, we performed a siRNA library screen against the human kinome (714 kinases) in two ERMS cell lines (RD and 381T). Each cell line was transfected with a pool of 3 siRNAs against each kinase, along with control (scramble) siRNAs, in 384-well low attachment plates to induce sphere formation. The sphere assay was used as a surrogate *in vitro* assay for assessing the self-renewal capacity of tumor cells[28]. RD and 381T cells were also transfected with the same set of siRNAs in adherent conditions for assessing cell growth. An ATP-based viability assay was performed on siRNA-transfected cells in adherent condition, and high-content imaging was performed on the spheres. The normalized ratio of self-renewal capacity to cell growth compared to controls for each kinase target was analyzed (see the volcano plot in Figure 1A). Of the 714 kinases screened, 6 top candidate genes (*FES, LTK, LYN, NME9, PIK3C2A, GRK5*)

showed differential effects on self-renewal compared to cell growth and were prioritized for further validation. We subsequently utilized a high-efficiency CRISPR/Cas9 gene targeting strategy[29] to validate the loss-of-function effect of each candidate kinase gene on self-renewal of 381T ERMS cells (Figure 1B). GRK5 was prioritized for further functional characterization due to consistent loss-of-function effects on self-renewal of RMS cells.

GRK5 is differentially expressed in RMS cells compared to normal tissue types and is present in both nuclear and cytoplasmic compartments.

GRK5 mRNA expression levels were analyzed in 4 RMS cell lines (381T and SMS-CTR of the ERMS subtype; Rh5 and Rh30 of the ARMS subtype) and compared against a primary myoblast line and an immortalized fibroblast line. In the 4 RMS cell lines, regardless of subtype, the expression level of *GRK5* is at least 2-fold higher compared to normal cell types (Figure 1C). Immunofluorescence showed both nuclear and cytoplasmic localization of GRK5 in RMS cells (Figure 1D). Immunohistochemistry performed on a tissue microarray (TMA) of primary human RMS tumors showed positive GRK5 expression in the majority of RMS samples including 8/10 ERMS and 10/17 ARMS samples (Figure 1E). In contrast, normal muscle samples from 4 patients showed very weak or negative GRK5 expression. From these findings, *GRK5* appears to be differentially expressed in RMS tumors and likely plays an important role in RMS pathogenesis.

GRK5 regulates self-renewal of both ERMS and ARMS.

To confirm effective disruption of *GRK5* by CRISPR/Cas9, gRNAs were designed to flank the catalytic, nuclear export (NES) and nuclear localization (NLS) functional domains of GRK5 (Figure 2A). Genetic disruption of *GRK5* was then verified via PCR amplification of the genomic deletion event, and depletion of the protein product was confirmed by Western blots (Figure 2A-B, Figure S1A). Immunofluorescence of SMS-CTR GRK5 targeted cells showed reduced GRK5 signal, highlighting specificity of our gene targeting (Figure S1B). We assessed the loss-of-function effect of GRK5 on tumor cell self-renewal using the sphere assay on a panel of ARMS (Rh5 and Rh30) and ERMS (381T and SMS-CTR) cell lines. CRISPR/Cas9-mediated disruption of *GRK5* resulted in a significant reduction (p-value < 0.05) in RMS self-renewal capacity via spheroid assay in 3 (381T, SMS-CTR, Rh5) out of the 4 RMS cancer cell lines (Figure 2C). Targeted disruption of *GRK5* in Rh30 showed a trend of reduced self-renewal capacity but was not statistically significant (p-value $= 0.086$). Spheroids generated from cells harboring targeted disruption of *GRK5* appeared to be both smaller and fewer in number (Figure

2C-D, Figure S1C). To determine the cellular mechanism underlying the loss-of-function effects of GRK5 on sphere formation, we performed a quantitative flow cytometry-based Annexin V assay to assess for any change in apoptosis. Loss of GRK5 resulted in a significant increase in early apoptotic events in the spheroids (Figure 2E-F), and approximately 2-fold increase in total apoptotic cells (Figure 2G) compared to the controls. Increased in cell death in GRK5-deficient spheroid cells was further supported by elevated levels of cleaved caspase 3 (CC3) protein (Figure 2H). To assess the effects of GRK5 loss-of-function on the self-renewal capacity of RMS cells *in vivo*, we performed limiting dilution experiments of ERMS (381T) and ARMS (Rh5) xenografts in immunocompromised NOD-scid-IL2Rgammanull (NSG) mice. In both RMS subtypes, targeted disruption of *GRK5* resulted in approximately 4 to 6-fold reduction in self-renewal frequency (Table 1). Taken together, our results indicate that loss of GRK5 in RMS cells results in decreased self-renewal capacity in part through induction of programmed cell death.

GRK5 regulates ERMS cell growth in a kinase-independent manner and is involved in regulating cell cycle progression.

We assessed the loss-of-function effect of GRK5 on tumor cell growth using an ATP-based viability assay on a panel of ARMS (Rh5 and Rh30) and ERMS (381T and SMS-CTR) cell lines. Loss of GRK5 resulted in a significant reduction in cell viability in all 4 RMS cell lines (p-value < 0.05) (Figure 3A). To assess the specificity of GRK5 loss-of-function effect on RMS cell growth, we overexpressed a Cas9-resistant form of GRK5 in the presence of CRISPR/Cas9-mediated *GRK5* gene disruption in SMS-CTR cells. Compared to GFP overexpression control, Cas9-resistant GRK5 rescued the growth phenotype of SMS-CTR cells following targeted disruption of *GRK5* (Figure 3B). Even though the GRK family proteins are known for their kinase-dependent roles, some studies have also implicated kinase-independent function of GRK5[20,30]. To determine whether GRK5 regulates RMS cell growth in a kinase dependent or independent manner, we generated a kinase dead (K215R) (KD) GRK5 mutant[25] that is resistant to targeted disruption by CRISPR/Cas9. Overexpression of KD GRK5 protein also restored cell growth in SMS-CTR cells with targeted disruption of *GRK5* (Figure 3B), indicating that GRK5 regulates ERMS cell growth in a kinase-independent manner. We next determined the cellular event that was responsible for GRK5 loss-of-function effect on RMS cell growth. While 381T and SMS-CTR cells with targeted disruption of *GRK5* showed no significant change in cellular differentiation or cell death (Figure 3C-D), they showed altered cell cycle progression in a flow cytometry-based cell cycle analysis following EdU pulse by day 6 of GRK5

knockout (Figure S2A). This delay in cell cycle progression is sustained till day 10 with a delay in the G1/S phase in 381T cells, and in the G2/M phase in SMS-CTR cells (Figure 3E-F). Overall, our results indicate that GRK5 functions in a kinase-independent manner to alter cell cycle progression in ERMS cells.

***NFAT1* expression is regulated by GRK5 in a kinase-independent manner.**

GRK5 has been previously shown to facilitate the transcriptional activity of NFAT as part of a DNA binding complex during cardiac hypertrophy in a kinase independent manner[20]. NFAT1 has been shown to function either as a positive or negative regulator of cell cycle progression[31,32]. To investigate the role of NFAT as a potential downstream component of the GRK5 pathway in regulating ERMS cell growth, we first showed that targeted disruption of *GRK5* led to decreased levels of NFAT1 expression in 381T and SMS-CTR cells (Figure 4A). Overexpression of wild-type or catalytically-dead GRK5 restored expression levels of *NFAT1* (Figure 4B). To determine the loss-of-function effects of NFAT1 on RMS cells, we showed that targeted disruption of *NFAT1* by CRISPR/Cas9 in ERMS cells (381T and SMS-CTR) significantly reduced cell growth (Figure 4C). Cell cycle analysis of *NFAT1*-targeted 381T and SMS-CTR cells showed significant alteration of cell cycle progression (Figure 4D-E). There was a delay in both G1/S and G2/M in *NFAT1*-disrupted 381T and SMS-CTR cells. To explore whether GRK5 interacts with NFAT1 in ERMS, we showed by immunofluorescence that GRK5 and NFAT1 appear to be co-localized in 381T cells (Figure 4F). By proximity ligation assay, we showed GRK5 and NFAT1 in close proximity in the nucleus and the cytoplasm of 381T cells, and that loss of GRK5 abrogated this interaction (Figure 4G). Taken together, our data indicate that NFAT1 is a potential downstream mediator of GRK5 function in regulating RMS cell growth.

Treatment of RMS tumor with CCG-215022, a GRK5 inhibitor, reduces tumor growth *in vivo.*

To assess the potential of GRK5 as a therapeutic target against RMS, 381T or Rh5 RMS xenografts established in NSG mice were treated with a GRK5-selective inhibitor, CCG-215022 (Figure 5A). Treatment duration (21 days for 381T tumors and 12 days for Rh5 tumors) was determined by how quickly DMSO vehicle control (CTRL) tumors reached experimental endpoint. Mice treated with CCG-215022 appeared to show delayed 381T and Rh5 tumor growth over time compared to mice treated with vehicle control (Figure 5B-C). CCG-215022 treated tumors showed a significant reduction in tumor growth in both 381T and Rh5 tumors compared to the mice treated with vehicle control (Figure 5D-F). Immunohistochemistry analysis

of CCG-215022 treated tumors shows a lower Ki-67 proliferation index compared to the vehicle control-treated tumors (Figure 5G). These results demonstrate the therapeutic potential of targeting GRK5 as an alternative treatment option to inhibit RMS tumor growth.

Discussion

While *GRK5* has been extensively studied for its role in the pathogenesis of cardiovascular disease, only in recent years has its role in cancer biology been brought to light[17–22]. GRK5 has been implicated as having a role in regulating lung, brain and prostate cancer cell growth[4,23,24]. However, the role of GRK5 in RMS has yet to be investigated. In this study, we show that GRK5 is a novel regulator of RMS cell growth through its interaction with NFAT1 to regulate cell cycle progression in a kinase-independent manner. Loss of GRK5 reduces the self-renewal capacity of RMS cells through increased programmed cell death, implicating it as a novel regulator of stem-like features in RMS. We demonstrate the potential for GRK5 as a therapeutic target through treatment of RMS xenografts with a selective GRK5 inhibitor, CCG-215022. RMS tumors treated with CCG-215022 show significant reduction in tumor growth and self-renewal capacity.

The studies characterizing the role of GRK5 in cancer pathogenesis to date have primarily investigated the functional requirement of its kinase activity[33,34]. TP53 phosphorylation by GRK5 leads to its degradation, resulting in inhibition of the TP53-dependent apoptotic response to genotoxicity in osteosarcoma cells[33]. A study using HeLa cells additionally shows a defect in proper cell cycle progression following *GRK5* gene knockdown[34]. However, we show through rescue experiments with a GRK5 kinase-dead mutant that GRK5 regulates RMS cell growth in a kinase-independent manner. We also show that targeted disruption of *GRK5* in two RMS cell lines with TP53 mutations, 381T with *TP53*(*R248W*) and Rh30 with *TP53*(*R237H)*[35,36], reduces RMS cell growth by inducing cell cycle arrest. Our findings indicate that GRK5 regulates RMS cell growth in a kinase- and TP53-independent manner.

Dysregulated activity of the NFAT family of transcription factors has been identified in cancer[37]. While NFAT proteins (NFAT1-5) share similar DNA binding targets, each member possesses both redundant and opposing functions, and their activity often requires cooperation with additional transcriptional partners[31,32,37]. NFAT1 has been shown to function both as a tumor suppressor through the transcriptional activation of the CDK4 promoter or as an oncogene by silencing p15 expression[20]. In a model of pathological cardiac hypertrophy, GRK5 promotes the transcriptional activity of NFAT in a kinase-independent manner as part of a DNA binding complex to regulate expression of hypertrophic genes[20]. In this study, both wild-type and

kinase-dead GRK5 are able to restore *NFAT1* expression following targeted disruption of *GRK5* in ERMS cell lines. We also show that GRK5 potentially interacts with NFAT1, and this interaction is abrogated with loss of GRK5. Our findings suggest a novel role for GRK5 acting in a kinase-independent manner to regulate the *NFAT1* expression. CRISPR/Cas9 mediated disruption of *NFAT1* phenocopies the loss-of-function effects of GRK5 on cell cycle progression. NFAT likely functions as an important downstream mediator to promote oncogenic activity of GRK5. Further study is required to determine whether GRK5 directly or indirectly interacts with NFAT1 in ERMS in regulating ERMS tumor cell growth.

TPCs undergo self-renewal to recapitulate the complex heterogeneity of a given malignant tumor and are thought to be the major drivers of cancer relapse and metastasis in selected cancer types[7,38]. Disease relapse or metastasis of RMS carries a poor survival prognosis[3]. Identifying potential targets that regulate TPC survival could potentially provide a solution for treating RMS disease relapse and metastasis. Our study shows that GRK5 loss-of-function significantly reduces the self-renewal capacity of RMS cells *in vitro* and *in vivo*. The stem-like RMS spheres harboring *GRK5* knockout show increased cell death. Our findings indicate that GRK5 is a promising therapeutic target against RMS stem-like features. Further investigation is required to assess whether loss of GRK5 leads to reduced heterogeneity of RMS tumors and thereby reduces the potential for resistance against standard-of-care therapies.

Inhibitors selective to GRK5 are currently limited. Amlexanox, an FDA-approved anti-inflammatory drug, has been shown to inhibit GRK5 activity[39]. However, amlexanox is a non-specific inhibitor with cross reactivity with other proteins and pathways such as IKBKE in the Hippo pathway[40]. CCG-215022, an investigational compound developed by John Tesmer's group at the University of Michigan, shows high selectivity against GRK5[41]. In our study, treatment of both ERMS and ARMS xenograft tumors treated with CCG-215022 significantly reduces tumor growth. CCG-215022-bound GRK5 shows disorder in the residues pertaining to the N-terminus, C-terminus and active site tether regions[41]. We show that a kinase deficient GRK5 mutant rescues the GRK5 loss-of-function growth phenotype. Based on this finding, it is possible that the functional domain of GRK5 that regulates RMS cell growth likely resides in one of these disordered regions. While additional testing to assess the toxicity profile of CCG-215022 in pre-clinical models is necessary, we have shown that inhibition of GRK5 is a promising therapeutic option for RMS patients.

With treatment options against RMS remaining relatively unchanged over last 3 decades, there remains a need for more effective therapeutic targets. From a comprehensive

siRNA library screen against the human kinome, we have identified GRK5 as a novel regulator of both RMS self-renewal and cell growth. Our functional characterization of GRK5 *in vitro* and *in vivo* demonstrates that GRK5 regulates ERMS cell growth in a kinase-independent manner and is essential for RMS self-renewal capacity. A GRK5 inhibitor, CCG-215022, recapitulates the loss-of-function effects of GRK5. Thus, our findings demonstrate the promise of GRK5 as a therapeutic target against RMS disease progression and relapse.

Material/Methods

siRNA kinome library screen

To identify potential candidate kinases that are important for the self-renewal of ERMS, we utilized the Quellos high-throughput screening core facility in the Institute of Stem Cell and Regenerative Medicine at the University of Washington to perform an siRNA library screen against the human kinome (714 kinases) in two different cell lines derived from ERMS (RD and 381T). Each cell line was transfected with a pool of 3 siRNAs against each kinase, along with control (scramble) siRNAs, in 384-well low attachment plates to induce sphere formation. The sphere assay was used as a surrogate *in vitro* assay for assessing the self-renewal capacity of tumor cell. The ATP-based Cell Titer Glo assay (Promega) was performed on the siRNA-treated adherent cells, and high-content imaging was performed at the Quellos core facility at day 5 post-siRNA transfection.

CRISPR/Cas9 gene targeting in human RMS cells

Single gene knockout was accomplished using lentiviral transduction of RMS cells with Cas9 expressing and gene-specific double gRNA constructs. Lentiviral transduced cells were placed under antibiotic selection and plated for assays 7 days later. Cloning of Cas9 and gRNA expression constructs was performed as described previously[36]. Overexpression constructs used in GRK5 functional experiments were amplified from cDNA generated from ERMS cancer cell RNA. Silent mutations to PAM sites were introduced to GRK5 overexpression constructs to generate Cas9 resistant GRK5 protein. RMS cells were then transduced with 3 separate viruses; Cas9 virus, dgRNA virus and GRK5 WT/KD overexpression virus. Domain mutations made to GRK5 to generate wildtype (WT) and kinase dead (KD) variants was done using Gibson cloning based off of previous studies[25].

The following gRNAs were used for targeting genes in human RMS cell lines:
GRK5: gRNA1- GGACCTGGTCTCCCAGACGG

gRNA2- GGAGCAGCCCTTTCTTGGG

NFAT1: gRNA1- GACGGAGTGATCTCGATCCG

gRNA2- GATCCCACAAGGCGAGTCCG

FES: gRNA1-GGCCGAGCTTCGTCTACTGG

gRNA2- GAGCCTGCTCATCCGGGAA

LTK: gRNA1- GCTGGCTCCAAGATACTAGG

gRNA2- GACCAGCGTGGTGGTGACCG

LYN: gRNA1- GTAGCCTTGTACCCCTATGA

gRNA2- GGAATGGCATACATCGAG

NME9: gRNA1- GACCTCGATCCTCATCTTC

gRNA2- GATGTCCTCGAAAAGTACAG

PIK3C2A: gRNA1- GCACAGGTTTATAACAAGC

gRNA2 - GGGGCGCTTGCTAATATTTT

Cell-based Assays

RMS cell growth was assessed via cell counts or an ATP-based luminescent cell viability assay, CellTiter-Glo (Promega, Madison, WI). Myogenic differentiation was performed following serum starvation of RMS cells in 2% horse serum/DMEM for 72 hours prior to fixation in 2% paraformaldehyde. Immunofluorescence against MF20 (myosin heavy chain) was then performed. Self-renewal was assessed by visual counts of rhabdospheres, induced in growth factors (EGF, bFGF, PDGF-A, PDGF-B) enriched neurobasal medium as previous described[42]. Apoptosis was assessed using a flow-cytometry based assay using the Annexin V, Alexa Fluor 647 conjugate (Life Technologies). Cell cycle analysis was done with flow cytometry on cells pulsed with EdU for 2 hours using the Click-iT EdU Alexa Fluor 647 Flow Cytometry Assay kit (Life Technologies, Carlsbad, CA).

Human Xenografts and Drug Treatment

All mouse experiments were approved by the University of Washington Subcommittee on Research Animal Care under IACUC protocol #4330-01. 6-7 immunocompromised NOD-

SCID IL2rg-/- (NSG) mice were xenografted via subcutaneous injections into the flanks with approximately 1-2x10^6 RMS cells (RH5 or 381T) suspended in Matrigel. At tumor onset, CCG-215022 (10mg/kg) or vehicle (DMSO) were given intraperitoneal every 3 days for up to 21 days or until tumors reached end point (750 mm^3). Tumor measurements were made with calipers every 3-4 days at tumor onset until tumors reached end point or at the end of drug treatment, whichever came first. For limiting dilution experiments, 6 NSG mice were given RMS cell injections (Rh5 or 381T) of either control or *GRK5* knock-out cells at either 2x10^3, 1x10^4, 5x10^4 dilutions in the same manner as previously described. Analysis of limiting dilution data was performed as previously described[43]. All mice were humanly euthanized for tumor tissue harvesting at the end of the experiment.

Immunohistochemistry and Immunofluorescence

The RMS tissue microarray was obtained from Seattle Children's Hospital. Immunohistochemistry was performed at the Histology and Imaging core facility at the University of Washington. Immunofluorescence was performed as previously described[29]. Duolink Proximity Ligation Assay (PLA) by Sigma Aldrich was used to visualize GRK5-NFAT1 activity. The following antibodies were used: rabbit polyclonal anti human mouse monoclonal anti human Ki-67, 1:100,(MIB1), Dako), Immunohistochemistry: GRK5 1:100 (N145/20) Abcam, Cambridge, MA), Immunofluorescence: GRK5 1:150, (N145/20), Abcam, Cambridge, MA), NFAT1 1:100, (D43B1), Cell Signaling Technology, Danvers, MA)

Western Blots

Cell lysates from RMS cells were counted and lysed in RIPA buffer (ThermoFisher #89900) with protease inhibitors plus 2x sample buffer (100mM Tris pH6.8, 4%SDS, 20% glycerol). Equal amounts of protein lysates were electrophoresed on a 4-15% gradient SDS-polyacrylamide gel (BioRad, Hercules, CA) and fast transferred to Immun-Blot PVDF membranes (BioRad, Hercules, CA) using the Turbo-Blot Transfer system (BioRad, Hercules, CA) We used the following antibodies: GRK5 (N145/20) 1:100 Abcam, Cambridge, MA), GAPDH (14C10) 1:2500 (Cell Signaling Technology, Danvers, MA), Cleaved Caspase 3 (Asp175) 1:200 (Cell Signaling Technology, Danvers, MA). Goat anti-mouse or anti-rabbit HRP conjugated IgG secondary antibodies from Santa Cruz Biotechnology. Membranes were blocked in 5% milk in Tris Buffered Saline plus Tween (20mM Tris, 136mM NaCl, 1% Tween 20, pH 7.4 TBST). Quantitative analysis of Western blot images was performed on ImageJ.

Human Expression Data Analysis

RNA was collected from human cell lines lysates (myoblasts, NHDF, 381T, SMSCTR, RH30, RH5) using Qiagen RNeasy Plus Mini Kit. cDNA was then generated using High Capacity cDNA Reverse Transcription Kit from Applied Biosystems. RT-PCR reactions were then run with iTaq Universal SYBR Green mix on a CFX Connect Real Time System (BioRad, Hercules, CA). RT-PCR primers used are listed below:

GRK5 FWD – GTCTGTCCACGAGTACCTGA

REV – CAGGCATACATTTTACCCGT

NFAT1 FWD - ACGAGCTTGACTTCTCCACC

REV - TGCATTCGGCTCTTCTTCGT

Statistics

Mann-Whitney statistical test was run on drug treated RMS tumor mouse experiments to assess statistical significance in differences between experimental and control. Two tailed Student's t-test was applied when appropriate.

Figures

FIGURE 1

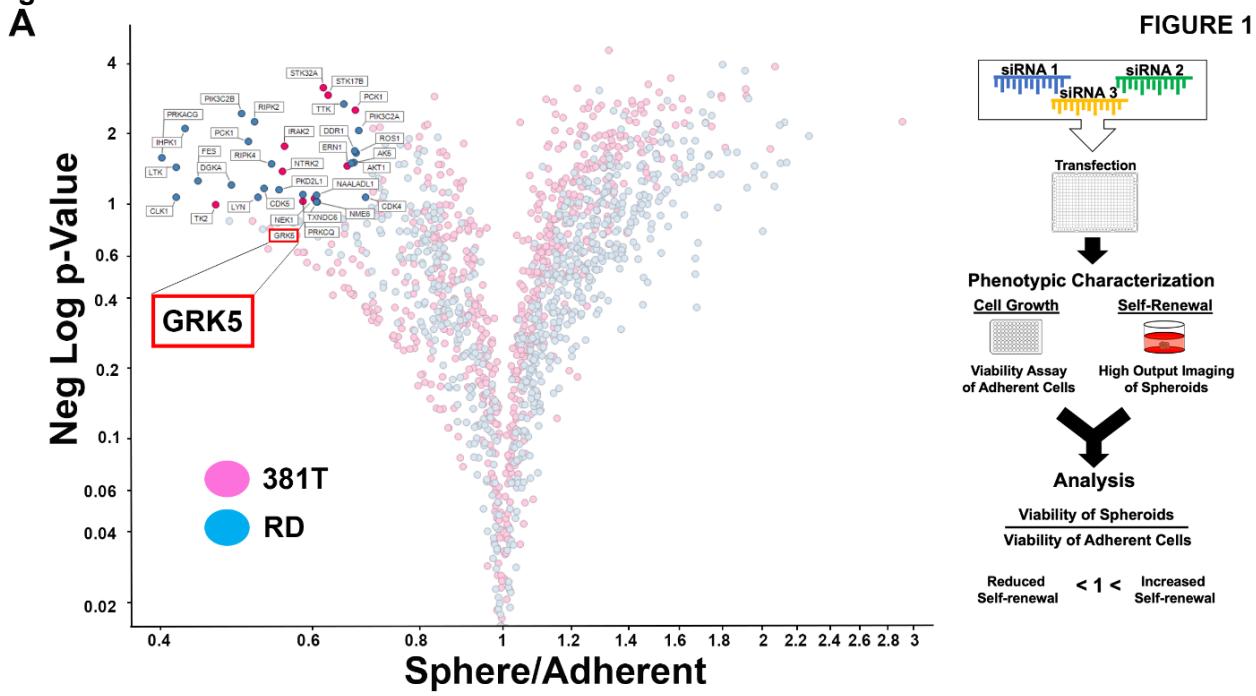

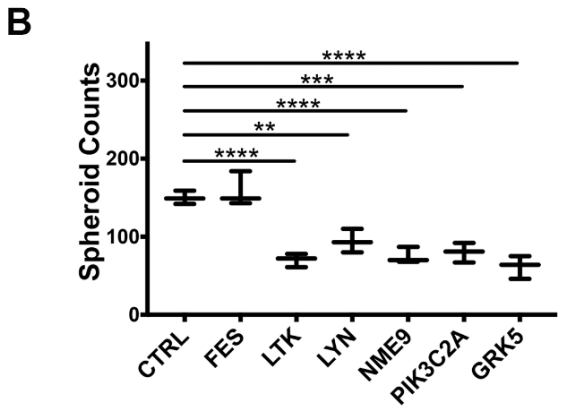

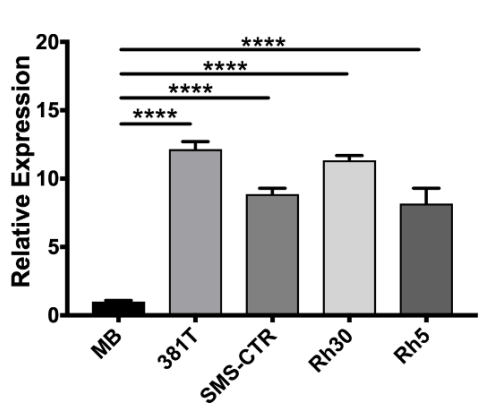

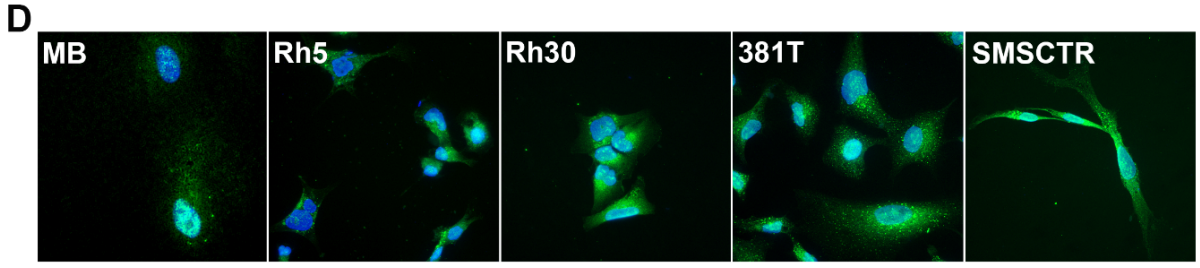

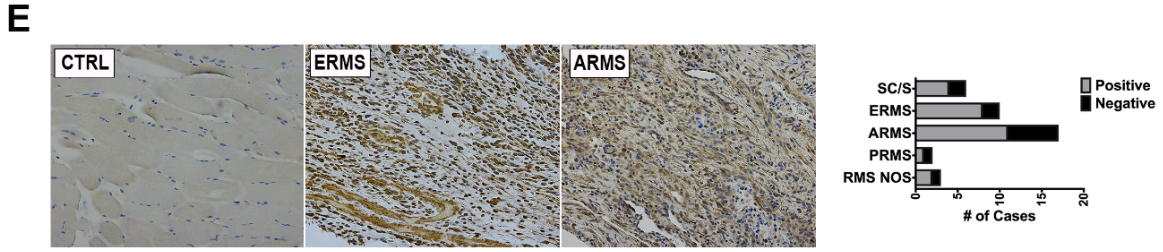

FIGURE 2

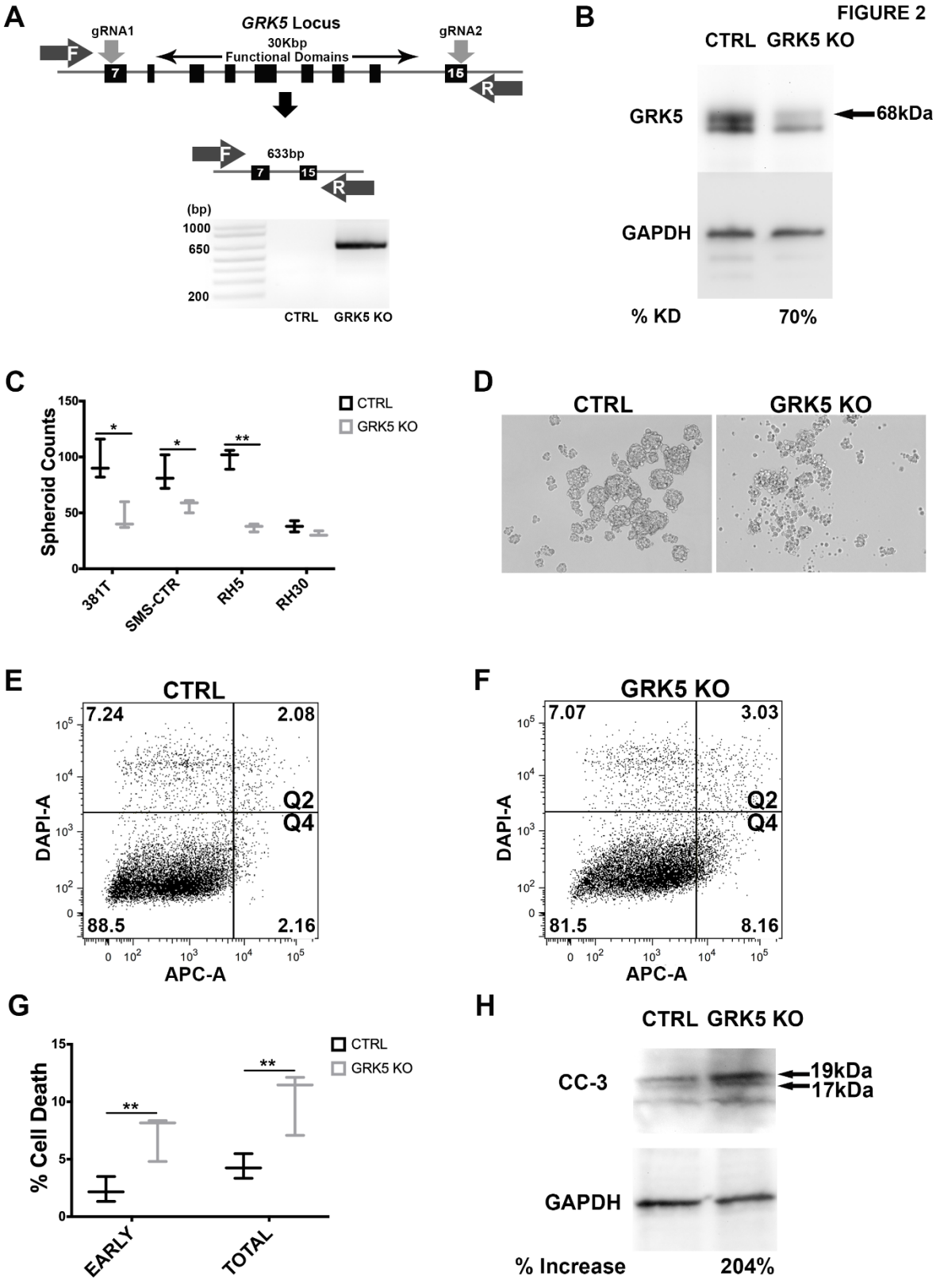
A
gRNA1
GRK5 Locus
30Kbp
Functional Domains
gRNA2
F
7
16
R
633bp
15
(bp)
1000
650
200
CTRL
GRK5 KO
B
CTRL GRK5 KO
GRK5
68kDa
GAPDH
% KD
70%
C
Spheroid Counts
CTRL
GRK5 KO
381T
SMS-CTR
RH5
RH30
D
CTRL
GRK5 KO
E
CTRL
7.24
2.08
Q2
Q4
88.5
2.16
DAPI-A
APC-A
F
GRK5 KO
7.07
3.03
81.5
8.16
G
% Cell Death
EARLY
TOTAL
H
CTRL GRK5 KO
CC-3
19kDa
17kDa
GAPDH
% Increase
204%

FIGURE 3

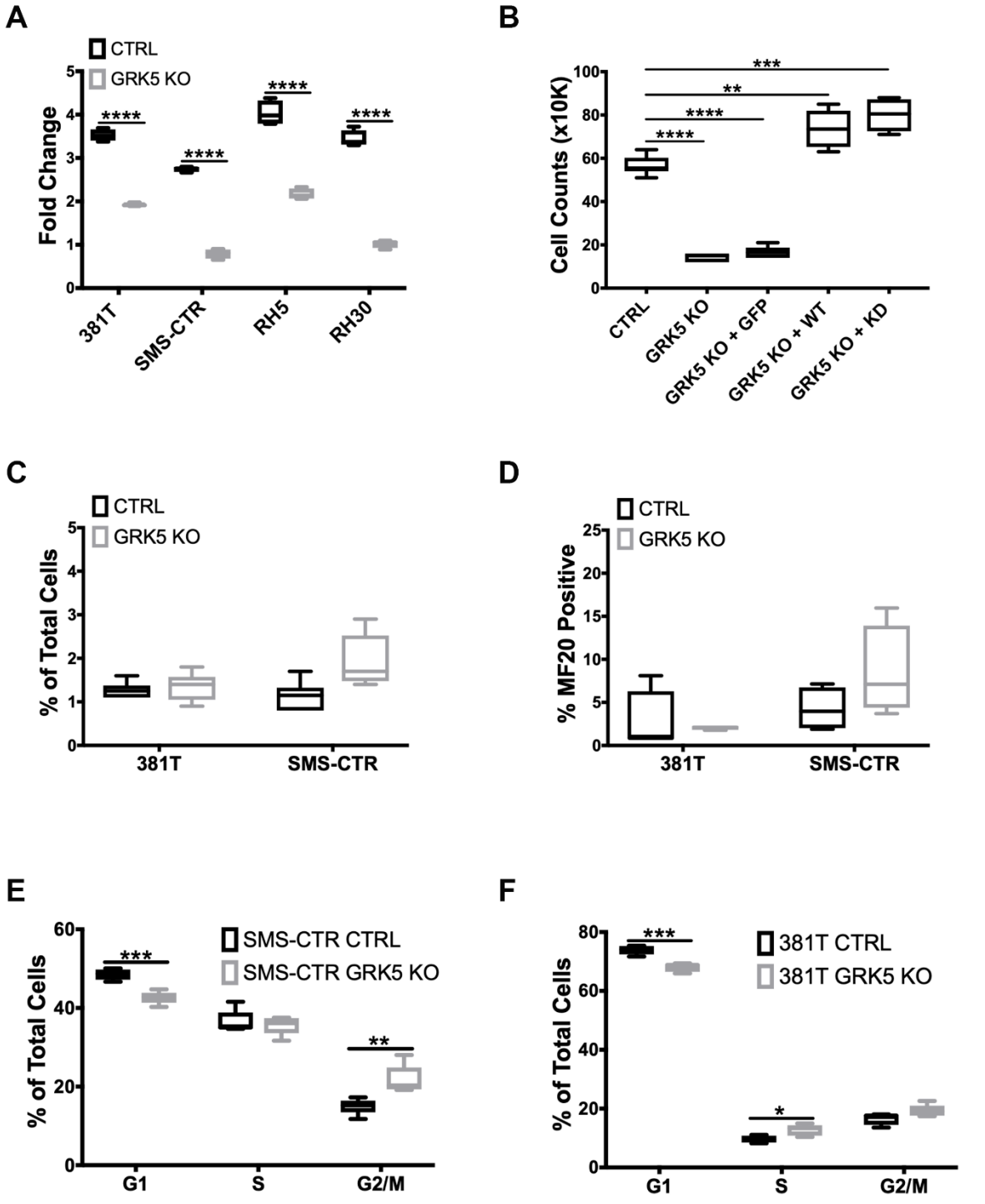
A
CTRL
GRK5 KO
Fold Change
****
381T
SMS-CTR
RH5
RH30
B
Cell Counts (x10K)
***
**
****
CTRL
GRK5 KO
GRK5 KO + GFP
GRK5 KO + WT
GRK5 KO + KD
C
% of Total Cells
381T
SMS-CTR
D
% MF20 Positive
E
SMS-CTR CTRL
SMS-CTR GRK5 KO
G1
S
G2/M
F
381T CTRL
381T GRK5 KO
*

FIGURE 4

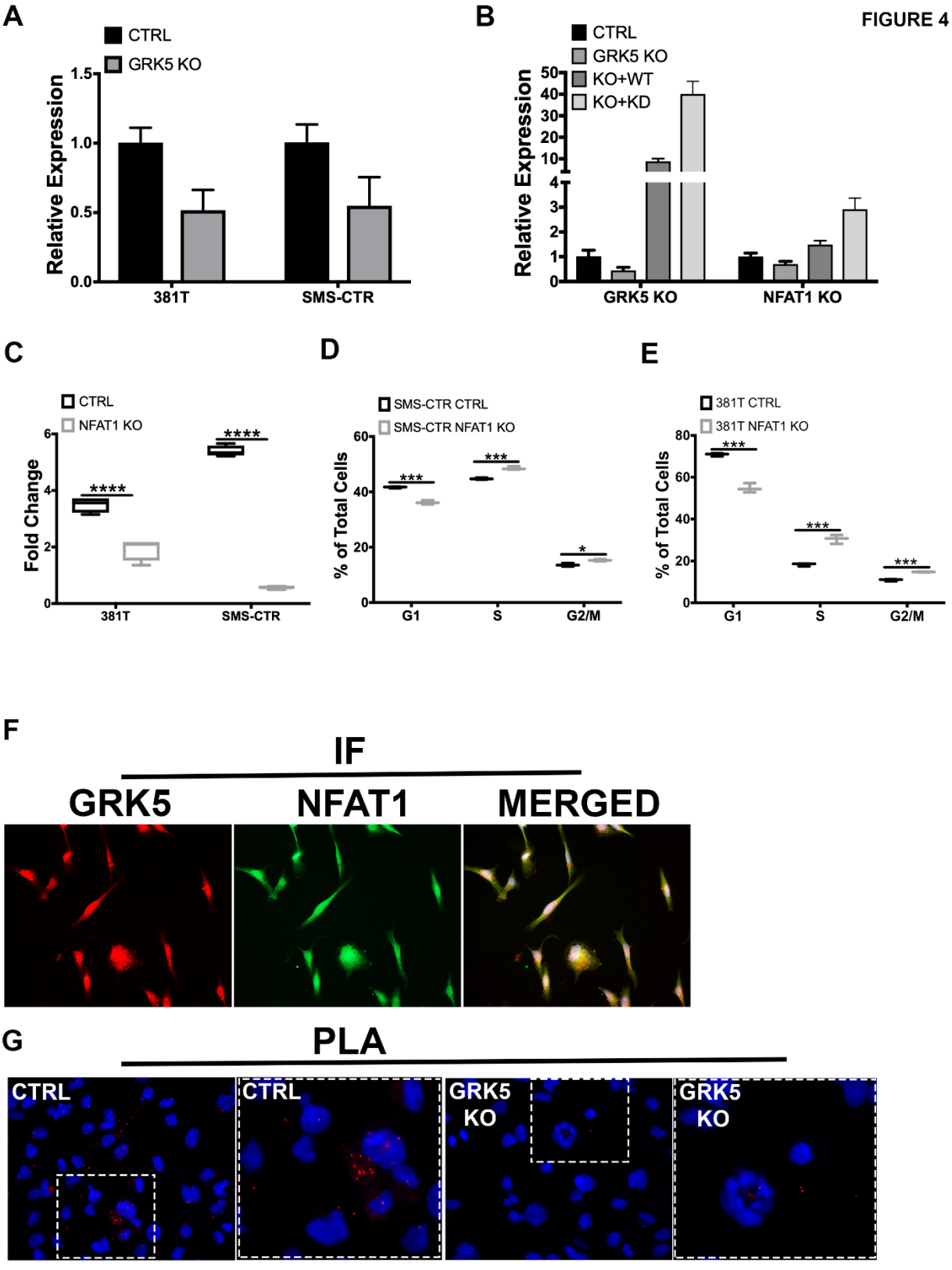
A
CTRL
GRK5 KO
Relative Expression
1.5
1.0
0.5
0.0
381T
SMS-CTR
B
CTRL
GRK5 KO
KO+WT
KO+KD
Relative Expression
50
40
30
20
10
4
3
2
1
0
GRK5 KO
NFAT1 KO
C
CTRL
NFAT1 KO
Fold Change
6
4
2
0
****
****
381T
SMS-CTR
D
SMS-CTR CTRL
SMS-CTR NFAT1 KO
% of Total Cells
60
40
20
0
***
***
*
G1
S
G2/M
E
381T CTRL
381T NFAT1 KO
% of Total Cells
80
60
40
20
0
***
***
***
G1
S
G2/M
F
IF
GRK5
NFAT1
MERGED
G
PLA
CTRL
CTRL
GRK5 KO
GRK5 KO

FIGURE 5

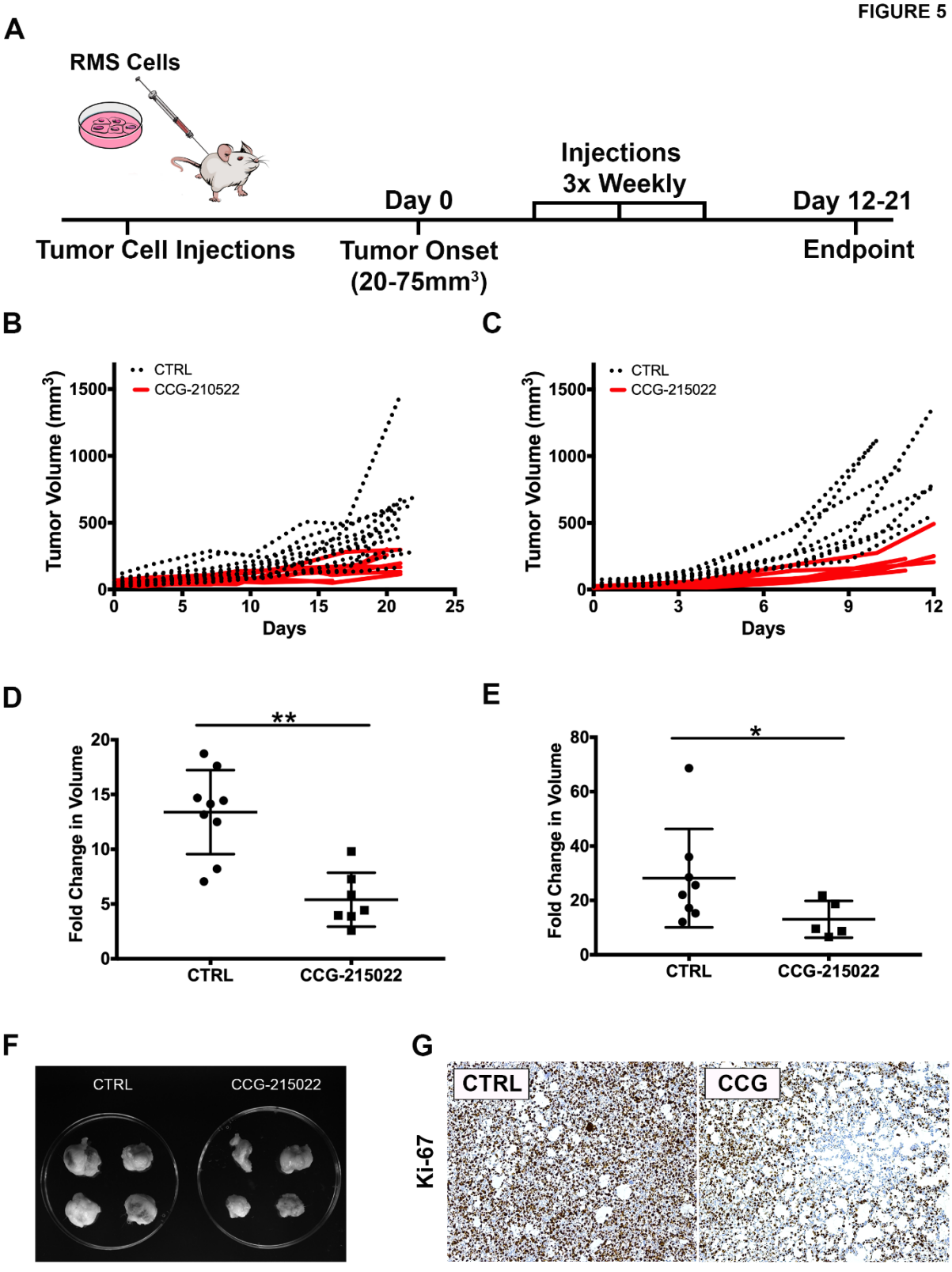
A
RMS Cells
Injections
3x Weekly
Day 0
Day 12-21
Tumor Cell Injections
Tumor Onset
(20-75mm3)
Endpoint
B
CTRL
CCG-210522
Tumor Volume (mm3)
Days
C
CTRL
CCG-215022
Tumor Volume (mm3)
Days
D
Fold Change in Volume
CTRL
CCG-215022
E
Fold Change in Volume
CTRL
CCG-215022
F
CTRL
CCG-215022
G
CTRL
CCG
Ki-67

Table 1. Summary of limiting dilution experiments

381T		
Cell No.	Control	GRK5 KO
50,000	6 of 6	6 of 6
10,000	6 of 6	5 of 6
2,000	5 of 6	3 of 6
TPC frequency	1115	4373*
95% CI	414-3002	1927-9922

* p = 0.0353

Rh5		
Cell No.	Control	GRK5 KO
50,000	6 of 6	6 of 6
10,000	6 of 6	4 of 6
2,000	5 of 6	3 of 6
TPC frequency	1115	6230**
95% CI	414-3002	2731-14214

** p = 0.00739

Sup. Figure 1

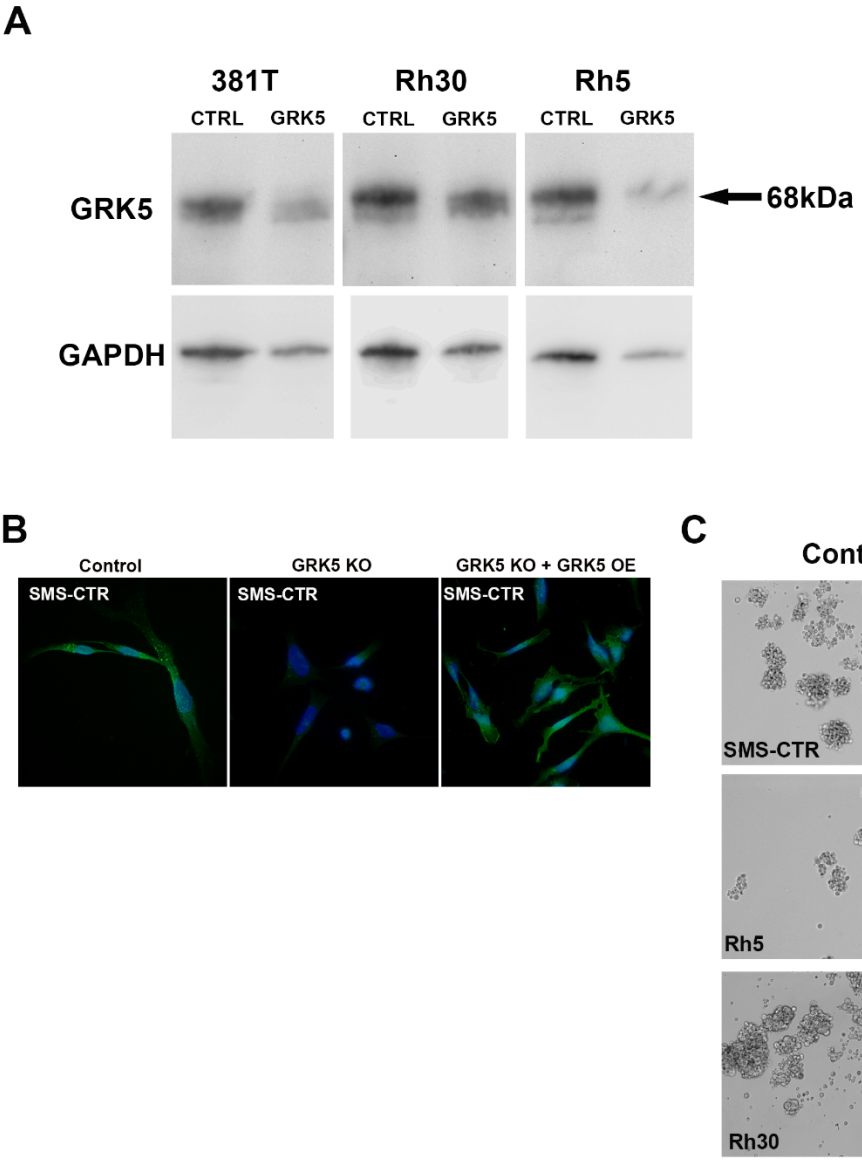
A
381T
Rh30
Rh5
CTRL
GRK5
CTRL
GRK5
CTRL
GRK5
GRK5
68kDa
GAPDH
B
Control
GRK5 KO
GRK5 KO + GRK5 OE
SMS-CTR
SMS-CTR
SMS-CTR
C
Control
GRK5 KO
SMS-CTR
SMS-CTR
Rh5
Rh5
Rh30
Rh30

Sup. Figure 2

A

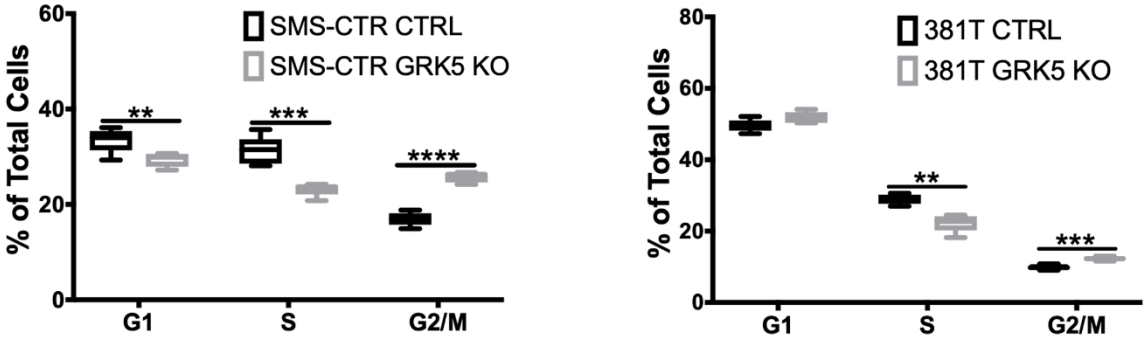

Figure Legends

Figure 1. An siRNA library screen of the human kinome identifies GRK5 as a novel regulator of ERMS self-renewal. (A) Volcano plot illustrating candidate kinases identified from an siRNA library screen against the human kinome in ERMS cancer cell lines (381T and RD). Significant hits are indicated as having a p-value (Y-axis) of < 0.05 and a Sphere/Adherent viability ratio (X-axis) of < 1.0. Diagram on the right illustrates workflow and analysis used in the siRNA library screen. GRK5 is highlighted as being a candidate kinase identified from the screen. (B) Spheroid counts to assess self-renewal capacity was performed on CRISPR/Cas9 mediated knockout of top 6 candidate kinases (*FES, LTK, LYN, NME9, PIK3C2A, GRK5)*. Error bars represent standard deviation of 3 technical replicates from an individual experiment that was repeated 3 times. (C) RT-PCR analysis of *GRK5* expression in human myoblasts (MB) compared to a panel of RMS cancer cell lines (381T, SMS-CTR, RH30, RH5). Error bars represent standard deviation of 3 technical replicates from an individual experiment that was repeated 3 times. (D) Immunofluorescence images showing GRK5 staining in MB and RMS cancer cell lines (381T, SMS-CTR, Rh30, Rh5). (E) Immunohistochemistry of GRK5 in skeletal muscle control (CTRL) and representative primary ERMS and ARMS tumors. Summary of IHC for GRK5 in primary RMS tumors spotted on a tissue microarray is shown on the right. Spindle cell RMS (SC/S), embryonal RMS (ERMS), alveolar RMS (ARMS), pleomorphic RMS (PRMS), RMS not otherwise specified (RMS NOS). Two-tailed t-test; ** = p <0.01; *** = p < 0.001, **** = p < 0.0001.

Figure 2. GRK5 regulates self-renewal of both ERMS and ARMS. (A) Schematic demonstrating CRISPR/Cas9 targeting of *GRK5*. Two gRNAs were designed to flank the region encoding functional domains of GRK5. Genetic disruption was confirmed via PCR amplification of the deleted *GRK5* domain followed by Western analysis of depleted protein (B). Spheroid counts to assess self-renewal (C). Representative images (D) of control (CTRL) and *GRK5* knockout (*GRK5* KO) spheroids are from 381T cells. Results shown are of 3 replicates from one of 3 independent experiments. (E-G) Annexin V Flow cytometry to assess the extent of apoptosis (quadrants 2 and 4) in SMS-CTR *GRK5* knockout spheroid cells (*GRK5* KO) compared to Cas9 only controls (CTRL). (H) Western analysis of cleaved Caspase 3 (CC3) comparing SMS-CTR *GRK*5 KO spheroids to controls (CTRL). Error bar represents standard deviation and two-tailed t-test (C, G) was performed on 3 replicates from one of three independent experiments. * = p <0.05; ** = p < 0.01.

Figure 3. GRK5 regulates ERMS cell growth in a kinase-independent manner and is involved in regulating cell cycle progression. (A) Cell Titer Glo viability assessment of *GRK5* knockout (*GRK5* KO) compared to controls (CTRL) in a panel of RMS cancer cell lines (381T, SMS-CTR, RH5, RH30). Data shown are 4 replicates from one of 3 independent experiments. Two-tailed t-test, **** = $p < 0.0001$. (B) Summary of cell count data from rescue experiment to demonstrate specificity of the *GRK5* KO growth phenotype. SMS-CTR cells were transduced with lentivirus expressing either Cas9 only (CTRL), Cas9 with *GRK5* gRNAs (*GRK5* KO), Cas9 with *GRK5* gRNAs and GFP overexpression *(GRK5* KO + GFP), Cas9 with *GRK5* gRNAs and Cas9 resistant, wildtype GRK5 (*GRK5* KO + WT), Cas9 with *GRK5* gRNAs and Cas9 resistant, kinase dead GRK5 (*GRK5* KO + KD). Data shown are 6 replicates from one of three independent experiments. Two-tailed t-test, ** = $p < 0.01$, *** = $p < 0.001$, (C) Annexin V Flow cytometry to assess apoptosis. (D) Quantitation of immunofluorescence (IF) against MF20 in RMS cells with *GRK5* knockout (*GRK5* KO) and Cas9 only controls (CTRL). (E-F) EdU flow cytometry-based cell cycle analysis of SMS-CTR and 381T cells with Cas9 only as control (CTRL) or *GRK5* knockout (*GRK5* KO). Data shown are from 6 independent experiments. Two-tailed t-test, * = $p < 0.05$, ** = $p < 0.01$, *** = $p < 0.001$, **** = $p < 0.0001$.

Figure 4. *NFAT1* expression is regulated by GRK5 in a kinase-independent manner. (A) Quantitative RT-PCR analysis of *NFAT1* expression in ERMS cells (381T and SMS-CTR) with Cas9 only control (CTRL) and *GRK5* knockout (*GRK5* KO). (B) RT-PCR analysis of *GRK5* and *NFAT1* expression in 381T cells following GRK5 rescue with wild-type and domain mutants. 381T cells were transduced with lentivirus expressing Cas9 only (CTRL), Cas9 with *GRK5* gRNAs (*GRK5* KO), Cas9 with *GRK5* gRNAs and Cas9 resistant, wildtype GRK5 (*GRK5* KO + WT), Cas9 with *GRK5* gRNAs and Cas9 resistant, kinase dead GRK5 (*GRK5* + KD). (C) Cell Titer Glo viability assessment of *NFAT1* knockout (*NFAT1* KO) compared to Cas9 only control (CTRL) in ERMS cancer cell lines (381T, SMS-CTR). Data shown are 4 replicates from one of 3 independent experiments, two-tailed t-test, **** = $p < 0.0001$. (D-E) EdU flow cytometry-based cell cycle analysis of 381T and SMS-CTR cells with Cas9 only as control (CTRL) or *NFAT1* knockout (*NFAT1* KO). Data shown are of 3 replicates from one of 3 independent experiments. Two-tailed t-test, * = $p < 0.05$, *** = $p < 0.001$. (F) Immunofluorescence images showing GRK5 (red) and NFAT1 (green) staining in 381T cells, with overlay of both channels (yellow). (G) Proximity Ligation Assay (PLA) to assess GRK5-NFAT1 protein interaction in GRK5 wildtype (CTRL) and *GRK5*-knockout 381T cells. Red dots represent points of GRK5-NFAT1 close proximity

Figure 5. Treatment of RMS tumor with CCG-215022, a GRK5 inhibitor, reduces tumor growth *in vivo.* (A) Schematic of the RMS xenograft in NSG mice experiment. (B-C) Summary of 381T (B) and Rh5 (C) daily tumor growth following CCG-215022 or DMSO control (CTRL) treatment. (D-E) Summary of 381T (D) and Rh5 (E) tumor volume fold change following CCG-215022 or DMSO control (CTRL) treatment. Each data point represents one mouse with error bars representing standard deviation. * = $p < 0.05$, ** = $p < 0.01$ (Mann-Whitney Statistical Test). (F) Representative images of Rh5 tumors harvested from DMSO vehicle control (CTRL) treated and CCG-215022 treated mice at the end of treatment period. (G) Representative images of Immunohistochemistry for Ki67 on DMSO control (CTRL) and CCG-215022 (CCG)-treated tumors.

Table 1. Summary of limiting dilution experiments.

381T and Rh5 RMS cells were injected into NSG mice at limiting dilutions of $2x10^3$, $1x10^4$, $5x10^4$ cells. TPC frequency was calculated as previously described. Confidence interval and statistics was performed on an n = 6 mice per control and GRK5 KO. * = $p < 0.05$; ** = $p < 0.01$.

Supplemental Figures

Figure S1. Confirmation of GRK5 knockdown and spheroid images. (A) Western analysis demonstrating GRK5 protein depletion in a panel of RMS cell lines (381T, Rh30, Rh5) with Cas9-mediated targeted disruption of *GRK5*. (B) Immunofluorescence images demonstrating the specificity of the GRK5 antibody. SMS-CTR cells with knockout (GRK5 KO) shows reduced staining compared to Cas9-only control (CTRL) cells and *GRK5* knockout cells rescued with Cas9-resistant wild-type GRK5 overexpression (GRK5 KO+GRK5 OE). (C) Representative images of spheroid formation comparing control (CTRL) and *GRK5* knockout (*GRK5* KO) in RMS cell lines (SMS-CTR, Rh5, Rh30).

Figure S2. Altered cell cycle progression day 6 following CRISPR/Cas9-mediated *GRK5* targeting. (A) EdU flow cytometry-based cell cycle analysis of SMS-CTR and 381T cells with Cas9 only control (CTRL) or *GRK5* knockout (*GRK5* KO). Data shown are from 5 independent experiments. Two-tailed t-test, ** = $p < 0.01$, *** = $p < 0.001$, **** = $p < 0.0001$.

References

1. Shern, J. F. *et al.* Comprehensive genomic analysis of rhabdomyosarcoma reveals a landscape of alterations affecting a common genetic axis in fusion-positive and fusion-negative tumors. *Cancer Discov* **4**, 216–231 (2014).

2. Barr, F. G. *et al.* Rearrangement of the PAX3 paired box gene in the paediatric solid tumour alveolar rhabdomyosarcoma. *Nat Genet* **3**, 113–117 (1993).

3. Pappo, A. S. *et al.* Survival After Relapse in Children and Adolescents With Rhabdomyosarcoma: A Report From the Intergroup Rhabdomyosarcoma Study Group. *JCO* **17**, 3487–3493 (1999).

4. Kaur, G. *et al.* G-protein coupled receptor kinase (GRK)-5 regulates proliferation of glioblastoma-derived stem cells. *Journal of Clinical Neuroscience* **20**, 1014–1018 (2013).

5. Lawson, D. A. *et al.* Single-cell analysis reveals a stem-cell program in human metastatic breast cancer cells. *Nature* **526**, 131–135 (2015).

6. Jahchan, N. S. *et al.* Identification and targeting of long-term tumor-propagating cells in small cell lung cancer. *Cell Rep* **16**, 644–656 (2016).

7. Kreso, A. & Dick, J. E. Evolution of the Cancer Stem Cell Model. *Cell Stem Cell* **14**, 275–291 (2014).

8. Ignatius, M. S. *et al.* In Vivo Imaging of Tumor-Propagating Cells, Regional Tumor Heterogeneity, and Dynamic Cell Movements in Embryonal Rhabdomyosarcoma. *Cancer Cell* **21**, 680–693 (2012).

9. Walter, D. *et al.* CD133 Positive Embryonal Rhabdomyosarcoma Stem-Like Cell Population Is Enriched in Rhabdospheres. *PLOS ONE* **6**, e19506 (2011).

10. Gross, S., Rahal, R., Stransky, N., Lengauer, C. & Hoeflich, K. P. Targeting cancer with kinase inhibitors. *J Clin Invest* **125**, 1780–1789 (2015).

11. Hanahan, D. & Weinberg, R. A. Hallmarks of Cancer: The Next Generation. *Cell* **144**, 646–674 (2011).

12. Roskoski, R. Properties of FDA-approved small molecule protein kinase inhibitors. *Pharmacological Research* **144**, 19–50 (2019).

13. Yohe, M. E. *et al.* MEK inhibition induces MYOG and remodels super-enhancers in RAS-driven rhabdomyosarcoma. *Science Translational Medicine* **10**, eaan4470 (2018).

14. Stewart, E. *et al.* Identification of Therapeutic Targets in Rhabdomyosarcoma through Integrated Genomic, Epigenomic, and Proteomic Analyses. *Cancer Cell* **0**, (2018).

15. Chen, E. Y. *et al.* Glycogen synthase kinase 3 inhibitors induce the canonical WNT/β-catenin pathway to suppress growth and self-renewal in embryonal rhabdomyosarcoma. *Proc Natl Acad Sci U S A* **111**, 5349–5354 (2014).

16. Willets, J. M., Challiss, R. A. J. & Nahorski, S. R. Non-visual GRKs: are we seeing the whole picture? *Trends in Pharmacological Sciences* **24**, 626–633 (2003).

17. Islam, K. N., Bae, J.-W., Gao, E. & Koch, W. J. Regulation of Nuclear Factor κB (NF-κB) in the Nucleus of Cardiomyocytes by G Protein-coupled Receptor Kinase 5 (GRK5). *J. Biol. Chem.* **288**, 35683–35689 (2013).

18. Philipp, M., Berger, I. M., Just, S. & Caron, M. G. Overlapping and Opposing Functions of G Protein-coupled Receptor Kinase 2 (GRK2) and GRK5 during Heart Development. *J Biol Chem* **289**, 26119–26130 (2014).

19. Zhang, Y. *et al.* Nuclear Effects of GRK5 on HDAC5-regulated Gene Transcription in Heart Failure. *Circ Heart Fail* **4**, 659–668 (2011).

20. Hullmann, J. E. *et al.* GRK5-Mediated Exacerbation of Pathological Cardiac Hypertrophy Involves Facilitation of Nuclear NFAT Activity. *Circ Res* **115**, 976–985 (2014).

21. Lessel, D. *et al.* The analysis of heterotaxy patients reveals new loss-of-function variants of GRK5. *Scientific Reports* **6**, 33231 (2016).

22. Martini, J. S. *et al.* Uncovering G protein-coupled receptor kinase-5 as a histone deacetylase kinase in the nucleus of cardiomyocytes. *Proc Natl Acad Sci U S A* **105**, 12457–12462 (2008).

23. Jiang, L.-P. *et al.* GRK5 functions as an oncogenic factor in non-small-cell lung cancer. *Cell Death Dis* **9**, (2018).

24. Kim, J. I., Chakraborty, P., Wang, Z. & Daaka, Y. G-Protein Coupled Receptor Kinase 5 Regulates Prostate Tumor Growth. *The Journal of Urology* **187**, 322–329 (2012).

25. Johnson, L. R., Robinson, J. D., Lester, K. N. & Pitcher, J. A. Distinct Structural Features of G Protein-Coupled Receptor Kinase 5 (GRK5) Regulate Its Nuclear Localization and DNA-Binding Ability. *PLOS ONE* **8**, e62508 (2013).

26. Sorriento, D. *et al.* The Amino-Terminal Domain of GRK5 Inhibits Cardiac Hypertrophy through the Regulation of Calcium-Calmodulin Dependent Transcription Factors. *Int J Mol Sci* **19**, (2018).

27. Macian, F. NFAT proteins: key regulators of T-cell development and function. *Nature Reviews Immunology* **5**, nri1632 (2005).

28. Pastrana, E., Silva-Vargas, V. & Doetsch, F. Eyes Wide Open: A Critical Review of Sphere-Formation as an Assay For Stem Cells. *Cell Stem Cell* **8**, 486–498 (2011).

29. Phelps, M. P., Bailey, J. N., Vleeshouwer-Neumann, T. & Chen, E. Y. CRISPR screen identifies the NCOR/HDAC3 complex as a major suppressor of differentiation in rhabdomyosarcoma. *PNAS* **113**, 15090–15095 (2016).

30. Watari, K., Nakaya, M. & Kurose, H. Multiple functions of G protein-coupled receptor kinases. *J Mol Signal* **9**, 1 (2014).

31. BAUMGART, S. *et al.* Restricted Heterochromatin Formation Links NFATc2 Repressor Activity With Growth Promotion in Pancreatic Cancer. *Gastroenterology* **142**, 388-98.e1–7 (2012).

32. Baumgart, S. *et al.* Inflammation induced NFATc1-STAT3 Transcription Complex Promotes Pancreatic Cancer initiation by KrasG12D. *Cancer Discov* **4**, 688–701 (2014).

33. Chen, X. *et al.* G-protein-coupled Receptor Kinase 5 Phosphorylates p53 and Inhibits DNA Damage-induced Apoptosis. *J Biol Chem* **285**, 12823–12830 (2010).

34. Michal, A. M. *et al.* G Protein-coupled Receptor Kinase 5 Is Localized to Centrosomes and Regulates Cell Cycle Progression. *J Biol Chem* **287**, 6928–6940 (2012).

35. Ognjanovic, S. *et al.* Low Prevalence of TP53 Mutations and MDM2 Amplifications in Pediatric Rhabdomyosarcoma. *Sarcoma* https://www.hindawi.com/journals/sarcoma/2012/492086/ (2012) doi:10.1155/2012/492086.

36. Hinson, A. R. P. *et al.* Human Rhabdomyosarcoma Cell Lines for Rhabdomyosarcoma Research: Utility and Pitfalls. *Front Oncol* **3**, (2013).

37. Mognol, G. P., Carneiro, F. R. G., Robbs, B. K., Faget, D. V. & Viola, J. P. B. Cell cycle and apoptosis regulation by NFAT transcription factors: new roles for an old player. *Cell Death Dis* **7**, e2199 (2016).

38. Saygin, C., Matei, D., Majeti, R., Reizes, O. & Lathia, J. D. Targeting Cancer Stemness in the Clinic: From Hype to Hope. *Cell Stem Cell* **24**, 25–40 (2019).

39. Homan, K. T., Wu, E., Cannavo, A., Koch, W. J. & Tesmer, J. J. G. Identification and Characterization of Amlexanox as a G Protein-Coupled Receptor Kinase 5 Inhibitor. *Molecules* **19**, 16937–16949 (2014).

40. Liu, Y. *et al.* Amlexanox, a selective inhibitor of IKBKE, generates anti-tumoral effects by disrupting the Hippo pathway in human glioblastoma cell lines. *Cell Death & Disease* **8**, e3022 (2017).

41. Homan, K. T. *et al.* Crystal Structure of G Protein-Coupled Receptor Kinase 5 in Complex with a Rationally Designed Inhibitor. *J. Biol. Chem.* jbc.M115.647370 (2015) doi:10.1074/jbc.M115.647370.

42. Vleeshouwer-Neumann, T. *et al.* Histone Deacetylase Inhibitors Antagonize Distinct Pathways to Suppress Tumorigenesis of Embryonal Rhabdomyosarcoma. *PLoS One* **10**, (2015).

43. Hu, Y. & Smyth, G. K. ELDA: Extreme limiting dilution analysis for comparing depleted and enriched populations in stem cell and other assays. *Journal of Immunological Methods* **347**, 70–78 (2009).

Chapter 3: HDAC6 promotes self-renewal and migration/invasion of rhabdomyosarcoma

AUTHORS: Thao Q. Pham[1], Kristin Robinson[1], Lin Xu[2,3], Stephen X. Skapek[2], Eleanor Y. Chen[1]

1. Department of Pathology, University of Washington, Seattle, WA

2. Department of Pediatrics,

3. Quantitative Biomedical Research Center, Department of Population & Data Sciences, University of Texas Southwestern Medical Center, Dallas, TX

Introduction

Rhabdomyosarcoma (RMS) is a devastating pediatric sarcoma that displays morphological and molecular evidence for incomplete myogenic differentiation. RMS is roughly divided into two major subtypes by histologic features, embryonal (ERMS) and alveolar (ARMS). Genetically, ERMS is characterized by mutations in the receptor tyrosine kinase/RAS/PIK3CA axis found in at least 90% of cases[1], and most ARMS cases harbor the PAX3 (or PAX7)-FOXO1 fusion transcript[2]. Despite the genetic differences, the prognosis for relapsed or metastatic disease remains poor regardless of the subtype. Effective targeted therapy is lacking due to our poor understanding of events leading to relapse or metastasis of RMS.

Several studies have shed some light on some of the genes and pathways that contribute to the metastatic potential of RMS. For example, Hepatocyte Growth Factor (HGF) and Stromal-derived Factor -1 (SDF-1) regulate metastatic behavior of cMet-positive RMS cells by directing them to the lymph nodes and the bone marrow[3], and downregulation of the MET-CXCR4 axis decreases the migration of RMS cells in response to the SDF-1 or HGF gradients in vitro[4]. Deficiency of tp53 in a conserved zebrafish model of ERMS increases the metastatic potential of ERMS cells[5]. Additional targets involved in the signaling pathways such as IL-4R and Plexin-A1 have also been shown to promote migratory and metastatic capacity of RMS cells[6,7]. However, the cellular and molecular mechanisms leading to invasion and metastasis of RMS cells remain to be elucidated. Specifically, the molecular players involved in altering the cytoskeletal dynamics to orchestrate RMS tumor cell invasion and metastasis remain to be identified and characterized.

Cancer stemness is mainly characterized by the self-renewal capacity of cancer cells to give rise to progeny cells that recapitulate the cancer heterogeneity[8]. The therapeutic potential of targeting cancer stem cells in solid tumors (e.g. skin squamous cell carcinoma, colorectal cancer and non-small cell lung cancer) has been demonstrated in a variety of pre-clinical animal models[9-11]. The inhibitors against several pathways involved in regulating the maintenance and survival of cancer stem cells (e.g. the Wnt , Notch and Hedgehog pathways) are in various phases of clinical trials[12,13]. However, the insight into the genes and pathways that regulate the stemness of RMS remains limited. Molecular markers such as Myf5, a marker for activated muscle satellite cells, and CD133, a transmembrane glycoprotein, have been used to enrich for tumor propagating cells in pre-clinical models of RMS[14,15]. Canonical and non-canonical Wnt pathways and TP53 have been shown to modulate the self-renewal capacity of RMS tumor-propagating cells[5,16,17]. Further investigation in preclinical models is necessary to identify

additional druggable targets against the cancer stemness of RMS and determine the therapeutic benefit of targeting cancer stemness in RMS.

In our previous CRISPR screen of the Histone Deacetylases (HDACs), HDAC6 is among the selected HDACs that are essential for RMS tumor cell growth[18]. Unlike the other HDACs, HDAC6 predominantly exerts its function in the cytoplasm and has been shown to interact with substrates such as Heat Shock Protein 90 (HSP90), Extracellular signal-related Kinase 1 (ERK1), KRAS, Tubulin and Cortactin to regulate diverse cellular processes such as cell migration, adhesion and growth in several normal and neoplastic cell types[19-23]. HDAC6 has been shown to either promote or suppress cancer cell invasion and metastasis depending on the cancer cell type[24,25]. Besides the studies on the role of HDAC6 in regulating the maintenance of glioma stem cells[26,27], there is limited knowledge on the function of HDAC6 in regulating self-renewal capacity of cancer cells.

In this study, we investigate the function of HDAC6 in various RMS features utilizing both in vitro and in vivo functional assays and demonstrate that HDAC6 is essential for RMS cell growth, migration/invasion and self-renewal. RAC1, a Rho GTPase, is a key player in mediating HDAC6 function in regulating RMS cell migration/invasion. High expression of RAC1 correlates with poor clinical survival of RMS patients. Overall, targeting the HDAC6-RAC1 axis may have significant therapeutic benefits for RMS patients.

Results

Expression of HDAC6 in RMS

We first assessed expression of HDAC6 in primary human RMS samples by immunohistochemistry. HDAC6 expression was detected primarily in the cytoplasm at variable intensity levels in most cases of ARMS (11 of 11) and ERMS (6 of 7) (Fig. 1 A-F). In contrast, five cases of pediatric muscle did not express HDAC6 (Fig. 1F). A panel of ERMS (RD and SMS-CTR) and ARMS cell lines (Rh5 and Rh30) also showed cytoplasmic and perinuclear expression of HDAC6 by immunofluorescence (Fig. 1 G-J). Overall, our findings showed that HDAC6 is differentially expressed in RMS cells compared to normal muscle, and that HDAC6 localizes predominantly in the cytoplasm of RMS cells.

Conserved role of HDAC6 in promoting tumor growth in RMS

To assess whether HDAC6 loss-of-function effects tumor cell growth, we generated CRISPR/Cas9-mediated HDAC6 gene knockout using two gRNAs targeting exons 5 and 8 (Fig. 1 K) in a panel of RMS cell lines (ERMS: RD, 381T, SMS-CTR; ARMS: Rh5 and Rh30) using

lentivirus. Targeted disruption of HDAC6 resulted in a significant reduction of tumor cell growth 5 days post-plating (Fig. 1 L). To assess the specificity of HDAC6 knockout on tumor cell growth, we performed rescue experiments in a stable RD cell line harboring tamoxifen-inducible Cas9 and the same set of HDAC6 gRNAs (Fig. 1 K) by overexpressing Green Fluorescent Protein (GFP) as a control, wild-type HDAC6 (modified to be Cas9-resistant) and catalytically-dead (cd) HDAC6 (modified to be Cas9-resistant) in RD cells harboring tamoxifen-inducible CRISPR/Cas9 targeting HDAC6. The two histidine-to-alanine mutations (H216A and H611A) inactivate the deacetylase activity of HDAC6 (23). Overexpression of Cas9-resistant wild-type HDAC6 alleviated the HDAC6 knockout-induced growth phenotype in comparison with overexpression of Cas9-resistant cd HDAC6 or GFP 6 days post-tamoxifen induction (Fig. 1 M). Similarly, overexpression of Cas9-resistant wild-type HDAC6 also rescued the growth phenotype in Rh5 cells with HDAC6 knockout (Fig. S1 A). Overexpressing HDAC6 alone did not affect RMS tumor cell growth significantly (Fig. S1 B). Our findings indicate that the effect of HDAC6 knockout on tumor cell growth is specific and that the catalytic activity of HDAC6 is required for its function in regulating RMS tumor cell growth. Depletion of HDAC6 protein from CRISPR/Cas9-mediated gene knockout in lentivirus-transduced and tamoxifen-inducible lines as well as overexpression of wild-type and cd HDAC6 were confirmed by Western blots (Fig. 1 N).

To assess the effects of HDAC6 loss-of-function on tumor growth in vivo, we generated CRISPR/Cas9-mediated *hdac6* knockout in a zebrafish model of KRAS(G12D)-induced ERMS[28]. Double gRNAs targeting exons 5 and 10 of *hdac6* generated an approximately 5-kb deletion (Fig. 1 O). Zebrafish ERMS tumors expressed hdac6 (Fig. S1 C), and depletion of *hdac6* mRNA was observed in 7 of 8 randomly selected *hdac6*-targeted zebrafish tumors (Fig. S1 D), indicating high targeting efficiency. Zebrafish ERMS tumors harboring *hdac6* knockout showed significantly reduced tumor growth by at least 50% compared to tumors harboring the GFP-scrambled gRNAs as a control (Fig. 1 P-T). In addition, targeted disruption of *hdac6* did not alter tumor onset but increased overall tumor-free survival in zebrafish (Fig. S1 E). Our findings indicate that *hdac6* has a conserved role in promoting ERMS tumor growth and progression.

HDAC6 promotes RMS tumor growth by modulating cell cycle progression and tumor cell differentiation

To determine the cellular mechanisms that contribute to reduced tumor cell growth following targeted disruption of HDAC6, we assessed for alterations in cell cycle progression,

cell death and cell differentiation in stable RD and Rh5 human cell lines harboring the tamoxifen-inducible Cas9/HDAC6 double gRNA cassette. RD and Rh5 cells with tamoxifen-induced HDAC6 knockout showed altered progression in G1 or G2/M phases of cell cycle day 6 post-tamoxifen induction (Fig. 2 A) but no significant change in programmed cell death at the same time point (Fig. 2 B). RMS cells show abnormal arrest in myogenic differentiation[16,18]. We have previously shown that CRISPR-mediated HDAC6 disruption resulted in a modest increase in myogenic differentiation of 381T ERMS cells[18]. Here we observed that on immunofluorescence staining for myosin heavy chain (MF20), targeted disruption of HDAC6 also resulted in a modest increase in myogenic differentiation of the RD ERMS line (approximately 1.5-2 fold; $p < 0.01$) compared to no tamoxifen-treated controls following 72-hour starvation in 2% horse serum starting at day 4 post-tamoxifen treatment (Fig. 2 C-E). There was a slightly larger increase in the percentage of MF20-positive cells in tamoxifen-treated Rh5 cells (approximately 2-3 folds increase) compared to the no tamoxifen-treated controls; $p < 0.01$) (Fig. 2 C, F-G). RD and Rh5 cells harboring targeted HDAC6 also showed variable increase in the expression levels of genes involved in myogenesis (e.g. MYOD1, MYH8, CKM) at distinct time points following targeted disruption of HDAC6 (Fig. 2 H-I). Based on our findings, HDAC6 promotes RMS tumor growth in part by modulating cell cycle progression and tumor cell differentiation.

HDAC6 promotes RMS tumor cell migration and self-renewal

The effects of HDAC6 loss-of-function on the migratory behavior and self-renewal capacity of RMS cells were also assessed in RD and Rh5 lines carrying the tamoxifen-inducible Cas9/HDAC6 double gRNA cassette. Following 3 days of tamoxifen-induced HDAC6 targeting, RD and Rh5 were plated for corresponding assays. RD and Rh5 cells with targeted disruption of HDAC6 showed reduced gap closure at 16 hours post-scratch in scratch wound healing assays (Fig. 3 A-B) as well as reduced transwell migration towards the chemoattractant (fetal bovine serum) 22 hours post-seeding in the top chamber (Fig. 3 C-D).

Using the sphere assay as a surrogate in vitro assay for assessing tumor cell stemness and self-renewal[29], we showed that RD and Rh5 cells with tamoxifen-induced CRISPR/Cas9-mediated HDAC6 gene disruption exhibited reduced frequency and size of sphere formation following 3 days of culturing in stem cell medium and low-attachment condition (Fig. 3 E-F). A previous study demonstrates that spheres generated from the RD line in stem cell medium show upregulated expression of stem cell markers such as NANOG, SOX2 and OCT4[14]. Here we showed that expression levels of SOX2, NANOG and OCT4 were reduced in RD sphere

cells with tamoxifen-induced HDAC6 knockout (Fig. 3 G). Overexpression of Cas9-resistant wild-type HDAC6 rescued the expression of these stem cell markers (Fig. 3 G).

Overall, our findings using in vitro functional assays suggest that HDAC6 plays an important role in regulating migratory and self-renewal capacity of RMS tumor cells.

HDAC6 alters the cytoskeletal dynamics to affect RMS cell migration via RAC1

HDAC6 has previously been shown to acetylate the elements of cytoskeleton such as tubulin and actin[20,30]. To assess whether HDAC6 plays a role in modulating the dynamics of cytoskeleton to promote migration of RMS tumor cells, we first showed that there were increased levels of acetylated tubulin in RD and Rh5 cells following targeted disruption of HDAC6 by CRISPR/Cas9 (Fig. 4 A). Overexpressing wild-type but not catalytically-dead (cd) Cas9-resistant HDAC6 in RD cells harboring targeted disruption of HDAC6 alleviated the migratory defect in comparison to overexpressing GFP as a control (Fig. 4 B; Fig. S2 A), indicating that the deacetylase activity is required for the HDAC6 function in regulating RMS cell migration. To assess the effects of HDAC6 loss-of-function on actin-dependent cytoskeletal dynamics, we showed by phalloidin staining that there was loss of membrane ruffles, folds and filopodia as well as altered organization of cytoplasmic actin filament in RD and Rh5 cells harboring Cas9-mediated targeted disruption of HDAC6 following Epidermal Growth Factor (EGF) stimulation in the setting of serum starvation (Fig. 4 C; Fig. S2 B).

RAC1 is a small GTPase of the Rho family which has been shown to mediate a variety of cellular events including cell adhesion, motility and polarity[31,32]. However, the causal relationship between HDAC6 and RAC1 in mediating the cytoskeletal dynamics to promote RMS cell migration is unclear. To assess whether RAC1 contributes to HDAC6-mediated changes in the cytoskeleton dynamics and cell motility of RMS cells, we first showed that RAC1 and HDAC6 co-localized in the regions of cell membrane ruffles and folds (Fig. 4 D; Fig. S2 C), and that RAC1-GTP levels were reduced in RMS cells with HDAC6 knockout (Fig. 4 E). Overexpressing the constitutively activated mutant form of RAC1 (RAC1V12) alleviated the migration phenotype (Fig. 4 F) but did not significantly alter the growth phenotype of RD cells with HDAC6 knockout (Fig. 4 G). A dominant-negative form of RAC1 (RAC1N17) and a constitutively active form of mutant RhoA (RhoAV14), another Rho family GTPase, did not rescue the migration defect or the growth defect in RMS cells with HDAC6 knockout (Fig. 4 F-G). Using a RAC1-GTP pull-down assay, RAC1V12 immunoprecipitated increased levels of RAC1-GTP compared to GFP control and RAC1N17, supporting the constitutive activity of RAC1V12 (Fig. 4 H). Taken together, HDAC6 alters the microtubule and actin-dependent

cytoskeletal dynamics to promote RMS cell migration via RAC1, and we find no evidence of cross talk between close members of Rho GTPases in this context.

RAC1 is essential for RMS cell migration and invasion

As RAC1 is a key mediator of HDAC6 function in regulating RMS cell migration, we next assessed whether RAC1 is essential for RMS cell migration and invasion through loss-of-function and gain-of-function studies. Cultured RD and Rh5 cells with CRISPR/Cas9-mediated targeted disruption of RAC1 showed reduced migratory capacity by the scratch wound healing assay (16 hours post-scratch, $p < 0.0001$; Fig. 5 A-B; Fig. S2 D). Overexpression of Cas9-resistant RAC1V12 rescued the loss-of-function effects of RAC1 on cell migration, indicating the specificity of the CRISPR/Cas9-mediated RAC1 targeting (Fig. 5 C). Targeted disruption of RAC1 had mild effect (approximately 10-15% reduction) on RD cell growth and no significant effect on Rh5 cell growth (7 days post-plating, $p < 0.0001$; Fig. 5 D). Finally, RD and Rh5 cells treated with the selective RAC1 inhibitor, EHop-016, also showed reduced migration (Figure S2 E).

To assess the gain-of-function effects of RAC1 on RMS cell growth and invasion in vivo, KRASG12D-driven zebrafish ERMS tumors co-expressing Green Fluorescent Protein (GFP) and either RAC1V12 or empty vector as a control were sorted for green fluorescence-positive cells and transplanted into syngeneic CG1 zebrafish at 10,000 cell per fish via dorsal subcutaneous route. The fish with engrafted tumors were imaged weekly and harvested after 21 days. RAC1V12-expressing tumors ($n = 12$) showed larger increase in tumor volume over 1-week period compared to control tumors ($n = 9$) (Fig. 5 E-F; Fig. S2 F). By 21 days, zebrafish ERMS tumor cells co-expressing RAC1V12 demonstrate more aggressive growth compared to the control empty vector co-expressing tumor cells (Fig. 5 E). On histologic analysis, RAC1V12 co-expressing zebrafish ERMS tumors are deeply invasive into the skeletal muscle compared to control empty vector co-expressing zebrafish ERMS tumors, which showed only superficial invasion in about the same time duration (Fig. 5 G).

RAC1 is associated with poor prognosis in RMS

To assess whether HDAC6 or RAC1 expression is associated with clinical prognosis in RMS, we correlated expression levels of HDAC6 or RAC1 mRNA expression in 81 human RMS cases with survival data (63 fusion-negative and 18 fusion-positive). Kaplan-Meier curves were generated based on gene expression values dichotomized into over- and under-expressed groups combining fusion-negative and fusion-positive patients using the median expression

value within each cohort as a cutoff. While expression of HDAC6 did not correlate with overall survival, high expression of RAC1 correlated with decreased overall survival (Fig. 5 H log rank test, p = 0.02842, HR = 2.36, 95% CI = 1.095 - 5.084). If we stratify the analysis by fusion status, RAC1 expression showed marginal significance for the fusion-negative (p= 0.07036) but not the fusion-positive cases (p=0.31) with respect to overall survival. Although the small sample size in both subsets compromises the ability to draw firm conclusions, our findings suggest that expression of RAC1 might be useful as a clinical prognostic biomarker, if these studies can be confirmed in a prospective analysis.

Treatment with HDAC6-selective inhibitors recapitulates the HDAC6 loss-of-function effects in RMS

To assess whether treatment of RMS cells with selective HDAC6 inhibitors, tubastatin A and tubacin, could recapitulate the loss-of-function effects of HDAC6 on RMS cells, we first showed that treating a panel of RMS cell lines (RD, SMS-CTR, Rh5 and Rh30) with tubastatin A and tubacin in vitro significantly inhibited tumor cell growth in a dose-dependent manner (Fig. 6 A; Fig. S3 A). RD and Rh5 cells treated with tubastatin A and tubacin showed increased levels of acetylated tubulin, a known substrate of HDAC6 (30) (Fig. 6 B; Fig. S3 B). In scratch wound healing assays, RD and Rh5 cells were treated with tubastatin A (200 nM) or tubacin (500 nM) for 24 hours prior to plating and kept under treatment throughout each assay. Tubastatin A or tubacin-treated RD and Rh5 cells showed reduced gap closure at 16 hours (Fig. 6 C-D; Fig. S3 C). RD and Rh5 cells treated with tubastatin A (200 nM) or tubacin (500 nM) in stem cell media for 3 days also showed reduced sphere formation (Fig. 6 E-F; Fig. S3 D).

To assess the effect of tubastatin A treatment on RMS tumor growth in vivo, RMS xenografts generated from RD and Rh5 cells were treated with tubastatin A by intraperitoneal injections at 10 mg per kg per mouse every 3 days for 21 days. RD and Rh5 xenografts harvested at the end of the treatment period showed increased expression of acetylated tubulin by immunohistochemistry (Fig. S4 A-H), indicating that treatment of tubastatin A selectively inhibited HDAC6 activity in vivo. RMS xenografts treated with tubastatin A showed at least 50% reduction in tumor growth compared to those treated with DMSO as a vehicle control (Fig. 6 G-H; Fig. S4 I-J). RMS xenograft tumors treated with tubastatin A also showed reduced Ki67 proliferation index based on immunohistochemistry analysis (Fig. S4 K-L).

To assess whether tubastatin A treatment affects the self-renewal capacity of RMS cells in vivo, we treated 20-21 days-old ERMS tumor-bearing zebrafish with tubastatin A (10 uM) and DMSO (vehicle) for 7 days and performed limiting dilution transplantation assays. A time course

analysis showed that zebrafish tumors treated with 10 uM of tubastatin showed increased levels of acetylated tubulin as early as 24 and 48 hours post-treatment compared to tumors treated with vehicle control (DMSO), indicating selective targeting of HDAC6 activity in zebrafish ERMS tumors (Fig. S4 M). Tumor engraftment was monitored weekly until day 30 post-transplantation. In 3 independent experiments, tubastatin A-treated ERMS tumors transplanted at limiting dilutions (104, 103 and 102 cells) showed approximately 6-9 fold decrease in self-renewal frequency by Extreme Limiting Dilution (ELDA) analysis (33) (Table 1). Overall, treatment of RMS cells with tubastatin A and tubacin mimics the loss-of-function effects of HDAC6 on tumor cell growth, migration and self-renewal capacity, thus identifying promising agents of targeted therapy for RMS.

Discussion

In this study, we have demonstrated through in vitro and in vivo functional assays that HDAC6 regulates RMS tumor growth by modulating cell cycle progression and differentiation. HDAC6 also plays an important role in regulating the self-renewal capacity and migration/invasion of RMS cells. RAC1 is an important mediator of HDAC6 function in RMS cell migration/invasion, and high expression of RAC1 correlates with poor clinical prognosis in RMS patients.

HDAC6 has been shown to deacetylate tubulin, a subunit of microtubule, and cortactin, an actin-associated protein, to affect cytoskeletal dynamics[20,30]. A study in mouse embryonic fibroblasts demonstrates that functional HDAC6 is required for RAC1 activation[23]. However, the functional relationships among HDAC6, microtubules and actin filaments in driving cancer cell invasion/migration is unclear. In our study, we showed that HDAC6 deacetylates the tubulin subunits of microtubules, and its deacetylase activity is required to promote RMS cell migration. HDAC6 also plays a crucial role in regulating the actin-dependent cytoskeletal dynamics required for RMS cell migration. This is supported by our findings that HDAC6 and RAC1 co-localize in membrane ruffles and filopodia, which are dynamic actin-regulated structures required for cell motility and invasion, and RMS cells with targeted disruption of HDAC6 showed reduced formation of membrane ruffling and filopodia. In addition, RAC1 has been shown previously to be required for actin polymerization, stress fiber formation and focal adhesion complex assembly[31]. In this study, loss of HDAC6 resulted in reduced RAC1 GTPase activity, and an activated mutant form of RAC1 (RAC1V12) alleviated the migration defect of RMS cells with HDAC6 knockout. Overall, our findings indicate that the deacetylase activity of HDAC6 and activation of RAC1 are essential for the HDAC6-mediated effects on actin-dependent

cytoskeletal dynamics required for RMS cell migration and invasion. The crosstalk between the microtubules and actin elements in regulating cellular processes such as cell migration is beginning to be recognized[34]. HDAC6 likely coordinates the direct or indirect interactions between the microtubules and the actin or its associated molecules to promote RMS cell migration and invasion. Further investigation is required to assess whether acetylation of tubulin or other substrates by HDAC6 directly affects RAC1 activation and, in turn, actin dynamics, or whether HDAC6 independently alters the microtubule and actin dynamics to regulate RMS cell motility.

RAC1 is required for actin cytoskeletal reorganization, a process required for cell migration/invasion during cancer metastasis. Increased expression or activity of RAC1 is associated with metastatic potential in multiple cancer types (e.g. breast, liver and upper urinary tract)[35-37]. In this study, we used loss-of-function and gain-of-function in vitro and in vivo studies to demonstrate that RAC1 is necessary and sufficient for active migration/invasion of RMS cells. Further investigation will be required to assess whether RAC1 is required to initiate metastasis of RMS cells.

Our analysis of clinical data showed that the expression levels of HDAC6 do not correlate with overall survival of RMS patients, suggesting that HDAC6 might be involved in a complex gene interaction network, and that epistatic interactions may mask the effect of HDAC6 on overall survival. By contrast, high expression of RAC1 correlates with poor overall survival in RMS patients. Additional analyses with larger data sets are needed to confirm the possible prognostic value of RAC1 expression within each subgroup (fusion-positive vs fusion-negative), and multivariate analyses are needed to evaluate whether its expression is independent of tumor stage or clinical risk groups already established to correlate with outcome for children with RMS. Beyond this, our findings indicate that HDAC6 and RAC1 can serve as therapeutic targets for reducing invasive and metastatic potential of RMS cells.

The self-renewal capacity of tumor initiating cells contributes to cancer relapse and therapy resistance[12]. So far there are limited studies on characterizing the role of HDAC6 in regulating cancer stemness and self-renewal capacity. In glioblastoma, HDAC6 is required for maintaining the glioma stem cell stemness and through its interaction with the Sonic Hedgehog (SHH) signaling pathway, promotes the radio-resistant phenotype[26]. Through in vitro sphere assays, stem cell marker analysis and in vivo limiting dilution assays, we showed that targeted disruption of HDAC6 by CRISPR technology and treatment with a selective HDAC6 inhibitor, tubastatin A or tubacin, resulted in reduced cancer stemness and self-renewal capacity of RMS cells. RMS spheres generated in vitro have been shown to be enriched for stem cell markers

and are resistant to treatment with standard-of-care chemotherapy agents[14]. While further investigation is required to determine the pathways modulated by HDAC6 to regulate self-renewal of RMS cells, our findings suggest that targeted therapy using HDAC6 selective inhibitors against cancer stemness represents a promising option for preventing relapse and treatment resistance in RMS.

Our knowledge of the molecular mechanisms underlying RMS self-renewal and metastasis is limited. Using in vitro and in vivo functional assays, we have characterized the unique role of HDAC6 in regulating RMS tumor growth, self-renewal and migration/invasion. As RAC1 serves as an essential downstream mediator of HDAC6 function in RMS cell migration and invasion, targeting the HDAC6-RAC1 axis will likely improve survival outcomes of RMS patients.

Material/Methods

CRISPR/Cas9 Gene Targeting in Human RMS Cell Lines

Single knockout was accomplished by transducing RMS cells with lentiviral virus expressing safe-harbor control or gene-specific double gRNAs and Cas9. Lentiviral transduced RMS cells were plated for cell-based assays following antibiotic selection 7 days post-transduction. Cloning of Cas9 and gRNA expression vectors was performed as described previously[18].

CRISPR/Cas9 inducible cells were created using piggybac transposition[1]. Stable cell lines were integrated with a construct containing double gRNAs and ERT2-Cas9-ERT2 fusion protein for tamoxifen inducible gene targeting. The coding portions of wild-type and cd *HDAC6* were amplified from the plasmids[38] obtained from Addgene (Watertown, MA) for cloning purposes. Lentiviral RAC1V12 and RHOAN17 expression constructs were obtained from the Langenau lab[17]. Silent mutations to alter PAM sites to create Cas9-resistant wild-type HDAC6, cd HDAC6 and RAC1V12 lentiviral overexpression constructs used in rescue and overexpression experiments were introduced using a 4-piece Gibson cloning strategy.

The following double gRNAs were used for targeting genes in human RMS cell lines:

HDAC6: gRNA1 - GCTTCCCGGAAGGCCCTGAGCGG

gRNA2 - GCTGGTGGATGCGGTCCTGGGGG

RAC1: gRNA1 - GATCCTTACTGTTTGCGGAT

gRNA2 – GAAAATGTCCGTGCAAAGGT

We used the same double gRNAs for targeting a safe-harbor region (Chr 4: 58110237-58110808; GRCH38.p2) as in our previously published study[18].

Assessing Tumor Growth and Self-renewal Using Zebrafish ERMS Model

Zebrafish were maintained in a shared facility at the University of Washington under protocol #4330-01 approved by the University of Washington Subcommittee on Research Animal Care. To introduce CRISPR/Cas9-mediated gene targeting in the zebrafish model of KRAS-driven ERMS, a cocktail of DNA constructs containing *rag2*:*KRAS(G12)*-U6-*hdac6* gRNAs, *rag2*:Cas9 and *myog*-H2B:RFP was injected into zebrafish embryos at 1-cell stage. Once RFP+ primary tumors were established (around day 15-20), fluorescent images of tumor fish that were randomly selected from each treatment condition and imaged at bright field and at the red channel at the starting time point and 7 days later using the same setting of a Nikon fluorescent dissecting scope. Tumor volume change was assessed over a 7-day period by measuring tumor area x intensity of fluorescence for each animal using ImageJ as previously described[39]. Deletion of *hdac6* in zebrafish tumors was confirmed by sequencing the PCR products amplified using the primers flanking the gRNA sites in the gene locus.

The *rag2*:*KRAS(G12D)*-U6:*hdac6* gRNAs construct was made by using the Gibson cloning strategy to insert the U6:*hdac6* gRNAs cassette into the *rag2*:KRAS(G12) construct obtained from the Langenau lab (Massachusetts General Hospital/Harvard Medical School). The *rag2* promoter and Cas9 coding region were inserted into the *rag2*:Cas9 expression construct using the Gibson cloning strategy.

The following gRNAs were used in zebrafish:

hdac6: gRNA1 - GCTGGGACGCTGTGTACAAG
gRNA2 - GCTGAGCATACCTTGTTCCA

GFP scrambled control: gRNA1 - GAATCCTGGCCCACTCGAGG
gRNA2 - GTCAACCACCGCGGTCTCAG

In limiting dilution assays to assess tumor cell self-renewal, zebrafish ERMS tumor cells were transplanted into 3-4 weeks-old juvenile fish and treated by soaking with DMSO (vehicle control) or Tubastatin A (10 uM) for 7 days with drug change daily except for drug holiday on day 4) prior to tumor cell harvesting and transplanting in limiting dilutions (10^4, 10^3 and 10^2 cells) into syngenetic adult CG1 zebrafish using the protocol as previously described[39].

Primary tumors co-expressing *rag2*:KRASG12D, *rag2*:GFP, and *rag2*:empty control vector or *rag2*:RAC1V12 were expanded by transplantation into 3-4 syngeneic adult CG1 fish. GFP-positive tumor cells were isolated by Fluorescent Activated Cell Sorting (FACs) and transplanted subcutaneously into the dorsal region at 10,000 cell per fish. Weekly imaging of tumor-bearing fish post-transplantation was performed using a Nikon fluorescent dissecting

scope. The weekly tumor volume change was quantified using the ImageJ software as previously described[39].

Cell-based Assays

RMS cell growth was quantified by direct cell counting or the ATP-based Cell Titer Glo luminescent cell viability assay (Promega, Madison, WI). For cell counts, RMS cells were transduced with lentivirus for 2 days and selected with the appropriate antibiotic for 3 days prior to plating. Cell counts were performed at 5-7 days post plating at a starting density of 10,000 cells per well in 24-well plates. For cell growth rescue experiments using the stable RD line harboring the tamoxifen-inducible Cas9/HDAC6 double gRNA cassette, cells was transduced first with lentivirus for Cas9-resistant GFP, wt HDAC6 and cd HDAC6 for 2 days. Following antibiotic selection for 3 days, inducible gene targeting *in vitro* was accomplished by treating RMS cells for 3 days with 2 μM 4-hydroxytamoxifen. Cell counts were performed 7 days post-tamoxifen induction. The Cell Titer Glo assay was used to assess dose-dependent effects of inhibitors (tubastatin A and tubacin) on cell growth. Cells were plated in 96-well plates at 1000-2000 cells per well and treated with each inhibitor at varying concentrations for 6 days (with drug change on day 3) prior to the Cell Titer Glo assay per manufacturer's manual. The luminescence was read using a microplate reader (BioTek Synergy H1, Winooski, VT).

To assess myogenic differentiation in RMS, cells were serum starved in 2% horse serum/DMEM for 72 hours prior to fixing in 2% paraformaldehyde for immunofluorescence against MF20 (myosin heavy chain).

A flow cytometry-based assay using the Annexin V, Alexa Fluor 647 conjugate (Thermo Fisher Scientific, Waltham, MA) was used to analyze apoptosis in tumor cells. For cell cycle analysis by flow cytometry, cells pulsed with EdU for 2 hours prior to being harvested and prepped using the Click-iT EdU Alexa Fluor 647 Flow Cytometry Assay kit (Life Technologies).

Spheres ("rhabdospheres") were induced in stem cell (neurobasal) medium enriched with growth factors (EGF, bFGF, PDGF-A and PDGF-B) as previously described[39]. For drug treatment studies, RD and Rh5 cells were incubated in the stem cell medium plus 250 nM of tubastatin A or 0.2% DMSO (vehicle) for 3 days. Tamoxifen-inducible Cas9/double *HDAC6* gRNA stable lines (RD and Rh5) were induced for 3 days with 2 □M of tamoxifen for 3 days prior to plating in low-attachment plates on day 4 for the sphere assays. Spheres were counted 3 days post-plating.

The scratch wound healing and transwell assays were performed as previously described[16]. Briefly, cells of different treatment conditions (control vs CRISPR-targeted or

DMSO vs drug treatment) were plated at similar density (~80-90% confluence) and analyzed at 16 hours post-scratch to minimize the confounding effects of cell proliferation difference. Transwell assays were performed using the Costar transwell clear polyester membrane inserts (6.5 mm diameter, growth area: 0.33 cm^2; pore size: 0.8 um) in 24-well plates. 200,000 cells were seeded into the insert in DMEM, and the bottom well was filled with 10% FBS/DMEM as a chemoattractant. Migrated cells in the transwell were fixed in formalin at 22 hours post-seeding and visualized by crystal violet staining.

Human Xenografts and Drug Treatment

Mouse studies were approved by the University of Washington Subcommittee on Research Animal Care under protocol #4330-01. To establish xenografts in immunocompromised NOD-SCID Il2rg-/- (NSG) mice, approximately 1-2 x 10^6 RMS cells (Rh5 or RD) were resuspended in Matrigel and injected subcutaneously into the flanks of each 6-7 week-old anesthetized mouse. As tumor size reached approximately 50-100 mm^3, tubastatin-A (10 mg/kg) or vehicle (DMSO) was administered by the intraperitoneal route every 3 days for up to 21 days or until tumor end point (750 mm^3). Tumor size was measured by caliper every 3-4 days at tumor onset until tumor end point or at the end of drug treatment (whichever is earlier). At the end of the experiment, all mice were humanely euthanized for tumor tissue harvesting.

Immunohistochemistry and Immunofluorescence

A tissue microarray created from archived paraffin tissue blocks for human RMS tumor samples was obtained from Seattle Children's Hospital. Immunohistochemistry was performed at the Histology and Imaging core facility at University of Washington. The following antibodies including dilutions were used: rabbit polyclonal anti human mouse monoclonal anti human Ki-67, (1:100, clone: MIB1, Dako, Santa Clara, CA), rabbit monoclonal anti human HDAC6 (1:100, clone, D2E5; Cell Signaling, Danvers, MA), mouse monoclonal anti human RAC1 (1:100, clone 102; BD Biosciences, San Jose, CA), mouse monoclonal anti acetylated alpha-tubulin (1:200; clone 6-11B-1; Santa Cruz Biotechnology, Dallas, TX) and mouse monocloncal anti-alpha-tubulin (1:200; B-5-1-2; Santa Cruz Biotechnology, Dallas, TX). Staining for F-actins was done using Phalloidin conjugated to fluorescent dye 488 (diluted 1:1000; Abnova, Tapei, Taiwan).

RAC1 Activation Assay

To assess the levels of RAC1 activation (GTP-bound form) in RMS cells, cultured cells were serum starved in DMEM for 24 hours prior to stimulation with EGF (50 ng/mL) for 10

minutes. Cells were harvested for RAC1-GTP pull down using the Rac1 Activation Assay Biochem Kit (Cytoskeleton, Inc., Denver, CO). Approximately 300 micrograms of protein in each treatment condition was used. Pull down products along with input lysate were run on Western blots to compare the levels of RAC1-GTP to total RAC1 using the antibody against RAC1.

Western Blots

Human cell line and zebrafish tumor whole cell lysates prepared in RIPA with protease inhibitors and 2x sample buffer were electrophoresed on a 4-15% gradient SDS-polyacrylamide gel (Bio-Rad, Hercules, CA) and transferred to PVDF membranes using the TurboTransblot (Bio-Rad, Hercules, CA). Blots blocked in 5% milk-TBST and probed using the following antibodies and dilutions: HDAC6 (1:1000; cloneD21B10, Cell Signaling, Danvers, MA); GAPDH (1:2000; Cell Signaling, Danvers, MA); mouse monoclonal anti acetylated alpha-tubulin (1:500; clone 6-11B-1; Santa Cruz Biotechnology, Dallas, TX), mouse monoclonal anti-alpha-tubulin (1:500; B-5-1-2; Santa Cruz Biotechnology, Dallas, TX) and RAC1 (1:1000; BD Biosciences, San Jose, CA). Goat anti-mouse or anti-rabbit HRP conjugated IgG secondary antibodies were obtained from Santa Cruz Biotechnology.

Survival Association Analysis in RMS patient cohort

The 81 RMS cases with survival and gene expression data were published previously[40]. For survival analysis, p value was calculated based on the log-rank test by R package Survival (https://cran.r-project.org/web/packages/survival/index.html). Note that study subject age and sex, available only on a subset of the data, were not incorporated into the survival analyses because those features are not generally accepted as influencing survival of RMS patients.

Quantitative RT-PCR

Human or zebrafish cells were lysed in TRIizol reagent (Thermo Fisher Scientific, Waltham, MA) and RNA was isolated per manufacturer's protocol. Approximately 1 microgram of RNA was used for cDNA synthesis using the High Capacity cDNA Reverse Transcription kit (Thermo Fisher Scientific, Waltham, MA). SYBR Green-based quantitative PCR was subsequently performed using gene-specific primers (Table S1) in a light cycler (CFX Connect Real-time PCR Detection System) from Bio-Rad (Hercules, CA).

Statistics

Two-tailed t-test and ANOVA tests were used to assess statistical significance in differences between experimental and control samples when appropriate. A p value <0.05 was considered statistically significant.

Figures

Figure 1

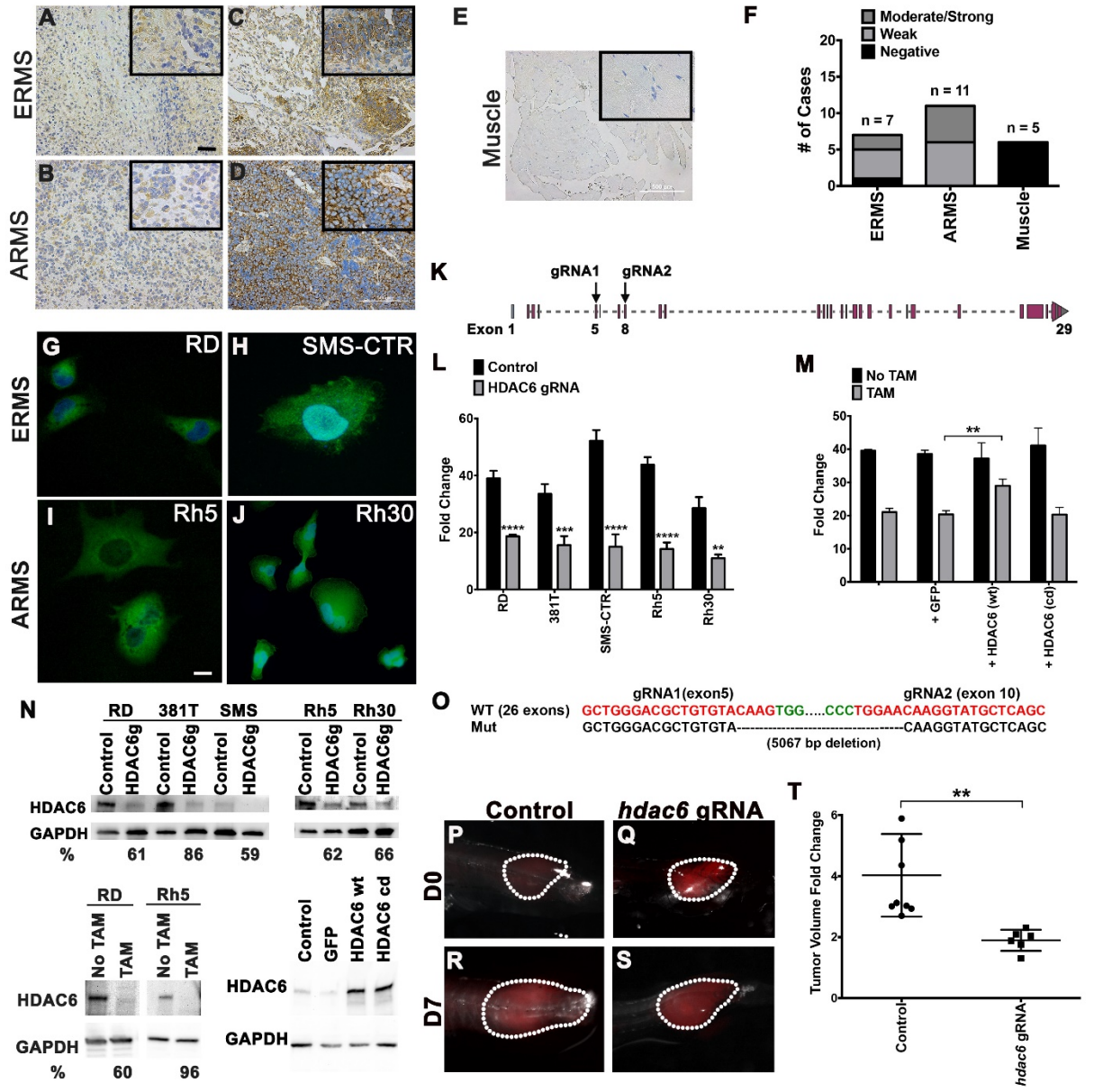

Figure 2

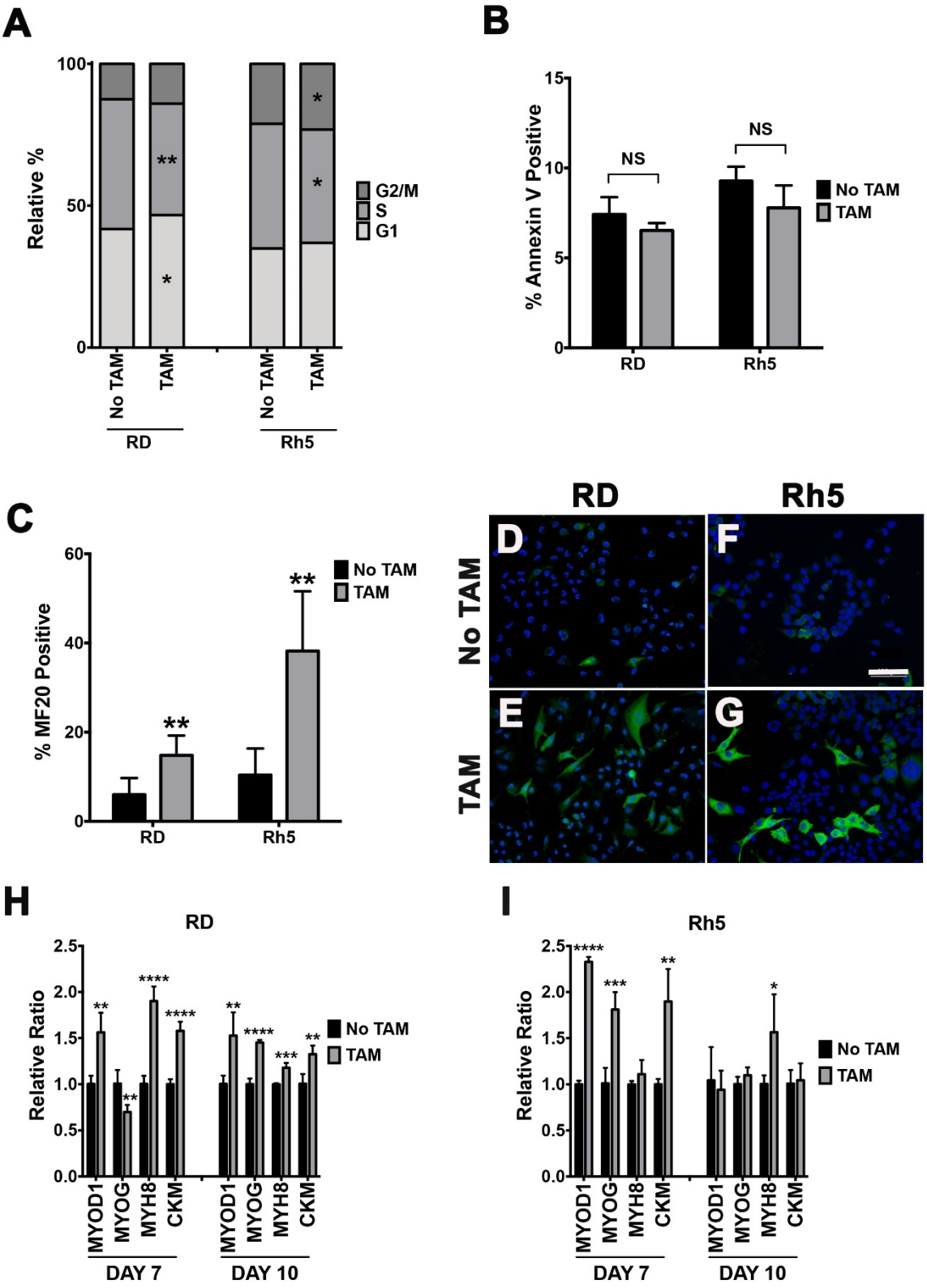
A
100
50
0
Relative %
**
*
*
*
G2/M
S
G1
No TAM
TAM
RD
Rh5
B
15
10
5
0
% Annexin V Positive
NS
NS
No TAM
TAM
RD
Rh5
C
60
40
20
0
% MF20 Positive
**
**
No TAM
TAM
RD
Rh5
RD
Rh5
No TAM
TAM
D
F
E
G
H
RD
2.5
2.0
1.5
1.0
0.5
0.0
Relative Ratio
**
**
****
****
**
****
***
**
No TAM
TAM
MYOD1
MYOG
MYH8
CKM
DAY 7
DAY 10
I
Rh5
2.5
2.0
1.5
1.0
0.5
0.0
Relative Ratio
****
***
**
*
No TAM
TAM
MYOD1
MYOG
MYH8
CKM
DAY 7
DAY 10

Figure 3

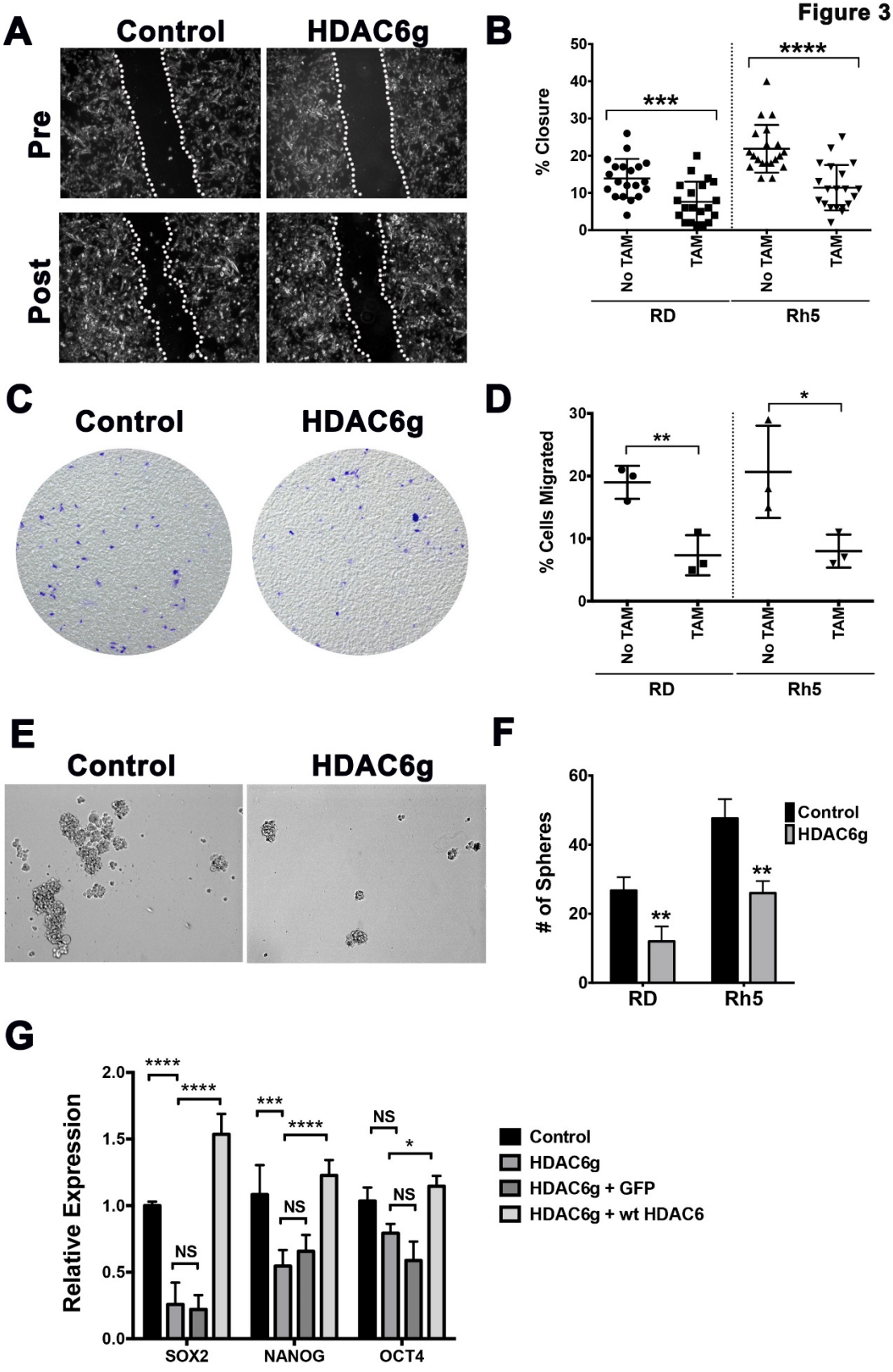
A
Control
HDAC6g
Pre
Post
B
% Closure
***
****
No TAM
TAM
No TAM
TAM
RD
Rh5
C
Control
HDAC6g
D
% Cells Migrated
**
*
No TAM
TAM
No TAM
TAM
RD
Rh5
E
Control
HDAC6g
F
# of Spheres
Control
HDAC6g
**
**
RD
Rh5
G
Relative Expression
****
****
***
****
NS
*
NS
NS
NS
SOX2
NANOG
OCT4
Control
HDAC6g
HDAC6g + GFP
HDAC6g + wt HDAC6

Figure 4

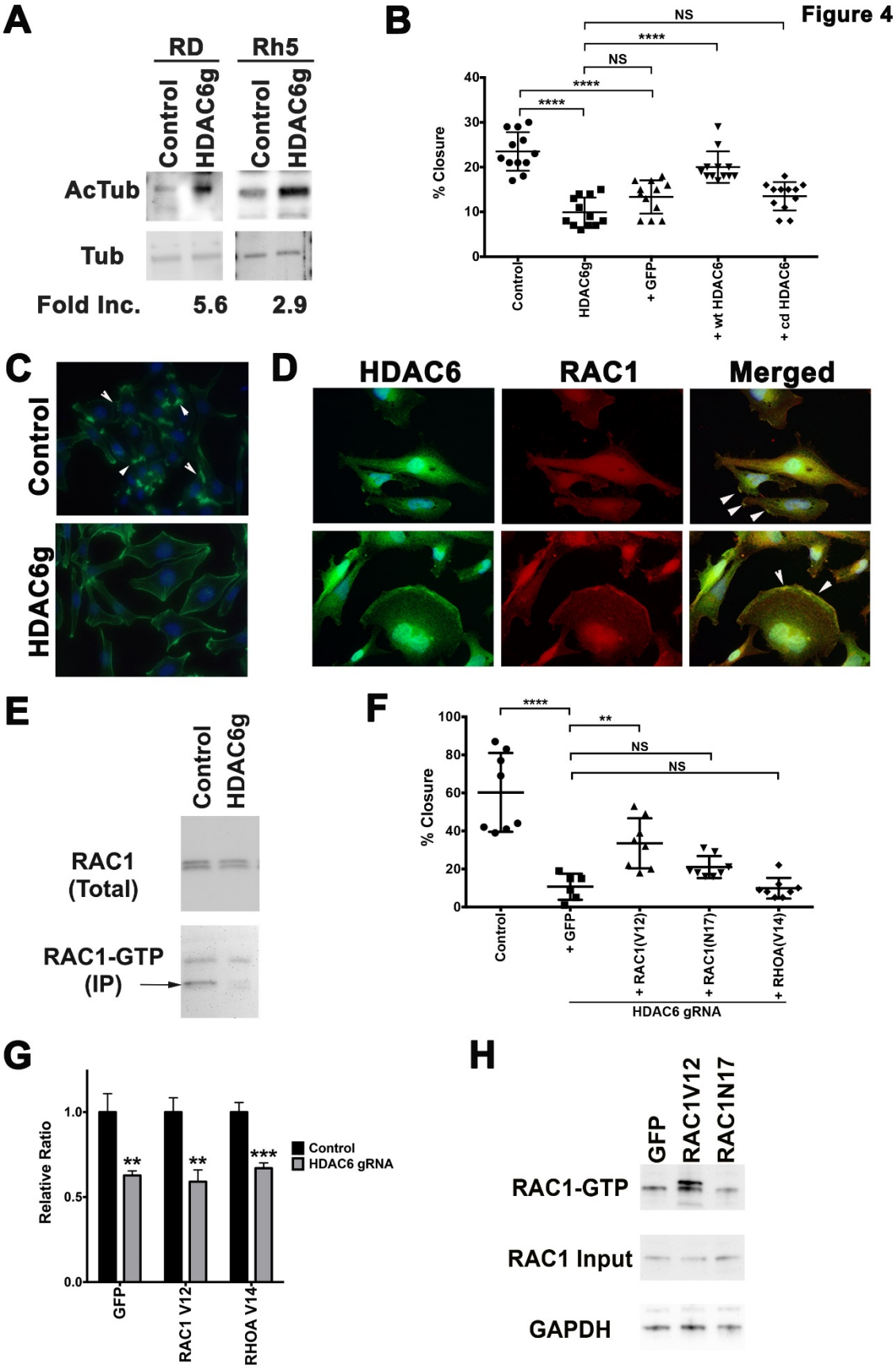
A
RD
Rh5
Control
HDAC6g
Control
HDAC6g
AcTub
Tub
Fold Inc.
5.6
2.9
B
NS
****
NS
****
****
% Closure
40
30
20
10
0
Control
HDAC6g
+ GFP
+ wt HDAC6
+ cd HDAC6
C
Control
HDAC6g
D
HDAC6
RAC1
Merged
E
Control
HDAC6g
RAC1
(Total)
RAC1-GTP
(IP)
F
****
**
NS
NS
% Closure
100
80
60
40
20
0
Control
+ GFP
+ RAC1(V12)
+ RAC1(N17)
+ RHOA(V14)
HDAC6 gRNA
G
Relative Ratio
1.0
0.5
0.0
**
**
***
Control
HDAC6 gRNA
GFP
RAC1 V12
RHOA V14
H
GFP
RAC1V12
RAC1N17
RAC1-GTP
RAC1 Input
GAPDH

Figure 5

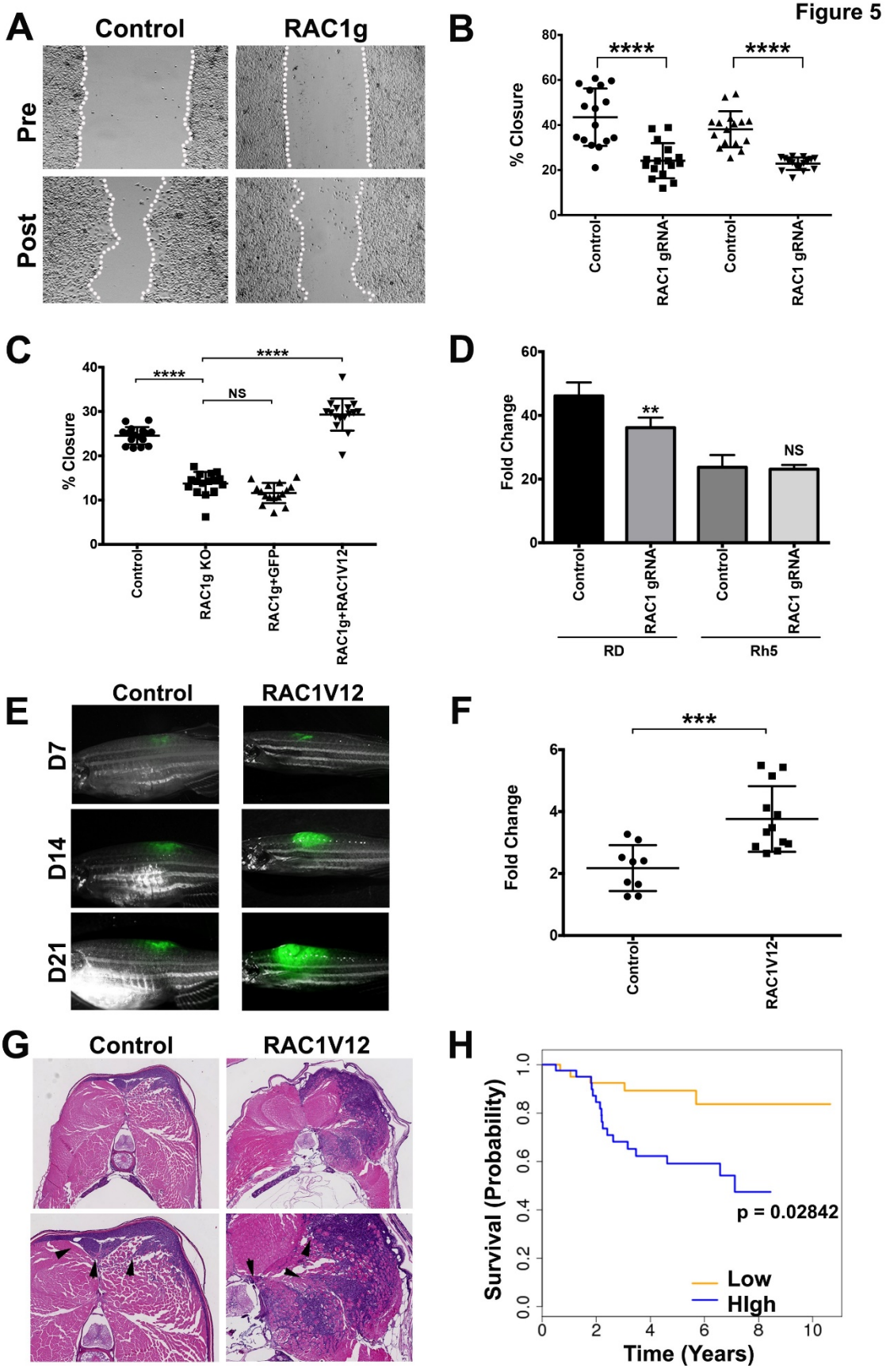
A
Control
RAC1g
Pre
Post
B
% Closure
****
****
Control
RAC1 gRNA
Control
RAC1 gRNA
C
% Closure
****
****
NS
Control
RAC1g KO
RAC1g+GFP
RAC1g+RAC1V12
D
Fold Change
**
NS
Control
RAC1 gRNA
Control
RAC1 gRNA
RD
Rh5
E
Control
RAC1V12
D7
D14
D21
F
Fold Change
***
Control
RAC1V12
G
Control
RAC1V12
H
Survival (Probability)
p = 0.02842
Low
HIgh
Time (Years)

Figure 6

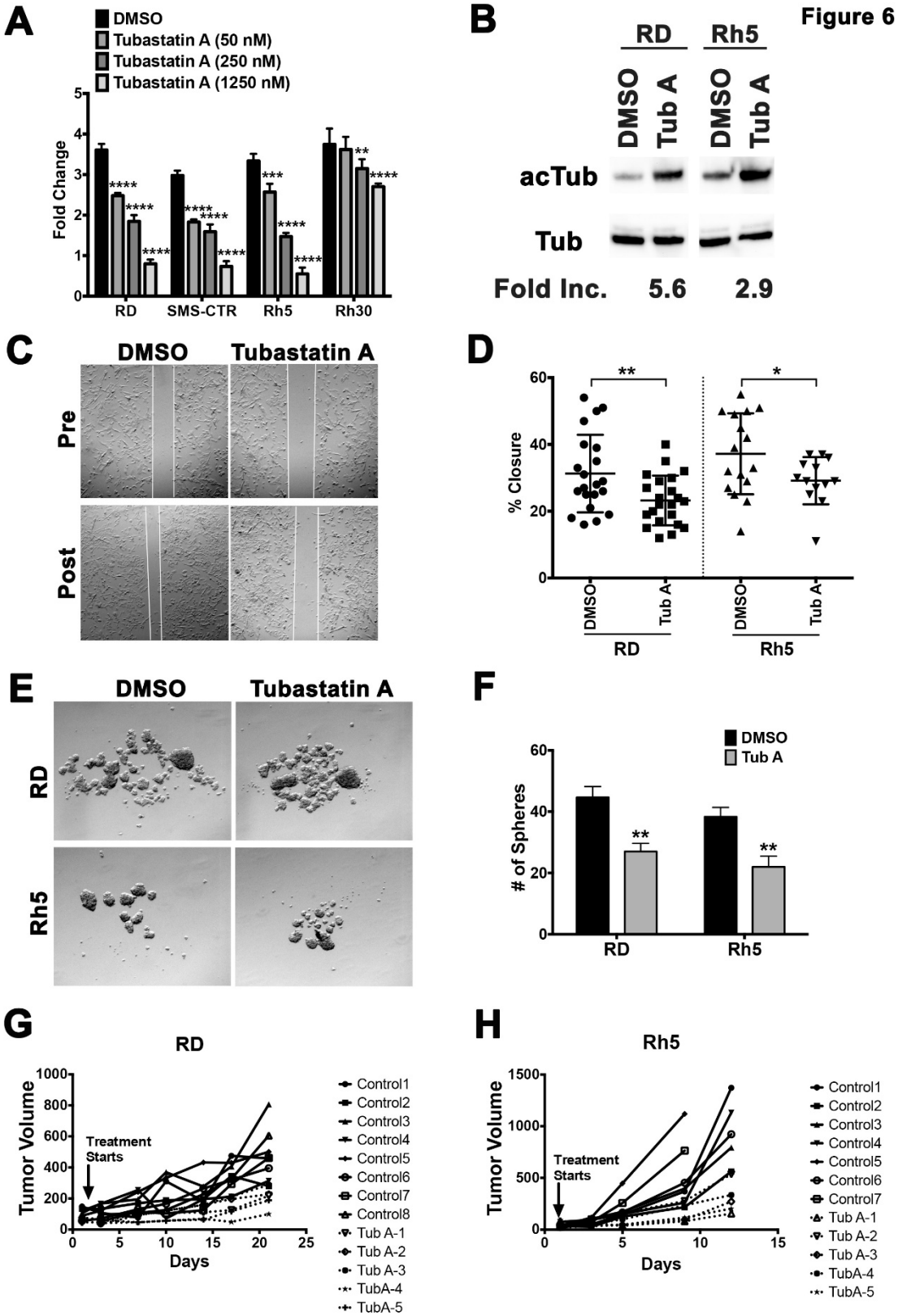
A
DMSO
Tubastatin A (50 nM)
Tubastatin A (250 nM)
Tubastatin A (1250 nM)
Fold Change
RD
SMS-CTR
Rh5
Rh30
B
RD
Rh5
DMSO
Tub A
acTub
Tub
Fold Inc.
5.6
2.9
C
DMSO
Tubastatin A
Pre
Post
D
% Closure
DMSO
Tub A
RD
Rh5
E
DMSO
Tubastatin A
RD
Rh5
F
DMSO
Tub A
# of Spheres
RD
Rh5
G
RD
Tumor Volume
Treatment Starts
Days
Control1
Control2
Control3
Control4
Control5
Control6
Control7
Control8
Tub A-1
Tub A-2
Tub A-3
TubA-4
TubA-5
H
Rh5
Tumor Volume
Treatment Starts
Days
Control1
Control2
Control3
Control4
Control5
Control6
Control7
Tub A-1
Tub A-2
Tub A-3
TubA-4
TubA-5

Table 1. Summary of Limiting Dilution Assays

	Experiment 1		Experiment 2		Experiment 3	
Cell No.	DMSO	Tubastatin A	DMSO	Tubastatin A	DMSO	Tubastatin A
10,000	6 of 6	7 of 7	8 of 8	6 of 10	6 of 6	6 of 7
1,000	5 of 6	5 of 10	6 of 10	3 of 10	9 of 10	6 of 10
100	3 of 6	1 of 10	2 of 9	0 of 10	4 of 10	2 of 9
TPC frequency	1350	9045*	908	8167*	332	2138*
95% CI	605-3017	3820-21419	605-3017	3820-21419	161-686	932-4908
		* p = 0.001		*p = 2.77e-0		*p = 9.82e-05

Figure S1

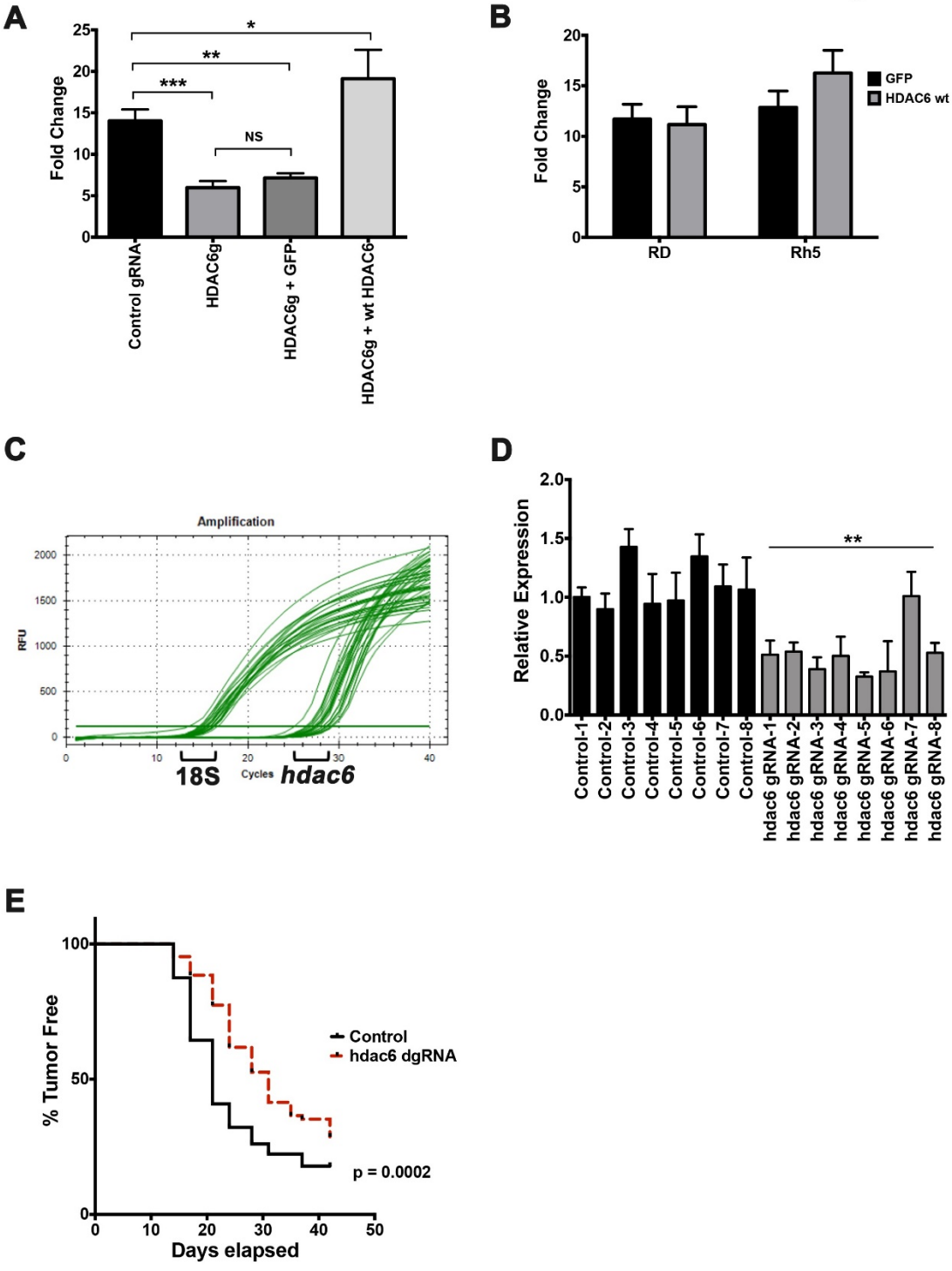
A
Fold Change
25
20
15
10
5
0
*
**
***
NS
Control gRNA
HDAC6g
HDAC6g + GFP
HDAC6g + wt HDAC6
B
Fold Change
20
15
10
5
0
GFP
HDAC6 wt
RD
Rh5
C
Amplification
RFU
2000
1500
1000
500
0
0
10
20
30
40
18S
Cycles
hdac6
D
Relative Expression
2.0
1.5
1.0
0.5
0.0
**
Control-1
Control-2
Control-3
Control-4
Control-5
Control-6
Control-7
Control-8
hdac6 gRNA-1
hdac6 gRNA-2
hdac6 gRNA-3
hdac6 gRNA-4
hdac6 gRNA-5
hdac6 gRNA-6
hdac6 gRNA-7
hdac6 gRNA-8
E
% Tumor Free
100
50
0
Control
hdac6 dgRNA
p = 0.0002
0
10
20
30
40
50
Days elapsed

Figure S2

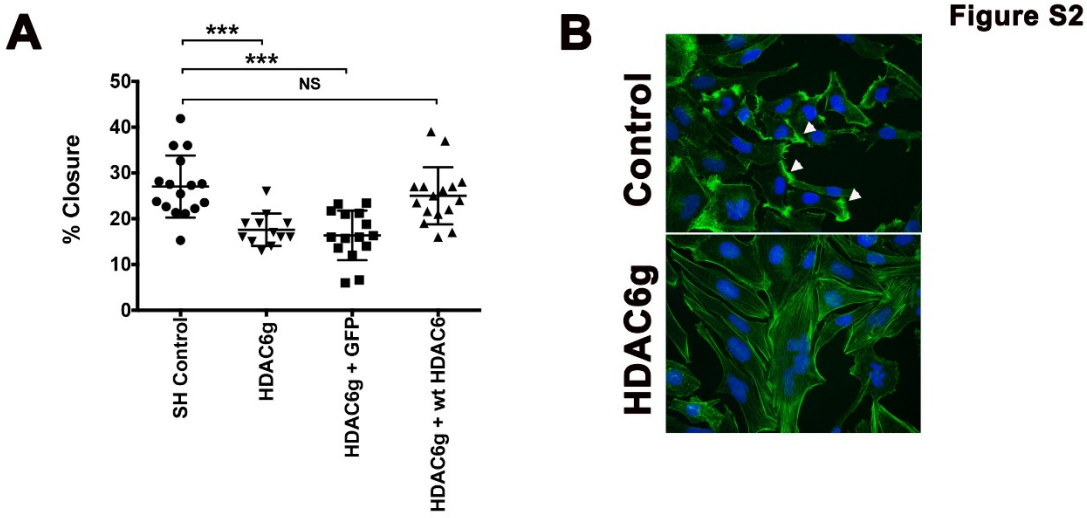
A
***
***
NS
% Closure
50
40
30
20
10
0
SH Control
HDAC6g
HDAC6g + GFP
HDAC6g + wt HDAC6
B
Control
HDAC6g

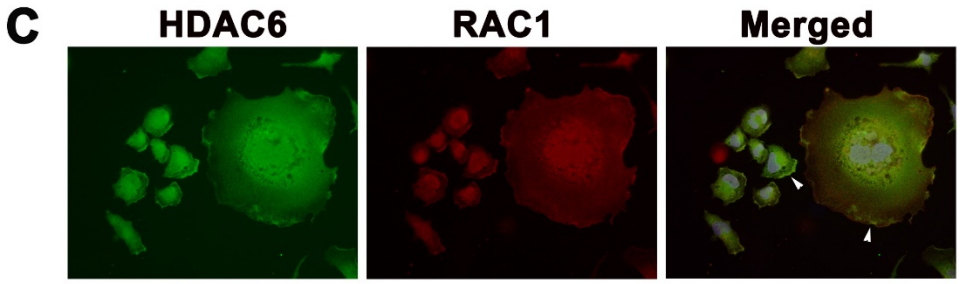
C
HDAC6
RAC1
Merged

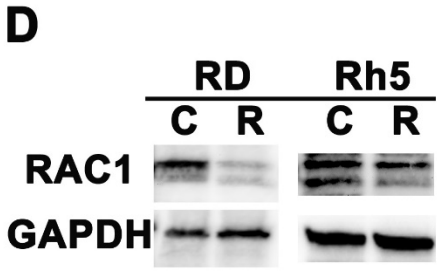
D
RD
Rh5
C
R
C
R
RAC1
GAPDH

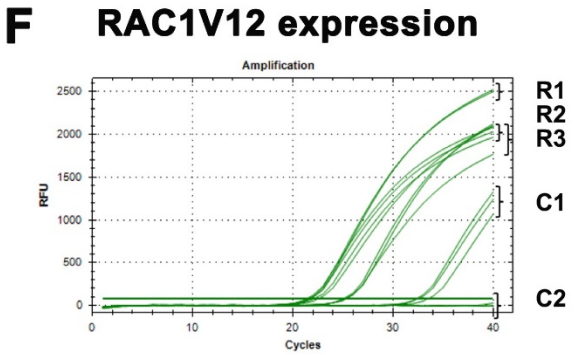
F
RAC1V12 expression
Amplification
RFU
2500
2000
1500
1000
500
0
0
10
20
30
40
Cycles
R1
R2
R3
C1
C2

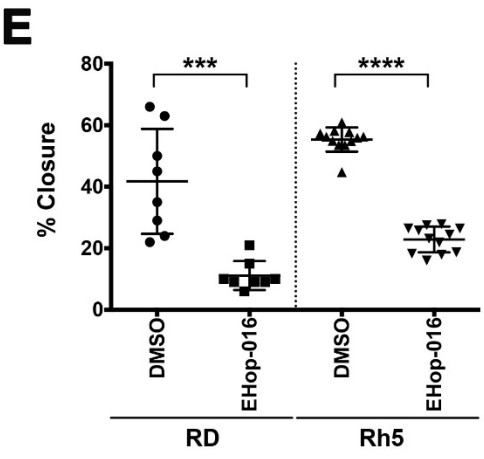
E
% Closure
80
60
40
20
0
***
****
DMSO
EHop-016
DMSO
EHop-016
RD
Rh5

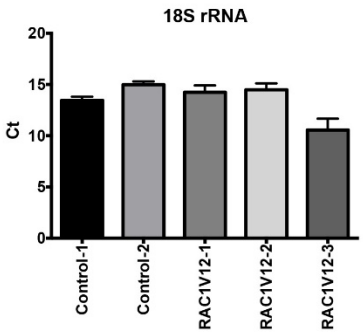
18S rRNA
Ct
20
15
10
5
0
Control-1
Control-2
RAC1V12-1
RAC1V12-2
RAC1V12-3

Figure S3

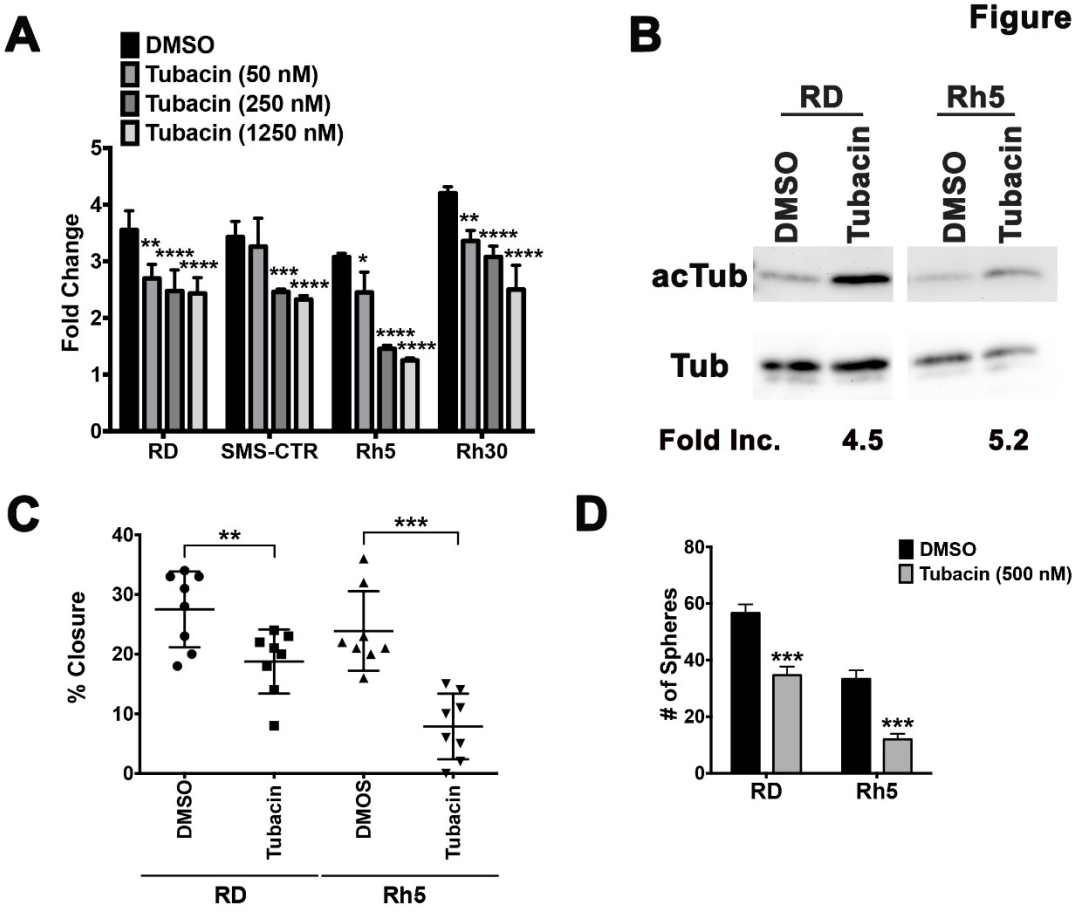
A
DMSO
Tubacin (50 nM)
Tubacin (250 nM)
Tubacin (1250 nM)
Fold Change
RD
SMS-CTR
Rh5
Rh30
B
RD
Rh5
DMSO
Tubacin
DMSO
Tubacin
acTub
Tub
Fold Inc.
4.5
5.2
C
% Closure
DMSO
Tubacin
DMOS
Tubacin
RD
Rh5
D
# of Spheres
DMSO
Tubacin (500 nM)
RD
Rh5

Fig. S4

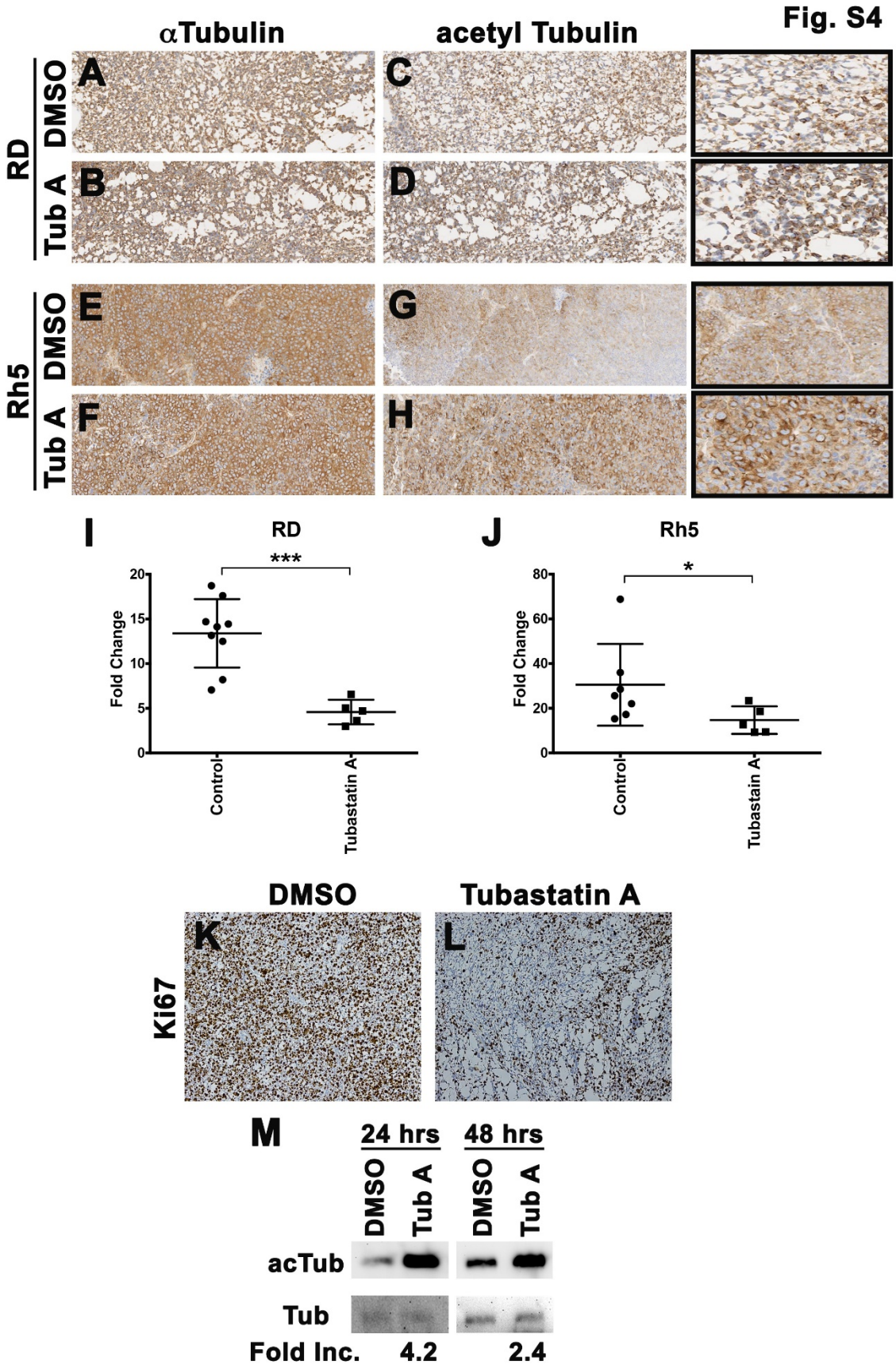
αTubulin
acetyl Tubulin
RD
DMSO
Tub A
Rh5
DMSO
Tub A
A
B
C
D
E
F
G
H
I
RD
***
Fold Change
20
15
10
5
0
Control
Tubastatin A
J
Rh5
*
Fold Change
80
60
40
20
0
Control
Tubastatin A
DMSO
Tubastatin A
Ki67
K
L
M
24 hrs
48 hrs
DMSO
Tub A
DMSO
Tub A
acTub
Tub
Fold Inc.
4.2
2.4

Table S1: RT-PCR Primers

Human	Forward	Reverse
MYOG	CCTGCCGTGGGCGTGTAAGG	GGACTGCAGGAGGCGCTGTG
MYOD1	AGCACTACAGCGGCGAT	GCGACTCAGAAGGCACGTC
CKM	CTCCTTCTCCGTCATGCTCT	GGTGGAGAAGCTCTCTGTGG
MYH8	ATTCTCGCGTGATCAGGATG	TGCCTACAGAGGCAAAAAGC
NANOG	TCTGGACACTGGCTGAATCCT	CGCTGATTAGGCTCCAACCAT
SOX2	GTCATTTGCTGTGGGTGATG	AGAAAAACGAGGGAAATGGG
POU5/OCT4	GGTTCTCGATACTGGTTCGC	GTGGAGGAAGCTGACAACAA
RAC1	AAACCGGTGAATCTGGGCTT	AAGAACACATCTGTTTGCGGA
Zebrafish	Forward	Reverse
hdac6	CTGAACACAGTTGGGCCTCTC	GCTCCGATCCATTCTGCCTT
18SrRNA	TCGCTAGTTGGCATCGTTTATG	CGGAGGTTCGAAGACGATCA

Figure Legends

Figure 1. HDAC6 expression in RMS and conserved function of HDAC6 in regulating RMS tumor growth. (A-E) Immunohistochemistry for HDAC6 in representative primary ERMS and ARMS tumors and skeletal muscle tissue. Weaker staining in (A-B) and stronger staining in (C-D). No staining in skeletal muscle (E). Scale bar = 100 um. Inset (outlined by bold rectangle) shows a higher-magnification view. (F) Summary of IHC results in ERMS (n = 7), ARMS (n = 11) and skeletal muscle (n = 5) from human patients. (G-J) Immunofluorescense for HDAC6 in (G-H) ERMS cell lines (RD and SMS-CTR) and (I and J) ARMS cell lines (Rh5 and Rh30). (K) A schematic of *hdac6* gRNA locations (exons 5 and 8) used for CRISPR-mediated gene targeting by lentivirus or tamoxifen-inducible system. (L) Summary of changes in cell growth by cell counts following transduction with lentivirus expressing Cas9 and double *HDAC6* gRNAs for gene knockout (KO) in a panel of RMS cell lines. The results shown are as fold change in cell counts 5 days post-plating and represent the average of 3 replicates for each cell line from one of 3 independent experiments. (M) Overexpression of GFP as a control, Cas9-resistant wild-type (wt) HDAC6 and Cas9-resistant catalytically-dead (cd) HDAC6 in tamoxifen (TAM)-inducible Cas9/*HDAC6* gRNA RD line to assess change in cell growth 6 days following TAM-induction. Results shown are the average of 4 replicates from one of 3 independent experiments. (N) Western blots against HDAC6 in ERMS cell lines (RD, 381T and SMS-CTR) and ARMS cell lines (Rh5 and Rh30) transduced with HDAC6 gRNAs and Cas9 6 days post-transduction (top panel); RD and Rh5 cells with TAM-inducible CRISPR-mediated targeted disruption of *HDAC6* (bottom left panel) and in RD TAM-inducible Cas9/*HDAC6* gRNA line overexpressing GFP, wt HDAC6 and cd HDAC6 (bottom right panel) 6 days post-TAM induction. *HDAC6*g = *HDAC6* gRNA. GAPDH was used as a loading control. % depletion relative to the control following normalization to GAPDH as the loading control was quantified by Image J. (O) A snapshot of genomic DNA sequencing results demonstrating a 5067-bp deletion in the *hdac6* locus in a representative CRISPR-targeted zebrafish tumor. gRNAs were designed against exons 5 and 10 of *hdac6*, which consists of 26 exons. (P-S) Representative zebrafish ERMS tumors expressing GFP scrambled gRNA control vector (P, R) and Cas9/*hdac6* gRNA (Q, S) over 7 days of growth. (T) Summary of tumor growth. n = 8 for control and n = 6 for *hdac6* gRNA-targeted ERMS tumors. Each error bar in graphs of L, M and T represents standard deviation. Two-tailed t-test; ** = $p < 0.01$; *** = $p < 0.001$; **** = $p < 0.0001$.

Figure 2. HDAC6 regulates RMS growth by modulating cell cycle progression and tumor cell differentiation. (A) EdU flow cytometry-based cell cycle analysis of tamoxifen-inducible Cas9-mediated *HDAC6* targeted RD and Rh5 cells day 6 post-tamoxifen treatment. *HDAC6*g =

HDAC6 gRNA. (B) Cell death analysis by Annexin V-based flow cytometry assay in the same RD and Rh5 cell lines 6 days post-tamoxifen treatment. Summary graphs in A-B are results from the average of 3 technical replicates from 1 representative experiment of 3 independent repeats. (C) Quantitation of immunofluorescence (IF) against MF20 in RD and Rh5 cells following 72 hours of serum starvation in 2% horse serum and 7 days post-tamoxifen-induced CRISPR/Cas9-mediated *HDAC6* targeting. Average of 4 fields at 400X for each condition was shown. (D-G) Representative IF images in RD (D-E) and Rh5 (F-G) cells. Scale bar = 100 microns. (H-I) Quantitative RT-PCR assessing expression of myogenic genes 7 days and 10 days post tamoxifen-induced CRISPR-mediated *HDAC6* gene disruption in RD and Rh5 cells. Results are the average of 4 replicates from one of three independent repeats. Two-tailed t-test was performed for data in A, B, C, H and I; * = $p < 0.05$; ** = $p < 0.01$; *** = $p < 0.001$; **** = $p < 0.0001$.

Figure 3. HDAC6 regulates RMS tumor cell migration and self-renewal. (A) Representative images from a wound healing scratch assay in RD cells with tamoxifen-induced CRISPR/Cas9 *HDAC6* targeting. Post = 16 hours post-scratch. Dashed lines indicate migrating fronts. (B) Summary of scratch assays in RD and Rh5 with tamoxifen-inducible CRISPR *HDAC6* targeting in RD and Rh5. Each datapoint represents a distinct area of the gap. The results shown are from one representative experiment of at least 3 repeats. (C) Representative images from a transwell migration assay. Cells migrated to the bottom chamber were stained with crystal violet at 22 hours post-seeding in the top chamber. (D) Summary of transwell migration assays in RD and Rh5 with tamoxifen-inducible CRISPR *HDAC6* targeting in RD and Rh5. Each data point represents a replicate well. Results shown are from one of 3 independent experiments. (E) Representative images from a sphere assay in RD cells. (F) Summary of sphere assays in RD and Rh5 cell lines 3 days post-plating. Shown are results of 4 replicates from one of 3 independent experiments. (G) RT-PCR analysis comparing expression levels of stem cell markers in RD sphere cells harboring no TAM control and TAM-induced *HDAC6*-targeting, TAM-induced *HDAC6*-targeting transduced with GFP expression construct and TAM-induced *HDAC6*-targeting transduced with Cas9-resistant wild-type HDAC6 expression construct harvested after 3 days of culturing in stem cell medium. Results were the average of 3 replicates from one of 3 independent experiments. Each error bar in B, D, F and G represents standard deviation. Two-tailed t-test in B, D and F; two-way ANOVA test in G; * = $p < 0.05$; ** = $p < 0.01$; *** = $p < 0.001$; **** = $p < 0.0001$.

Figure 4. HDAC6 regulates cytoskeletal dynamics to affect RMS cell migration. (A) Western blots against acetylated alpha-Tubulin and alpha-Tubulin in RD and Rh 5 cells with tamoxifen-induced CRISPR-mediated targeted disruption of *HDAC6* (day 6 post-tamoxifen). Fold increase in the levels of acetylated alpha-tubulin following normalization to the levels of alpha-tubulin was quantified using Image J. (B) Scratch assay assessing effects of adding back Cas9-resistant wild-type (wt) HDAC6 and catalytically-dead (cd) HDAC6 in RD cells with tamoxifen-induced *HDAC6* targeting. Results at 16 hours post-scratch are shown from one representative experiment of at least 3 repeats. (C) Phalloidin staining in RD cells with no tamoxifen control and tamoxifen-induced *HDAC6* CRISPR targeting following serum starvation and 15-minute EGF (50 ng/mL) treatment at day 6 post-tamoxifen treatment. Arrowheads point to representative areas of membrane ruffles and filopodia formation. Green = phalloidin, Blue = DAPI. (D) Double IF against HDAC6 (green) and RAC1 (red) in RD, showing HDAC6 and RAC1 expression in the regions of membrane ruffles (top panels) and folds (bottom panels), also highlighted by the arrowheads in merged panels. (E) RAC1 GTP pulldown assay in RD cells harboring no tamoxifen control and tamoxifen-induced *HDAC6* CRISPR targeting. (F) Summary of scratch assays assessing the effects of lentiviral overexpression of GFP as a control, RAC1V12, RAC1N17 and RHOAV14 in the presence of tamoxifen-induced CRISPR-mediated targeted disruption of *HDAC6* in RD cells at 16 hours post-scratch following 24 hours of serum starvation and 15 minutes of EGF (50 ng/mL) treatment. (G) Summary of cell growth change by cell counts over 6 days assessing the effects of overexpressing GFP as a control, RAC1V12 and RAC1N17 on cell growth of RD cells with tamoxifen-induced targeted disruption of *HDAC6*. Results were normalized to the no tamoxifen control for each comparison and represent the average of 4 replicates in one of 3 independent experiments. (H) RAC1-GTP pulldown assay in RD cells overexpressing GFP, RAC1V12 and RAC1N17 following 24 hours of serum starvation and 15 minutes of EGF (50 ng/mL) treatment. Each error bar in B, F and G represents standard deviation. Two-tailed t-test in B and G, one-way ANOVA test in F; NS = no significance, $p < 0.05$; ** = $p < 0.01$; *** = $p < 0.001$; **** = $p < 0.0001$.

Figure 5. RAC1V12 promotes ERMS tumor growth and invasion. (A) Representative images of RD cells harboring safe-harbor control targeting and *RAC1* gRNA targeting in a wound healing scratch assay. Dashed lines indicate migrating fronts. (B) Summary of scratch assays in RD and Rh5 cells with targeted disruption of *RAC1*. Each assay was analyzed at 16 hours post-scratch. The results from one of 3 independent replicate experiments are shown. (C) Summary of scratch assays in RD cells transduced with lentivirus expressing safe-habor control gRNA, *RAC1* gRNA, *RAC1* gRNA + GFP, *RAC1* gRNA + RAC1V12 and analyzed at 16 hours post-

scratch following plating at the same cell density at 80-90% confluence. (D) Summary of cell counts in RD and Rh5 cells at 7 days post-plating following lentiviral CRISPR/Cas9-mediated *RAC1* gene disruption (starting cell density = 10,000). (E) Representative images of KRASG12D-induced zebrafish ERMS tumors co-expressing GFP and an empty vector (control) or mutant RAC1V12 at day 7, 14 and 21 post-transplantation. (F) Summary growth volume change for each fish over the first 7 days. n = 8 for control and n = 12 for human RAC1V12-expressing tumors. (G) Representative H&E images of control and RAC1V12 expressing zebrafish ERMS tumors. Lower panels show higher magnification with arrow heads indicating areas of skeletal muscle invasion by tumor cells. (H) Correlation of *RAC1* expression levels with overall survival outcome in RMS patients (63 fusion-negative and 18 fusion-positive) by Kaplan-Meier analysis. Error bars in graphs of B, C, D and F represent standard deviation. Two-tailed t-test in B, D and F. One-way ANOVA with multiple comparisons in C; *** = $p < 0.001$; **** = $p < 0.0001$.

Figure 6. Tubastatin A treatment of RMS cells mimics the HDAC6 loss-of-function phenotypes. (A) Cell Titer Glo viability assays assessing the dose-dependent effect of tubastatin A on cell growth of RD and Rh5 cells over 5 days. Each dose was done in 4 replicate wells. Results from one representative experiment of at least 3 repeats are shown. (B) Western blots with antibodies against acetylated alpha-tubulin (acTub) and alpha-tubulin (Tub) in RD and Rh5 cells treated with DMSO (vehicle control) or tubastatin A (200 nM) at 24 hours. Fold increase in the levels of acetylated alpha-tubulin following normalization to the levels of alpha-tubulin was quantified using Image J. (C) Representative images from a scratch assay in RD cells following treatment with DMSO (vehicle) or tubastatin A (200 nM). (D) Summary of scratch assay analysis in RD and Rh5 cells treated with DMSO or tubastatin A (16 hours post-scratch). Results shown are from one representative experiment of 3 repeats. (E) Representative images of sphere assays in RD and Rh5 cells treated with DMSO or tubastatin A (200 nM) for 3 days. (F) Summary of sphere assay analysis in RD and Rh5 cells from one representative experiment of 3 repeats. (G-H) RMS xenografts were established using the RD cell line (G) and Rh5 cell line (H) and treated with tubastatin A (10 mg per kg per mouse, intraperitoneal injections every 3 days for up to 21 days). Treatment for Rh5 xenografts ended early due to many control tumors reaching tumor end point (750 mm^3) per approved animal protocol. Tumor volume change over the treatment period is shown for each tumor-bearing mouse. Each data point represents a mouse. Each error bar in the graphs of A, D and F represents standard deviation. Two-tailed Student's t-test; * = $p < 0.05$; ** = $p < 0.01$; *** = $p < 0.001$; **** = $p < 0.0001$.

SUPPLEMENTAL FIGURE LEGENDS

Figure S1. Conserved role of HDAC6 in regulating RMS cell growth. (A) Summary of cell counts. Rh5 cells transduced with lentivirus expressing safe-harbor control gRNAs, *HDAC6* gRNAs, *HDAC6* gRNAs in combination with Cas9-resistant wild-type (wt) HDAC6 or GFP were plated for cell counts at day 5 post-transduction, and cell counts were performed on day 5 post-plating. NS = no significance; * $p < 0.05$; ** $p < 0.01$; *** $p < 0.001$ by one-way ANOVA test with multiple comparisons. (B) Summary of cell counts in RD and Rh5 cells transduced with GFP and wild-type HDAC6 lentiviral expression constructs. Counts were done 5 days post-plating. $p > 0.05$ by two-tailed t-test. (C) Left panel: Quantitative PCR amplification plot showing expression of *hdac6* and 18S rRNA (loading control) in 8 zebrafish ERMS tumors. (D) Summary of quantitative RT-PCR showing expression of *hdac6* in 8 zebrafish ERMS tumors targeted with GFP scrambled control gRNAs and 8 zebrafish tumors targeted with *hdac6* gRNAs. Expression was normalized to control tumor 1 for easier data visualization. ** = $p < 0.01$ by Mann Whitney non-parametric test. Error bar represents standard deviation of 3 technical replicates. (E) Kaplan-Meier analysis of tumor-free survival. n = 227 for GFP scrambled control gRNA-injected tumor fish, and n = 277 for *hdac6* double gRNA-injected tumor fish. Log rank test was performed.

Figure S2. HDAC6 and RAC1 regulate cytoskeletal changes required for RMS cell migration. (A) Summary of scratch assays in Rh5 cells transduced with lentivirus expressing safe-harbor (SH) control gRNAs, *HDAC6* gRNAs, *HDAC6* gRNAs and GFP, *HDAC6* gRNAs and Cas9-resistant wild-type HDAC6. Gap closure was assessed at 16 hours post-scratch. (B) Phalloidin IF staining of Rh5 cells with no tamoxifen-induced targeting (top panel) and tamoxifen-induced *HDAC6* gene targeting by CRISPR/Cas9 (bottom panel). HDAC6g = *HDAC6* gRNA. Arrowheads point to examples of membrane ruffles. (C) Co-IF staining of HDAC6 and RAC1 in Rh5 cells following serum starvation and 15-minute EGF (50 ng/ml) treatment. Green = HDAC6, Red = RAC1. Arrow heads indicate co-localization of HDAC6 and RAC1 at membrane ruffles. (D) Western blots against RAC1 and GAPDH (loading control) using lysates isolated from RD and Rh5 harboring either safe-harbor control (C) or *RAC1* gRNA (R) targeting. (E) Scratch assays of RD and Rh5 cells treated with 1 □M EHop-016 and DMSO (vehicle). The results are from one representative experiment of at least 3 repeats. Error bar represents standard deviation. *** = $p < 0.001$, **** = $p < 0.0001$ by unpaired t-test. (F) Top panel: Quantitative PCR amplification plot showing expressing of human *RAC1V12* in 3 independent zebrafish ERMS tumors, but no or non-specific amplification after cycle 30 in 2 independent

empty vector-expressing control tumors. Bottom panel: Ct values of 18S rRNA (as loading control) in all samples.

Figure S3. Treatment with tubacin inhibits RMS tumor growth, migration and self-renewal. (A) ATP-based Cell Titer Glo viability assays to assess cell growth in RD, SMS-CTR, Rh5 and Rh30 cells treated with tubacin at varying concentrations over 5 days. Results from one representative experiment (4 replicates per drug concentration) of 3 repeats are shown. Error bar represents standard deviation. One-way ANOVA test, ** = $p < 0.01$; *** = $p < 0.001$; **** = $p < 0.0001$. (B) Western blots against acetylated alpha-tubulin and alpha-tubulin in RD and Rh5 cells treated with 500 nM of tubacin at 24 hours. Fold increase in the levels of acetylated alpha-tubulin was quantified using ImageJ. (C) Summary of scratch assay analysis in RD and Rh5 cells treated with DMSO or tubacin (500 nM) at 16 hours post-scratch. Results shown are from one representative experiment of 3 repeats. Two-tailed t-test, ** = $p < 0.01$; *** = $p < 0.001$. (D) Summary of sphere assay analysis in RD and Rh5 cells treated with tubacin (500 nM) for 3 days from one representative experiment of 3 repeats. Two-tailed t-test, *** = $p < 0.001$.

Figure S4. Treatment with tubastatin A inhibits HDAC6 activity *in vivo*. (A-H) Immunohistochemistry at 100x magnification for alpha-tubulin (A-B, E-F) and acetylated alpha-tubulin (C-D, G-H) performed on paraffinized tissue sections from RD (A-D) and Rh5 (E-H) tumor xenografts harvested at the end of treatment period with tubastain A. Inset panels with higher magnification (~800x) are shown in boxed panels on the far right. (I-J) Summary of tumor volume change over treatment period in xenografts established using RD (I) and Rh5 (J) cells treated with DMSO (vehicle control) and tubastatin A (10 mg per kg per mouse, drug injection every 3 days for up to 21 days). (K-L) Immunohistochemistry for Ki67 performed on RD xenografts treated with DMSO (K) and tubastatin A (L) harvested at treatment endpoint. Representative images were taken at 100x magnification. (M) Western blots against acetylated alpha-tubulin and alpha-tubulin in tumors isolated from 21-day-old ERMS tumor-bearing fish treated with 10 mM tubastatin A or DMSO (vehicle control) for 24 hours and 48 hours. Fold increase in the levels of acetylated alpha-tubulin following normalization to the levels of alpha-tubulin was quantified using ImageJ.

Table S1. RT-PCR primers. Human and zebrafish RT-PCR primer sequences.

References

1. Shern, J. F. *et al.* Comprehensive genomic analysis of rhabdomyosarcoma reveals a landscape of alterations affecting a common genetic axis in fusion-positive and fusion-negative tumors. *Cancer Discov* **4**, 216–31 (2014).

2. Barr, F. G. *et al.* Rearrangement of the PAX3 paired box gene in the paediatric solid tumour alveolar rhabdomyosarcoma. *Nat Genet* **3**, 113–7 (1993).

3. Jankowski, K. *et al.* Both hepatocyte growth factor (HGF) and stromal-derived factor-1 regulate the metastatic behavior of human rhabdomyosarcoma cells, but only HGF enhances their resistance to radiochemotherapy. *Cancer Res* **63**, 7926–35 (2003).

4. Miekus, K. *et al.* The decreased metastatic potential of rhabdomyosarcoma cells obtained through MET receptor downregulation and the induction of differentiation. *Cell Death Dis* **4**, e459 (2013).

5. Ignatius, M. S. *et al.* tp53 deficiency causes a wide tumor spectrum and increases embryonal rhabdomyosarcoma metastasis in zebrafish. *Elife* **7**, (2018).

6. Hosoyama, T. *et al.* IL-4R drives dedifferentiation, mitogenesis, and metastasis in rhabdomyosarcoma. *Clin Cancer Res* **17**, 2757–66 (2011).

7. Chen, E. Y. *et al.* Cross-species array comparative genomic hybridization identifies novel oncogenic events in zebrafish and human embryonal rhabdomyosarcoma. *PLoS Genet* **9**, e1003727 (2013).

8. Kreso, A. & Dick, J. E. Evolution of the cancer stem cell model. *Cell Stem Cell* **14**, 275–91 (2014).

9. Chen, D. *et al.* Targeting BMI1(+) Cancer Stem Cells Overcomes Chemoresistance and Inhibits Metastases in Squamous Cell Carcinoma. *Cell Stem Cell* **20**, 621-634 e6 (2017).

10. Hu, S. *et al.* Antagonism of EGFR and Notch limits resistance to EGFR inhibitors and radiation by decreasing tumor-initiating cell frequency. *Sci Transl Med* **9**, (2017).

11. Goto, N. *et al.* Lineage tracing and targeting of IL17RB(+) tuft cell-like human colorectal cancer stem cells. *Proc Natl Acad Sci U A* **116**, 12996–13005 (2019).

12. Saygin, C., Matei, D., Majeti, R., Reizes, O. & Lathia, J. D. Targeting Cancer Stemness in the Clinic: From Hype to Hope. *Cell Stem Cell* **24**, 25–40 (2019).

13. Du, F. Y., Zhou, Q. F., Sun, W. J. & Chen, G. L. Targeting cancer stem cells in drug discovery: Current state and future perspectives. *World J Stem Cells* **11**, 398–420 (2019).

14. Walter, D. *et al.* CD133 positive embryonal rhabdomyosarcoma stem-like cell population is enriched in rhabdospheres. *PLoS One* **6**, e19506 (2011).

15. Ignatius, M. S. *et al.* In vivo imaging of tumor-propagating cells, regional tumor heterogeneity, and dynamic cell movements in embryonal rhabdomyosarcoma. *Cancer Cell* **21**, 680–93 (2012).

16. Chen, E. Y. *et al.* Glycogen synthase kinase 3 inhibitors induce the canonical WNT/beta-catenin pathway to suppress growth and self-renewal in embryonal rhabdomyosarcoma. *Proc Natl Acad Sci U A* **111**, 5349–54 (2014).

17. Hayes, M. N. *et al.* Vangl2/RhoA Signaling Pathway Regulates Stem Cell Self-Renewal Programs and Growth in Rhabdomyosarcoma. *Cell Stem Cell* **22**, 414-427 e6 (2018).

18. Phelps, M. P., Bailey, J. N., Vleeshouwer-Neumann, T. & Chen, E. Y. CRISPR screen identifies the NCOR/HDAC3 complex as a major suppressor of differentiation in rhabdomyosarcoma. *Proc Natl Acad Sci U A* (2016) doi:10.1073/pnas.1610270114.

19. Tran, A. D. *et al.* HDAC6 deacetylation of tubulin modulates dynamics of cellular adhesions. *J Cell Sci* **120**, 1469–79 (2007).

20. Zhang, X. *et al.* HDAC6 modulates cell motility by altering the acetylation level of cortactin. *Mol Cell* **27**, 197–213 (2007).

21. Wu, J. Y. *et al.* Histone deacetylase 6 (HDAC6) deacetylates extracellular signal-regulated kinase 1 (ERK1) and thereby stimulates ERK1 activity. *J Biol Chem* **293**, 1976–1993 (2018).

22. Yang, M. H. *et al.* HDAC6 and SIRT2 regulate the acetylation state and oncogenic activity of mutant K-RAS. *Mol Cancer Res* **11**, 1072–7 (2013).

23. Gao, Y. S. *et al.* Histone deacetylase 6 regulates growth factor-induced actin remodeling and endocytosis. *Mol Cell Biol* **27**, 8637–47 (2007).

24. Kozyreva, V. K. *et al.* NEDD9 regulates actin dynamics through cortactin deacetylation in an AURKA/HDAC6-dependent manner. *Mol Cancer Res* **12**, 681–93 (2014).

25. Yin, Z., Xu, W., Xu, H., Zheng, J. & Gu, Y. Overexpression of HDAC6 suppresses tumor cell proliferation and metastasis by inhibition of the canonical Wnt/beta-catenin signaling pathway in hepatocellular carcinoma. *Oncol Lett* **16**, 7082–7090 (2018).

26. Marampon, F. *et al.* HDAC4 and HDAC6 sustain DNA double strand break repair and stem-like phenotype by promoting radioresistance in glioblastoma cells. *Cancer Lett* **397**, 1–11 (2017).

27. Yang, W., Liu, Y., Gao, R., Yu, H. & Sun, T. HDAC6 inhibition induces glioma stem cells differentiation and enhances cellular radiation sensitivity through the SHH/Gli1 signaling pathway. *Cancer Lett* **415**, 164–176 (2018).

28. Langenau, D. M. *et al.* Effects of RAS on the genesis of embryonal rhabdomyosarcoma. *Genes Dev* **21**, 1382–95 (2007).

29. Pastrana, E., Silva-Vargas, V. & Doetsch, F. Eyes wide open: a critical review of sphere-formation as an assay for stem cells. *Cell Stem Cell* **8**, 486–98 (2011).

30. Hubbert, C. *et al.* HDAC6 is a microtubule-associated deacetylase. *Nature* **417**, 455–8 (2002).

31. Guo, F., Debidda, M., Yang, L., Williams, D. A. & Zheng, Y. Genetic deletion of Rac1 GTPase reveals its critical role in actin stress fiber formation and focal adhesion complex assembly. *J Biol Chem* **281**, 18652–9 (2006).

32. Lof-Ohlin, Z. M. *et al.* EGFR signalling controls cellular fate and pancreatic organogenesis by regulating apicobasal polarity. *Nat Cell Biol* **19**, 1313–1325 (2017).

33. Hu, Y. & Smyth, G. K. ELDA: extreme limiting dilution analysis for comparing depleted and enriched populations in stem cell and other assays. *J Immunol Methods* **347**, 70–8 (2009).

34. Dogterom, M. & Koenderink, G. H. Actin–microtubule crosstalk in cell biology. *Nat. Rev. Mol. Cell Biol.* **20**, 38–54 (2019).

35. Zhuang, X. *et al.* Differential effects on lung and bone metastasis of breast cancer by Wnt signalling inhibitor DKK1. *Nat Cell Biol* **19**, 1274–1285 (2017).

36. Kamai, T. *et al.* Increased Rac1 activity and Pak1 overexpression are associated with lymphovascular invasion and lymph node metastasis of upper urinary tract cancer. *BMC Cancer* **10**, 164 (2010).

37. Wu, L. *et al.* MicroRNA-142-3p, a new regulator of RAC1, suppresses the migration and invasion of hepatocellular carcinoma cells. *FEBS Lett* **585**, 1322–30 (2011).

38. Kawaguchi, Y. *et al.* The deacetylase HDAC6 regulates aggresome formation and cell viability in response to misfolded protein stress. *Cell* **115**, 727–738 (2003).

39. Vleeshouwer-Neumann, T. *et al.* Histone Deacetylase Inhibitors Antagonize Distinct Pathways to Suppress Tumorigenesis of Embryonal Rhabdomyosarcoma. *PLoS One* **10**, e0144320 (2015).

40. Xu, L. *et al.* Integrative Bayesian Analysis Identifies Rhabdomyosarcoma Disease Genes. *Cell Rep* **24**, 238–251 (2018).

Chapter 4: Identifying rhabdomyosarcoma (RMS) tumor propagating cell (TPC) markers to study RMS disease relapse

AUTHORS: Thao Pham[1], Phuong Van[2], Xiao Chu Lin[3], Eleanor Y. Chen[1]

1. Department of Pathology, University of Washington, Seattle, WA

2. Fred Hutchinson Cancer Research Institute, Seattle, WA

3. Emory University, Atlanta, GA

Introduction

Rhabdomyosarcoma (RMS) is a common pediatric soft-tissue sarcoma with a poor patient survival outlook following RMS disease relapse[1]. Tumor propagating cells (TPCs) are believed to be responsible for disease relapse and metastasis of some cancer types, such as breast and lung cancer[2–4]. TPCs possess stem cell-like characteristics that allow for the recapitulation of tumor heterogeneity in its entirety[5]. A zebrafish ERMS disease model successfully identified *myf5* as a marker for TPCs[6]. Serial transplantation of *myf5* expressing ERMS tumor cells into new zebrafish hosts results in the formation of new heterogenous tumors[6]. However, there is currently no validated marker for studying TPCs in human RMS cancer cells. The spheroid assay is a surrogate *in vitro* assay that is commonly used to assess self-renewal[7]. Cells are grown in suspension in medium containing a collection of various growth factors (EGF, FGF, bFGF, etc.) that promote the growth and expansion of cells with stem-cell like characteristics[7]. As such, the spheroid assay is an imperfect tool for the study of TPCs, as any cell that possesses stem-cell like characteristics may proliferate. The ability to more accurately define and isolate RMS TPCs would allow for identification of novel therapeutic avenues for treating RMS disease relapse and metastasis

CD133 is a transmembrane glycoprotein that is commonly used as a marker of both cancer and non-cancerous stem cells[8–11]. Several studies have also implicated the role of CD133 as a potential marker of RMS TPCs. CD133 labels a subpopulation of chemo-resistant RMS cancer cells that express high levels of genes associated with muscle satellite cells[10–13]. While CD133 shows promise as a potential marker of RMS TPCs, current studies are limited to using expensive, antibody-based labeling of CD133 positive cells. Commonly recognized CD133 epitopes have the potential to be hidden or inaccessible due to changes in glycosylation patterns, which may impact accurate CD133 representation[14,15]. Thus, there exists a need for a cheaper and more consistent form of CD133 cell labeling.

Endoplasmic reticulum to nucleus signaling 1 (ERN1), also known as IRE1α, is a transmembrane protein kinase that is part of the unfolded protein response (UPR) pathway[16]. Upon endoplasmic reticulum (ER) stress, ERN1 may initiate downstream signaling of the UPR pathway through unconventional splicing of *XBP1* or post-transcriptional modifications via Regulated IRE1-dependent Decay (RIDD) of RNA[16,17]. ERN1 activity has also been implicated in some cancer types, such as breast, colon and pre-leukemic stem cells. In a breast cancer cell line, siRNA mediated knockdown of ERN1 reduces tumor cell growth *in vitro* and *in vivo*[18]*.* Knockdown of ERNS also suppresses proliferation of colon cancer cells *in vitro* and xenograft growth *in vivo*[19]*.* Loss of ERN1 also reduces spheroid formation capacity of colon cancer stem

cells[19]. NRASG12D, an oncogenic mutant form of wild-type NRAS, activates ERN1-XBP1 in mouse hematopoietic stem cells (HSCs), reducing ER-stress induced apoptosis in both quiescent and proliferative HSCs[20]. However, we currently lack insight into the role of ERN1 in RMS pathogenesis. ERN1 was identified as a potential regulator of RMS self-renewal through an siRNA library screen against the human kinome. Having been implicated in regulating TPC activity in other cancer types, ERN1 is a promising candidate for its role in regulating the function of RMS TPCs.

In this chapter, I investigate the potential role of CD133 as an ERMS TPC marker and show through RT-PCR expression analysis that CD133 is highly upregulated in ERMS spheroid cells compared to adherent controls. Using a novel CRISPR/Cas9 mediated gene knock-in approach, we generated an ERMS CD133-GFP reporter cell line. My findings so far show that ERN1 is a novel regulator of both ERMS cell growth and self-renewal. Overall, this chapter highlights preliminary findings from my experiments investigating the potential of CD133 as an ERMS TPC marker and proposes future directions.

Results

Identification of *CD133* as a potential ERMS TPC marker and creation of a novel reporter cell line.

To identify potential gene markers for an ERMS TPC population, we performed RT-PCR expression analysis on a panel of candidate genes (*MYF5, PAX7, CD82, CD133)* in an ERMS cell line (381T). *MYF5, PAX7,* and *CD82* were identified due to their role in regulating muscle satellite cell homeostasis and myogenic fate commitment[21,22]. *CD133* expression has been shown to be enriched following ERMS spheroid induction[13]. Expression of each candidate gene was compared between adherent and spheroid cells from increasing number of passages. We observed that *CD133* expression significantly increased following serial passaging of 381T, SMS-CTR and JR1 ERMS spheroids (Figure 1A-B). Expression of *MYF5, PAX7* and *CD82* did not see any significant change between adherent and spheroid cells (Figure 1A). In order to rapidly identify and isolate *CD133*-expressing ERMS spheroid cells, we developed a novel CRISPR/Cas9 mediated gene knock-in approach to endogenously label *CD133* expression with green fluorescent protein (GFP) (Figure 1C). We tested our knock-in approach in SMS-CTR cells and isolated clonal populations. Following clonal isolation of spheroid cell populations, we identified one SMS-CTR clonal population (Clone 9) with successful endogenous integration of the knock-in GFP reporter cassette through PCR amplification and sequencing (Figure 1D). Future references from here on out regarding our SMS-CTR CD133-GFP reporter cell line will

be referring to Clone 9. To determine whether our SMS-CTR CD133-GFP reporter cell line behaves similarly to wild-type SMS-CTR cells, we compared cell growth kinetics. Preliminary ATP-based viability data showed that our SMS-CTR CD133-GFP reporter cell line grew at a similar rate as wild-type SMS-CTR cells (Figure 1E). Following culturing in the stem cell medium, approximately 0.45% of the spheroid cells generated from the SMS-CTR CD133-GFP reporter cell line expressed GFP (Figure 1F). Serial passaging of spheroids increased the percentage of GFP expressing cells to 2.4% (~5x fold) (Figure 1F). In summary, preliminary findings showed that *CD133* expression was upregulated in ERMS spheroid cells compared to adherent cells. Using a novel CRISPR/Cas9 mediated gene knock-in approach, we generated a *CD133-GFP* reporter cell line. Serial passaging of our CD133 reporter cell line increased *CD133* expression, in line with our RT-PCR data. Together, it appears *CD133* has potential for being a promising gene marker for ERMS TPCs.

Characterization of *ERN1* and other potential TPC regulators using a CD313 ERMS reporter cell line.

Previous work from our lab identified GRK5 and HDAC6 as novel regulators of RMS self-renewal capacity (Chapters 2, 3). GRK5 was identified through a siRNA library screen against the human kinome (714 kinases) in two ERMS cell lines (RD and 381T). To identify potential candidate kinases that specifically regulate self-renewal of ERMS, we performed RT-PCR on candidate kinase genes to identify those upregulated in spheroid cells compared to adherent cells. RT-PCR analysis identified *ERN1* in a panel of ERMS cell lines (381T, SMS-CTR, JR1) as being upregulated in spheroids compared to adherent cells (Figure 2A). We subsequently utilized a high-efficiency CRISPR/Cas9 gene targeting strategy[23] to validate the loss-of-function effect of *ERN1* on self-renewal of 381T and SMS-CTR ERMS cells (Figure 2B). Genetic disruption of *ERN1* was then verified via PCR amplification of the genomic deletion event (Figure 2B). CRISPR/Cas9-mediated disruption of *ERN1* significantly reduced (p-value < 0.05) the self-renewal capacity of ERMS cells via spheroid assay in both cell lines (381T, SMS-CTR) (Figure 2C). Loss of ERN1 also resulted in a significant reduction in cell viability in both ERMS cell lines (381T, SMS-CTR) (p-value < 0.05) through an ATP-based viability assay (Figure 2D). To determine the effect of ERN1, GRK5 or HDAC6 depletion on TPC proportions, we utilized our previously described SMS-CTR CD133-GFP reporter cell line. Preliminary findings showed that CRISPR/Cas9 mediated disruption of *GRK5, ERN1*, or *HDAC6* resulted in an increase percentage of *CD133* positive cells of 5.3%, 15.2% and 3.8% respectively, compared to controls (2.3%) (Figure 2E). From our preliminary results, we have identified *ERN1*

as a novel regulator of both ERMS self-renewal and cell growth, with loss of ERN1 resulting in an increase of CD133 positive cells.

Future experiments for validation of SMS-CTR CD133-GFP reporter cell line.

In this section, I will propose potential future directions and experiments for completion of the ERMS CD133 project. The first major goal is to validate our SMS-CTR CD133-GFP cell line as a potential reporter of ERMS TPCs. *In vivo* limiting dilution xenograft experiments are considered a gold standard for studying self-renewal potential of TPCs. Therefore, I propose performing limiting dilution xenograft experiments in immunocompromised NOD-scid-IL2Rgammanull (NSG) mice using our SMS-CTR CD133-GFP reporter cell line (Figure 3A). If CD133 labels ERMS TPCs, I hypothesize that there will be a significantly higher rate of engraftment for CD133 (+) ERMS cells compared to CD133 (-) cells (Figure 3A). To determine whether GFP expression is an accurate readout of CD133 in spheroid cells, I propose assessing *CD133* expression using RT-PCR in GFP positive and negative SMS-CTR CD133-GFP spheroid cells (Figure 3B). I hypothesize that GFP positive cells will show enriched *CD133* expression compared to GFP negative cells. As TPCs have been shown to possess drug resistance to chemotherapeutic agents, I propose treating CD133 (+) and CD133 (-) cells with vincristine, a standard-of-care chemotherapy agent for RMS and assess growth kinetics via an ATP-based assay (Figure 3B). If CD133 labels ERMS TPCs, I hypothesize CD133 (+) cells to show enhanced resistance compared to CD133 (-) cells response to the treatment with vincristine. Time lapse imaging of SMS-CTR CD133-GFP single cell suspensions using high resolution fluorescent microscopy would allow for visual characterization of ERMS TPCs cellular division dynamics (Figure 3C). If CD133 (+) cells give rise to CD133 (+) daughter cells following symmetric or asymmetric division, this would support the hypothesis of CD133 as an ERMS TPC marker and that TPC exist as a constant population (Figure 3C). If we instead see that CD133 (-) cells can give rise to CD133 (+) daughter cells following division, this could mean CD133 may label mature ERMS TPCs instead of more naïve ERMS TPCs. It is also possible that ERMS TPCs exist as a transitory state and CD133 mark ERMS cells that are currently ERMS TPCs. These experiments will help determine whether our SMS-CTR CD133-GFP cell line sufficiently functions as a potential ERMS TPCs reporter cell line.

Following validation of our SMS-CTR CD133-GFP cell line, I propose using it to assess the role of novel regulators of RMS self-renewal (e.g. *GRK5, HDAC6, ERN1)* in regulating ERMS TPCs cell cycle, apoptosis and senescence (Figure 3D). Following CRISPR/Cas9 mediated knockout of a gene of interest using our SMS-CTR CD133-GFP cell line, flow

cytometry-based cell sorting of spheroid cells will enrich for CD133 (+) and CD133 (-) populations (Figure 3D). From here, EdU-based cell labeling for cell cycle analysis, Annexin V assay for apoptosis, or β-Galactosidase staining to assess senescence can be performed (Figure 3D). This will allow us to better determine whether a reduction in self-renewal capacity through use of the spheroid assay is due to alterations in ERMS TPC cell cycle progression, cell death or senescence.

Ongoing projects.

In collaboration with Cailyn Spurrell of the Brotman Baty Institute at the University of Washington, we performed single cell RNA (scRNA) sequencing of 381T wild-type and GRK5 depleted spheroid cells. We have recently received the raw data and are currently working to analyze it with the help of Dr. Jing-Ru Jhan, a post-doctoral fellow in the Chen lab (Figure 3C). By studying the genetic composition of ERMS spheroids, we hope to gain insight into the heterogeneity of cell sub-populations, molecular signatures of CD133+ cell population and additional candidate TPC gene markers (Figure 3C). If we see unique population clustering based on CD133 expression, it will lend additional support to our SMS-CTR CD133-GFP cell line as a reporter of ERMS TPCs.

To study the role of TPCs in relapse ERMS tumors, we generated chemo resistant RMS cancer cell lines. RMS cancer cell lines of embryonal (RD) and alveolar (Rh30) subtypes were grown in gradually increasing doses of common chemotherapeutics, vincristine and D-actinomycin (Figure 3C). To confirm resistance to drug treatment, we will assess viability of wild-type and drug-resistant RMS cells in varying doses of vincristine or D-actinomycin. We hypothesize that resistant cells are less sensitive to drug treatment compared to wild-type RMS cells. We hope to investigate the role of TPCs in mediating treatment resistance in our chemo-resistant cell lines and their role in driving RMS disease relapses (Figure 3D).

Discussion

In this chapter we have shown preliminary data in characterizing the potential role of CD133 as an ERMS TPC marker. RT-PCR expression analysis of CD133 shows upregulation in ERMS spheroid cells compared to adherent controls. To quickly and inexpensively identify CD133 expressing ERMS spheroid cells for characterization, we generated an ERMS CD133-GFP reporter cell line. ERN1 was identified as a novel regulator of ERMS tumor cell growth and self-renewal. Loss of ERN1 resulted in an increase percentage of SMS-CTR CD133 positive spheroid cells compared to controls. We also introduce future directions that include validation

of our SMS-CTR CD133-GFP reporter cell line, analysis of ERMS spheroid scRNA sequencing results, and characterization of TPCs in chemo resistant RMS cancer cell lines.

In human ERMS cancer cell lines, we found low levels of MYF5 expression in both adherent and spheroid cells, therefore MYF5 is not an ideal TPC marker for human ERMS. CD133-positive RMS cells express higher levels of muscle progenitor genes and are more resistant to chemotherapeutic agents, making it a promising marker for potential TPCs[12,13]. We found enriched expression of *CD133* in ERMS spheroid cells of 3 independent ERMS cancer cell lines (381T, SMS-CTR, JR1). We subsequently generated a novel SMS-CTR CD133-GFP reporter cell line. Serial passaging of SMS-CTR CD133-GFP spheroid cells showed a similar fold increase in GFP expressing cells as *CD133* expression. *In vivo* limiting dilution xenograft experiments using our SMS-CTR CD133-GFP reporter cell line is required to validate potential labeling of ERMS TPCs. A study using antibody based cell sorting showed xenografted CD133 positive ERMS spheroid cells giving rise to heterogenous tumors in mice[13]. Interestingly, the reported percentage of CD133 positive adherent and spheroid cells, differ greatly amongst different studies as well as our SMS-CTR CD133-GFP reporter cell line[12,13,15]. This variance could be due to known CD133 epitope masking resulting from changes in glycosylation patterns[15]. Additionally, the use of antibodies for large cell sorting experiments can be expensive and different brands have been shown to report different percentages of CD133 positive adherent and spheroid cells[12,13,15]. The use of a CD133-GFP reporter line would be less expensive and fewer technical complications than antibodies[15]. We have also recently begun analyzing scRNA sequencing data of 381T spheroid cells to study the genetic composition of potential TPCs. This could allow for the identification of additional, or more precise, ERMS TPCs gene markers. In addition, a CRISPR/Cas9 knockout screen against genes identified in our scRNA sequence data could help find key essential regulators of ERMS TPC survival.

Increased ERN1 activity has been proposed to prevent ER stress induced apoptosis in cancer cells and pre-leukemic HSCs[18,19]. In this chapter, we present preliminary results that indicate ERN1 as a novel regulator of ERMS cell growth and self-renewal. Early findings see, while loss of ERN1 reduced self-renewal capacity in the form of fewer spheroids, depletion of ERN1 in our SMS-CTR CD133-GFP reporter cell line resulted in an increase in GFP positive cells. This finding was unexpected, as we hypothesized a reduction in spheroid size and numbers following loss of ERN1 would result in fewer ERMS TPCs. If our SMS-CTR CD133-GFP cell line is found to label ERMS TPCS, we would then be able to characterize CD133 (+) vs CD133 (-) ERN1 loss of function spheroid cells. We could investigate whether the increase in GFP positive cells is due to increased cell death in CD133 (-) or induced senescence in CD133

(+) cells. Further study is required to understand how loss of ERN1 effects ERMS TPC behavior.

Tumor cell heterogeneity is believed to contribute to cancer cell resistance of chemotherapeutic agents[24]. Along with a glim survival outlook, patients with relapsed or metastatic RMS disease respond poorly to previously used chemotherapeutics[1]. A majority of chemotherapeutic agents target rapidly diving cells, which are ineffective against TPCs[5,24]. CD133 expressing ERMS spheroid cells were shown to be more tumorigenic and less responsive to commonly used chemotherapeutics[13]. By generating chemo resistant RMS cancer cell lines, we hope to understand the mechanisms driving RMS chemotherapeutic resistance.

Our understanding of how RMS TPCs function in disease relapse remains limited. While a zebrafish ERMS disease model allows for rapid identification and isolation of TPCs for study, a similar approach in human ERMS cancer cell lines currently do not exist. In this chapter, we show preliminary results that indicate CD133 as a promising marker of human ERMS TPCs. We have developed a novel SMS-CTR CD133-GFP reporter cell line that would allow for inexpensive and rapid isolation of potential TPCs for characterization. By understanding the mechanism behind RMS TPC self-renewal in the context of chemo and NRAS resistance, we may identify novel therapeutic targets against RMS disease relapse and metastasis.

Materials/Methods

CRISPR/Cas9 Mediated Gene Knockout

SMS-CTR cells were transfected using the Neon Transfection System with two separate DNA plasmids. Our CRISPR/Cas9 plasmid is responsible for generating both targeting gRNAs as well as the Cas9 enzyme. The second plasmid contains our replacement template, which has fuses a self-cleaving T2A peptide sequence linked to *GFP* to the last exon of *CD133.* Following CRISPR/Cas9 mediated double stranded DNA break of the endogenous *CD133* sites and our replacement template, NHEJ will insert our replacement sequence, bumping down the endogenous last exon of *CD133.* The addition of a puromycin selectable marker driven by the PGK promoter allows for selection of successful transfection. Cells are grown under antibiotic selection for at least 2 weeks before plating for clonal isolation. Clonal expansions are kept under continuous antibiotic selection. PCR amplification of knock-in junction and Sanger sequencing is performed to confirm correct integration.

Confirmation Primers Sequence

FWD - GGATGGATATACTGTCTGGAGGAGA

REV - CGTCGCCGTCCAGCTCGACCAG

CRISPR/Cas9 gene targeting in human RMS cells

Single gene knockout was accomplished using lentiviral transduction of RMS cells with Cas9 expressing and gene-specific double gRNA constructs. Lentiviral transduced cells were placed under antibiotic selection and plated for assays 7 days later. Cloning of Cas9 and gRNA expression constructs was performed as described previously[20].

The following gRNAs were used for targeting genes in human RMS cell lines:

GRK5: gRNA1- GGACCTGGTCTCCCAGACGG

gRNA2- GGAGCAGCCCTTTCTTGGG

HDAC6: gRNA1 - GCTTCCCGGAAGGCCCTGAGCGG

gRNA2 - GCTGGTGGATGCGGTCCTGGGGG

ERN1: gRNA1 - GGCCGCATAGTCAAAGTAGGNGG

gRNA2 - GTATTTCCCAACATACAGAGNGG

Human Expression Data Analysis

RNA was collected from human cell lines lysates (381T, SMSCTR, JR1) using Qiagen RNeasy Plus Mini Kit. cDNA was then generated using High Capacity cDNA Reverse Transcription Kit from Applied Biosystems. RT-PCR reactions were then run with iTaq Universal SYBR Green mix on a CFX Connect Real Time System (BioRad, Hercules, CA). RT-PCR primers used are listed below: MYF5 and PAX7 RT-PCR primer sequences were from a previously published article[29].

The following qPCR primers were used:

CD82: FWD - GGAGCAGAAAGCAGAACCC

REV - GGAGCTTCCTTCCACGAAAC

CD133: FWD - ACTCCCATAAAGCTGGACCC

REV - TCAATTTTGGATTCATATGCCTT

ERN1: FWD - GAGACCCTGCGCTATCTGAC

REV - CTTGGCCTCTGTCTCCTTGG

Cell-based Assays

RMS cell growth was quantified by direct cell counting or the ATP-based Cell Titer Glo luminescent cell viability assay (Promega, Madison, WI). Spheres (“rhabdospheres”) were induced in stem cell (neurobasal) medium enriched with growth factors (EGF, bFGF, PDGF-A and PDGF-B). Tumor palpations will be made 3 times a week until tumor engraftment. Analysis

of limiting dilution data was performed as previously described[30]. All mice were humanly euthanized for tumor tissue harvesting at the end of the experiment.

Human Xenografts

We will generate spheroids from SMS-CTR CD133-GFP cells and live cell flow cytometry sort GFP positive and GFP negative cells. 4 immunocompromised NOD-SCID IL2rg-/- (NSG) mice will be xenografted via subcutaneous injections into the flanks with either GFP positive, GFP negative, bulk spheroids and adherent cells at approximately 10, 100, 1000 counts suspended in Matrigel. Tumor palpations will be made 3 times a week until tumor engraftment. Analysis of limiting dilution data was performed as previously described[30]. All mice were humanly euthanized for tumor tissue harvesting at the end of the experiment.

Generating Chemo Resistant RMS Cells

RD and Rh30 RMS cancer cells were seeded at approximately 80,000 cells per well. Both cell lines were started at 0.1nM concentrations of either vincristine, D-actinomycin or DMSO vehicle control. Dosage was increased between 0.2-0.5 nM every 3-4 days while monitoring number of dead cells per well. If cells respond with heavy cell death, revert to the previous drug concentration. Continue until cells are able to survive in at least 4.5nM drug concentration.

Figures

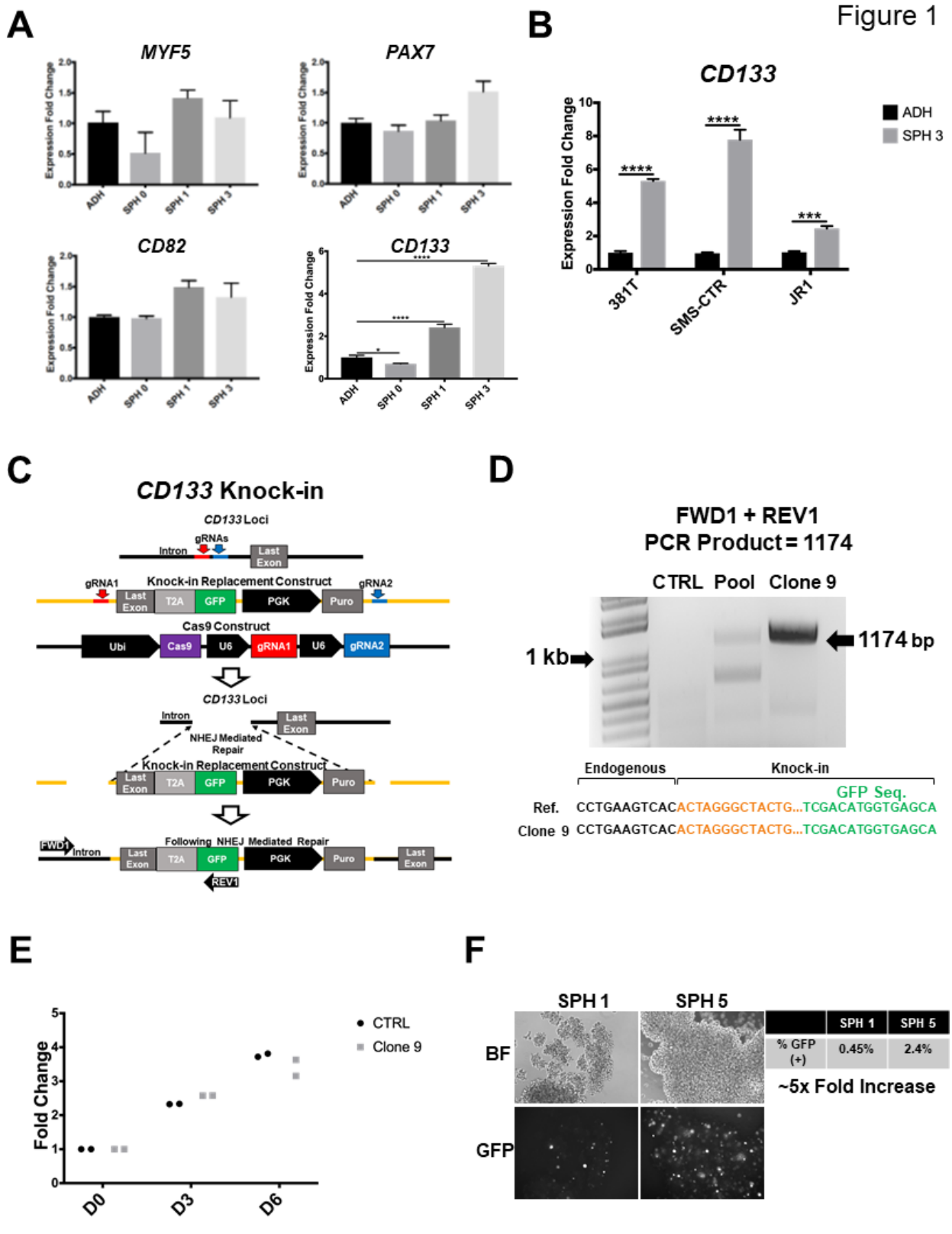
Figure 1
A
MYF5
PAX7
CD82
CD133
Expression Fold Change
ADH
SPH 0
SPH 1
SPH 3
B
CD133
ADH
SPH 3
****
***
381T
SMS-CTR
JR1
C
CD133 Knock-in
CD133 Loci
gRNAs
Intron
Last Exon
gRNA1
gRNA2
Knock-in Replacement Construct
T2A
GFP
PGK
Puro
Cas9 Construct
Ubi
Cas9
U6
gRNA1
U6
gRNA2
NHEJ Mediated Repair
Following NHEJ Mediated Repair
FWD1
REV1
D
FWD1 + REV1
PCR Product = 1174
CTRL
Pool
Clone 9
1 kb
1174 bp
Endogenous
Knock-in
GFP Seq.
Ref. CCTGAAGTCACACTAGGGCTACTG...TCGACATGGTGAGCA
Clone 9 CCTGAAGTCACACTAGGGCTACTG...TCGACATGGTGAGCA
E
Fold Change
CTRL
Clone 9
D0
D3
D6
F
SPH 1
SPH 5
BF
GFP
% GFP (+)
0.45%
2.4%
~5x Fold Increase

Figure 2

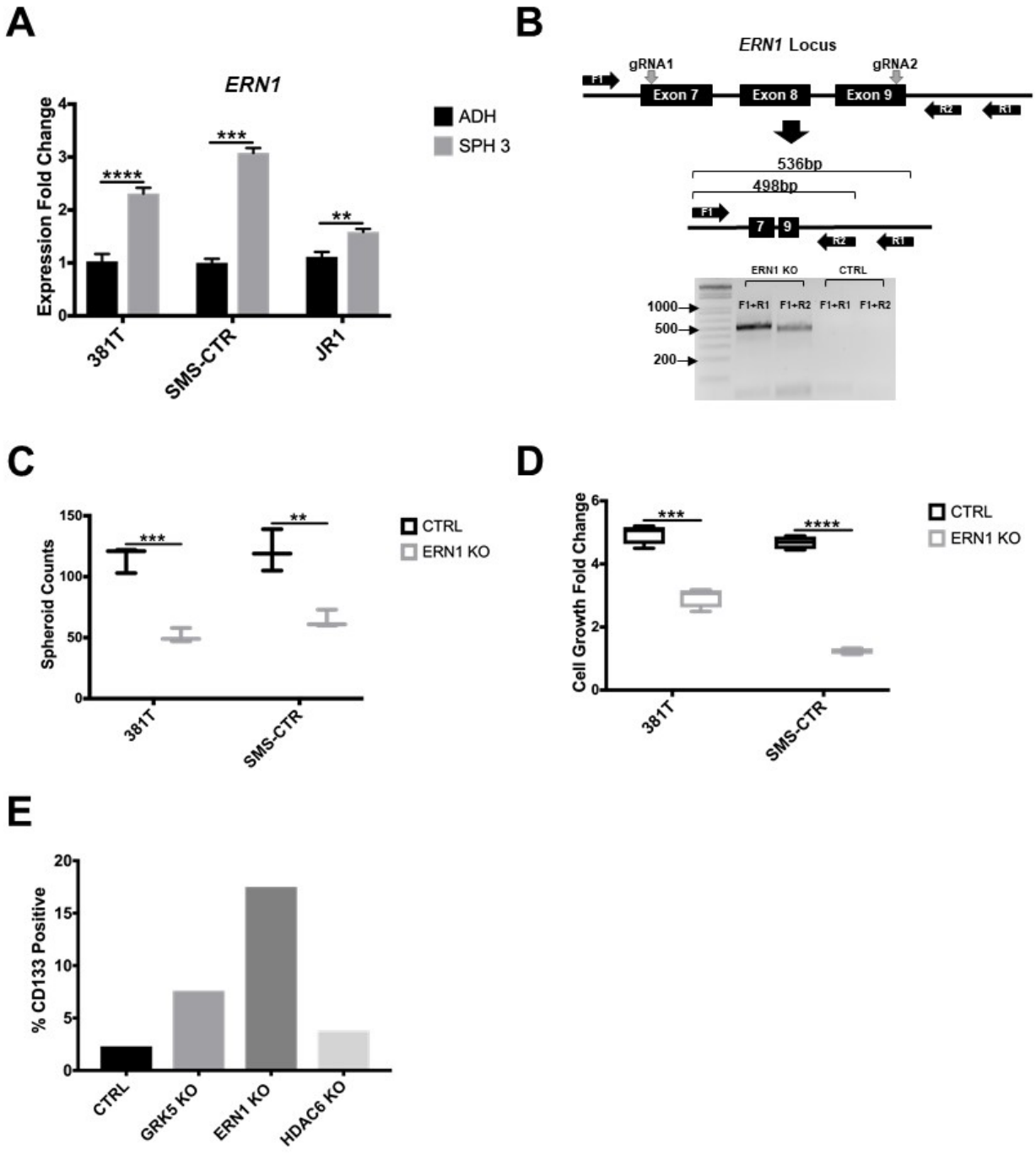
A
ERN1
Expression Fold Change
ADH
SPH 3
****
***
**
381T
SMS-CTR
JR1
B
ERN1 Locus
gRNA1
gRNA2
Exon 7
Exon 8
Exon 9
F1
R2
R1
536bp
498bp
7
9
ERN1 KO
CTRL
F1+R1
F1+R2
F1+R1
F1+R2
1000
500
200
C
Spheroid Counts
CTRL
ERN1 KO
***
**
381T
SMS-CTR
D
Cell Growth Fold Change
CTRL
ERN1 KO
***
****
381T
SMS-CTR
E
% CD133 Positive
CTRL
GRK5 KO
ERN1 KO
HDAC6 KO

Figure 3

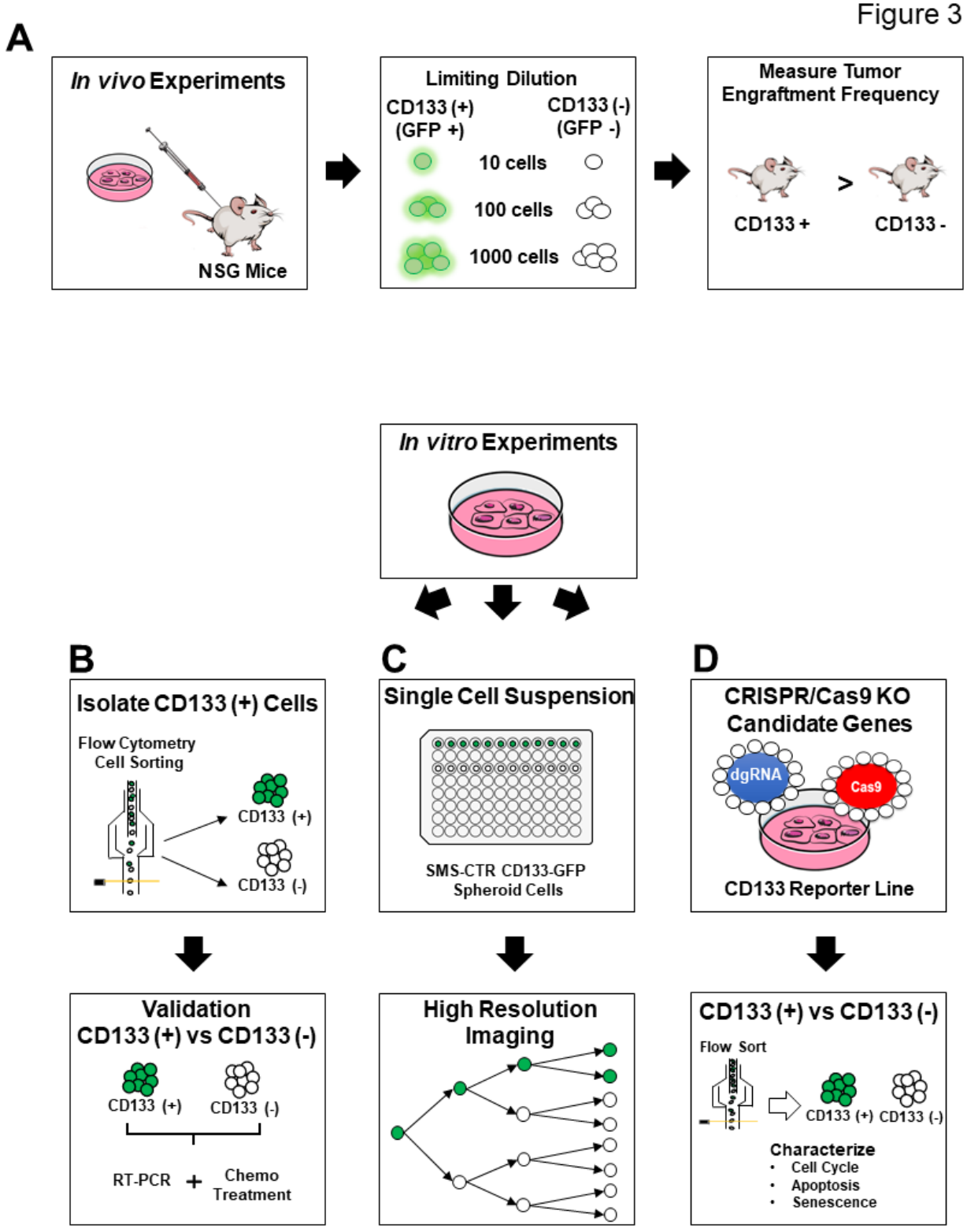
A
In vivo Experiments
NSG Mice
Limiting Dilution
CD133 (+) (GFP +)
CD133 (-) (GFP -)
10 cells
100 cells
1000 cells
Measure Tumor Engraftment Frequency
CD133 +
>
CD133 -
In vitro Experiments
B
Isolate CD133 (+) Cells
Flow Cytometry Cell Sorting
CD133 (+)
CD133 (-)
C
Single Cell Suspension
SMS-CTR CD133-GFP Spheroid Cells
D
CRISPR/Cas9 KO Candidate Genes
dgRNA
Cas9
CD133 Reporter Line
Validation CD133 (+) vs CD133 (-)
CD133 (+)
CD133 (-)
RT-PCR + Chemo Treatment
High Resolution Imaging
CD133 (+) vs CD133 (-)
Flow Sort
CD133 (+)
CD133 (-)
Characterize
Cell Cycle
Apoptosis
Senescence

Figure 4

A

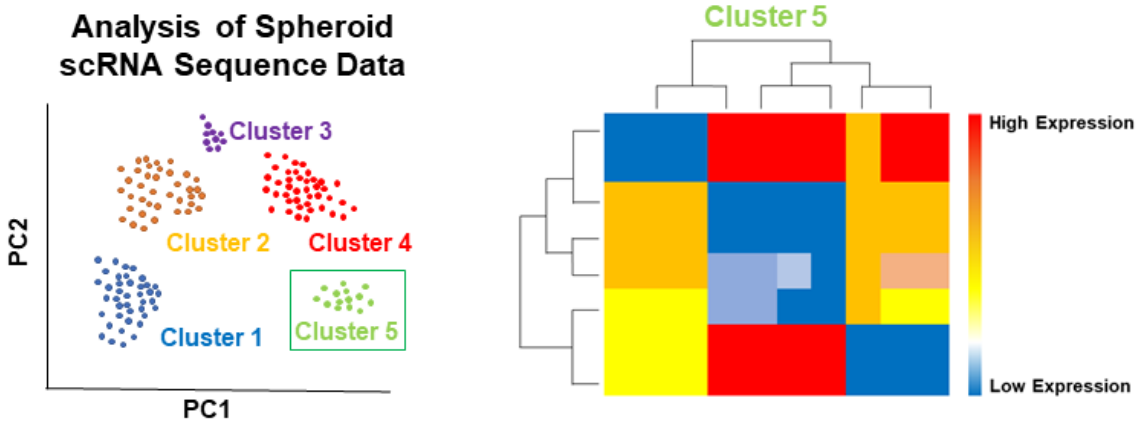
Analysis of Spheroid scRNA Sequence Data
Cluster 3
Cluster 2
Cluster 4
Cluster 1
Cluster 5
PC2
PC1
Cluster 5
High Expression
Low Expression

B

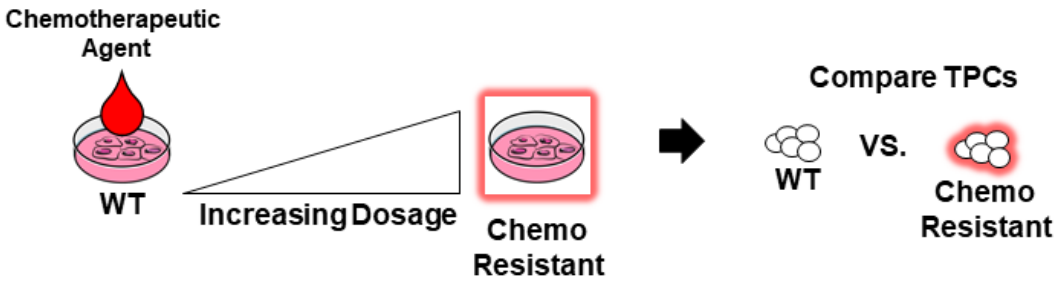
Chemotherapeutic Agent
WT
Increasing Dosage
Chemo Resistant
Compare TPCs
WT
VS.
Chemo Resistant

Figure Legends

Figure 1: Identification of *CD133* as a potential ERMS TPC marker and creation of a novel reporter cell line. (A) RT-PCR analysis of candidate TPC marker genes (*MYF5, PAX7, CD82, CD133)* comparing adherent 381T cells (ADH) and spheroids passaged 0, 1, 3 times (SPH 0, SPH 1, SPH 3). (B) RT-PCR analysis of *CD133* expression in a panel of 3 ERMS cell lines (381T, SMS-CTR, JR1) comparing adherent (ADH) to spheroid cells passaged 3 times (SPH 3). RT-PCR error bars represent standard deviation of 3 technical replicates from an individual experiment repeated 3 times. (C) Schematic illustrating CRISPR/Cas9 mediated gene knock-in of *GFP* to the *CD133* loci of SMS-CTR cells. Confirmation of successful knock-in was done through PCR amplification (FWD1 + REV1) across region spanning endogenous *CD133* and knock-in sequence (D) Gel electrophoresis of knock-in confirmation PCR in SMS-CTR control cells (CTRL), heterogenous knock-in population (POOL) and isolated clone #9 (Clone 9). Sanger sequencing for Clone 9 shows confirms correct knock-in. (E) Cell Titer Glo viability assessment of SMS-CTR CD133-GFP clone 9 (Clone 9) compared to SMS-CTR controls (CTRL). (F) Brightfield (BF) and fluorescent GFP images (GFP) of SMS-CTR CD133-GFP Clone 9 spheroids at passage 1 (SPH 1) and 5 (SPH 5). Flow cytometry-based cell sorting to determine changes in GFP (+) population. Each data point represents one technical replicate. Two-tailed t-test and one-way ANOVA; * = $p < 0.05$; *** = $p < 0.001$, **** = $p < 0.0001$.

Figure 2: Characterization of *ERN1* and other potential TPC regulators using a CD313 ERMS reporter cell line. (A) RT-PCR analysis of *ERN1* expression comparing adherent (ADH) to spheroid cells passaged 3 times (SPH 3) in a panel of ERMS cell lines (381T, SMS-CTR, JR1). RT-PCR error bars represent standard deviation of 3 technical replicates from an individual experiment repeated 3 times. (B) Schematic demonstrating CRISPR/Cas9 targeting of *ERN1*. Two gRNAs were designed to disrupt 2 separate exons to maximize targeting efficiency. (C) Spheroid counts to assess self-renewal. Data shown are 4 replicates from one of 3 independent experiments. (D) Cell Titer Glo viability assessment of *ERN1* knockout (ERN1 KO) compared to controls (CTRL) in two independent ERMS cell lines (381T and SMS-CTR). Data shown are 3 replicates from one of 3 independent experiments. (E) Preliminary flow cytometry results comparing change in GFP positive SMS-CTR CD133-GFP spheroid cells between control (CTRL) and CRISPR/Cas9 mediated knock out of *GRK5, ERN1,* and *HDAC6* cells. Data shown is from 1 technical replicate from 1 experiment. Two-tailed t-test; ** = $p < 0.01$; *** = $p < 0.001$, **** = $p < 0.0001$.

Figure 3: Future experiments for validation of SMS-CTR CD133-GFP reporter cell line. (A-D) Flow chart schematic illustrating future *in vivo* and *in vitro* experiments to validate SMS-CTR CD133 reporter cell line.

Figure 4: Ongoing projects. (A) Illustration of unsupervised clustering and gene expression analysis required of single cell RNA (scRNA) sequencing results in 381T spheroid cells. (B) Schematic illustrating method for generating chemo resistant RMS cell lines from wild-type (WT) cells to compare potential changes to TPCs.

References

1. Pappo, A. S. *et al.* Survival After Relapse in Children and Adolescents With Rhabdomyosarcoma: A Report From the Intergroup Rhabdomyosarcoma Study Group. *JCO* **17**, 3487–3493 (1999).

2. Kaur, G. *et al.* G-protein coupled receptor kinase (GRK)-5 regulates proliferation of glioblastoma-derived stem cells. *Journal of Clinical Neuroscience* **20**, 1014–1018 (2013).

3. Lawson, D. A. *et al.* Single-cell analysis reveals a stem-cell program in human metastatic breast cancer cells. *Nature* **526**, 131–135 (2015).

4. Jahchan, N. S. *et al.* Identification and targeting of long-term tumor-propagating cells in small cell lung cancer. *Cell Rep* **16**, 644–656 (2016).

5. Kreso, A. & Dick, J. E. Evolution of the Cancer Stem Cell Model. *Cell Stem Cell* **14**, 275–291 (2014).

6. Ignatius, M. S. *et al.* In Vivo Imaging of Tumor-Propagating Cells, Regional Tumor Heterogeneity, and Dynamic Cell Movements in Embryonal Rhabdomyosarcoma. *Cancer Cell* **21**, 680–693 (2012).

7. Pastrana, E., Silva-Vargas, V. & Doetsch, F. Eyes Wide Open: A Critical Review of Sphere-Formation as an Assay For Stem Cells. *Cell Stem Cell* **8**, 486–498 (2011).

8. Chen, X. *et al.* p53 positively regulates the expression of cancer stem cell marker CD133 in HCT116 colon cancer cells. *Oncol Lett* **16**, 431–438 (2018).

9. Liu, G. *et al.* Analysis of gene expression and chemoresistance of CD133+ cancer stem cells in glioblastoma. *Mol Cancer* **5**, 67 (2006).

10. Negroni, E. *et al.* In Vivo Myogenic Potential of Human CD133+ Muscle-derived Stem Cells: A Quantitative Study. *Molecular Therapy* **17**, 1771–1778 (2009).

11. Meng, J., Muntoni, F. & Morgan, J. CD133+ cells derived from skeletal muscles of Duchenne muscular dystrophy patients have a compromised myogenic and muscle regenerative capability. *Stem Cell Research* **30**, 43–52 (2018).

12. Pressey, J. G. *et al.* CD133 marks a myogenically primitive subpopulation in rhabdomyosarcoma cell lines that are relatively chemoresistant but sensitive to mutant HSV. *Pediatric Blood & Cancer* **60**, 45–52 (2013).

13. Walter, D. *et al.* CD133 Positive Embryonal Rhabdomyosarcoma Stem-Like Cell Population Is Enriched in Rhabdospheres. *PLOS ONE* **6**, e19506 (2011).

14. Bidlingmaier, S., Zhu, X. & Liu, B. The utility and limitations of glycosylated human CD133 epitopes in defining cancer stem cells. *J Mol Med (Berl)* **86**, 1025–1032 (2008).

15. Glumac, P. M. & LeBeau, A. M. The role of CD133 in cancer: a concise review. *Clinical and Translational Medicine* **7**, 18 (2018).

16. Chen, Y. & Brandizzi, F. IRE1: ER stress sensor and cell fate executor. *Trends in Cell Biology* **23**, 547–555 (2013).

17. Maurel, M., Chevet, E., Tavernier, J. & Gerlo, S. Getting RIDD of RNA: IRE1 in cell fate regulation. *Trends in Biochemical Sciences* **39**, 245–254 (2014).

18. Strietz, J. *et al.* ERN1 and ALPK1 inhibit differentiation of bi-potential tumor-initiating cells in human breast cancer. *Oncotarget* **7**, 83278–83293 (2016).

19. Li, X.-X. *et al.* Knockdown of IRE1α inhibits colonic tumorigenesis through decreasing β-catenin and IRE1α targeting suppresses colon cancer cells. *Oncogene* **36**, 6738–6746 (2017).

20. Liu, L. *et al.* Adaptive endoplasmic reticulum stress signalling via IRE1α–XBP1 preserves self-renewal of haematopoietic and pre-leukaemic stem cells. *Nature Cell Biology* **21**, 328 (2019).

21. Alexander, M. S. *et al.* CD82 Is a Marker for Prospective Isolation of Human Muscle Satellite Cells and Is Linked to Muscular Dystrophies. *Cell Stem Cell* doi:10.1016/j.stem.2016.08.006.

22. Bentzinger, C. F., Wang, Y. X. & Rudnicki, M. A. Building Muscle: Molecular Regulation of Myogenesis. *Cold Spring Harb Perspect Biol* **4**, a008342 (2012).

23. Phelps, M. P., Bailey, J. N., Vleeshouwer-Neumann, T. & Chen, E. Y. CRISPR screen identifies the NCOR/HDAC3 complex as a major suppressor of differentiation in rhabdomyosarcoma. *PNAS* **113**, 15090–15095 (2016).

24. Sui, X. *et al.* Autophagy and chemotherapy resistance: a promising therapeutic target for cancer treatment. *Cell Death & Disease* **4**, e838–e838 (2013).

25. Tenente, I. M. *et al.* Myogenic regulatory transcription factors regulate growth in rhabdomyosarcoma. *eLife* **6**,.

26. Hu, Y. & Smyth, G. K. ELDA: Extreme limiting dilution analysis for comparing depleted and enriched populations in stem cell and other assays. *Journal of Immunological Methods* **347**, 70–78 (2009).

Chapter 5: Concluding Remarks

While great advancements have been in made in the field of cancer therapy, disease relapse remains a major concern for cancer patients. Cancer TPCs are believed to evade therapeutic targeting and are responsible for driving disease relapse and metastasis[1]. Self-renewal of TPCs allows for recapitulation of the tumor heterogeneity in its entirety[1]. Laboratory findings show that targeting regulators of TPC activity, in combination with standard therapeutic agents, may improve tumor killing and reduce disease relapse in patients[2–7]. For RMS patients, disease relapse comes along with a very poor survival outlook[8]. Therefore, there exists a need for identifying novel therapeutic targets against RMS disease relapse and metastasis.

To help identify novel therapeutic targets against RMS disease relapse, our lab utilized a siRNA library screen against the entire human kinome. From this screen, we discovered GRK5 regulates ERMS self-renewal and cell growth in a kinase-independent manner. Interestingly, loss of GRK5 results in a significant increase of ERMS spheroid cell death but not adherent ERMS cancer cells. While we are uncertain whether this effect is specific to ERMS TPCs or all spheroid cells, it provides novel insight into GRK5 potentially having distinct activity in ERMS TPCs vs non-TPCs. As GRK5 was shown to regulate ERMS cell growth in a kinase independent manner, it would be interesting to investigate whether GRK5 possesses unique regulatory gene transcription activity when it comes to NFAT1 transcription. Such additional mechanistic insights may help in developing therapeutic agents against GRK5 mediated ERMS tumor cell growth.

From a previously performed CRISPR/Cas9 screen on histone deacetylases (HDAC), we identified HDAC6 as a potent regulator of RMS cell growth[9]. HDAC6 was found to regulate RMS tumor cell growth, self-renewal and cell motility. RMS loss-of-function spheroid cells showed reduced expression of stem-cell markers compared to controls. Characterization of HDAC6 loss-of-function spheroid cells to assess cell death and cell cycle may provide additional insight into how HDAC6 may regulate RMS TPC activity. As HDAC6 was shown to alter RMS cytoskeletal dynamics via RAC1, I believe it would be interesting to look at HDAC6 loss-of-function spheroid cell division and how this may affect RMS TPC self-renewal capacity.

In order to more accurately study human ERMS TPCs, I set out to develop a human TPCs reporter cell line. CD133 was identified as a potential ERMS TPC marker as it was shown to be highly upregulated in ERMS spheroid cells. We successfully generated a SMS-CTR CD133-GFP reporter cell line using CRISPR/Cas9 mediated gene knock-in. While additional validation studies must still be performed, the development of a SMS-CTR CD133-GFP cell line will allow for the isolation and characterization of ERMS TPCs behavior. ERN1 was also identified as a novel regulator of ERMS self-renewal and cell growth. ERN1 loss-of-function

spheroid cells were found to be smaller and fewer in number. Expecting to see a decrease in CD133 (+) ERN1 loss-of-function spheroid cells, we instead saw a dramatic increase in CD133 (+) spheroid cells. If our preliminary findings prove to be accurate, it may mean a reduction in RMS self-renewal capacity seen through sphere assays may not only be the result of TPC death.

Targeting of GRK5 or HDAC6, *in vivo,* via small molecule inhibitors significantly reduced RMS tumor cell growth, highlighting their potential as novel RMS therapeutic targets. While we have characterized the role of GRK5 and HDAC6 in regulating RMS self-renewal *in vitro* and *in vivo*, there are still important questions left unanswered regarding their role in RMS TPCs. TPCs are a heterogeneous population, with cells potentially existing in different stages of quiescence, proliferation, differentiation and apoptosis. While loss of GRK5, HDAC6 and ERN1 may result in reduced ERMS self-renewal capacity, we are still uncertain of their role is specific to ERMS TPCs or non-TPC spheroid cells. By utilizing new technology and techniques, such as our SMS-CTR CD133-GFP reporter cell line, I hope to tackle such uncertainties and provide novel insights into RMS TPC behavior. With the help of current advancements in single cell RNA sequencing and gene editing techniques, we are beginning to also directly look at RMS TPCs to illicit potential therapeutic markers and targets. I hope that my contributions to the field of RMS and cancer biology today may lay the foundation for promising therapeutic options for RMS patients tomorrow.

References

1. Kreso, A. & Dick, J. E. Evolution of the Cancer Stem Cell Model. *Cell Stem Cell* **14**, 275–291 (2014).

2. Hirsch, H. A., Iliopoulos, D., Tsichlis, P. N. & Struhl, K. Metformin Selectively Targets Cancer Stem Cells, and Acts Together with Chemotherapy to Block Tumor Growth and Prolong Remission. *Cancer Res* **69**, 7507–7511 (2009).

3. Li, Y., Wang, M., Zhi, P., You, J. & Gao, J.-Q. Metformin synergistically suppress tumor growth with doxorubicin and reverse drug resistance by inhibiting the expression and function of P-glycoprotein in MCF7/ADR cells and xenograft models. *Oncotarget* **9**, 2158–2174 (2017).

4. Heidel, F. H. *et al.* Genetic and Pharmacologic Inhibition of β-Catenin Targets Imatinib-Resistant Leukemia Stem Cells in CML. *Cell Stem Cell* **10**, 412–424 (2012).

5. Li, Y. *et al.* Suppression of cancer relapse and metastasis by inhibiting cancer stemness. *PNAS* **112**, 1839–1844 (2015).

6. Vazquez-Martin, A., Oliveras-Ferraros, C., Barco, S. D., Martin-Castillo, B. & Menendez, J. A. The anti-diabetic drug metformin suppresses self-renewal and proliferation of trastuzumab-resistant tumor-initiating breast cancer stem cells. *Breast Cancer Res Treat* **126**, 355–364 (2011).

7. Zhang, B. *et al.* Effective Targeting of Quiescent Chronic Myelogenous Leukemia Stem Cells by Histone Deacetylase Inhibitors in Combination with Imatinib Mesylate. *Cancer Cell* **17**, 427–442 (2010).

8. Pappo, A. S. *et al.* Survival After Relapse in Children and Adolescents With Rhabdomyosarcoma: A Report From the Intergroup Rhabdomyosarcoma Study Group. *JCO* **17**, 3487–3493 (1999).

9. Phelps, M. P., Bailey, J. N., Vleeshouwer-Neumann, T. & Chen, E. Y. CRISPR screen identifies the NCOR/HDAC3 complex as a major suppressor of differentiation in rhabdomyosarcoma. *PNAS* **113**, 15090–15095 (2016).